

FINAL REPORT  
JULY 1973

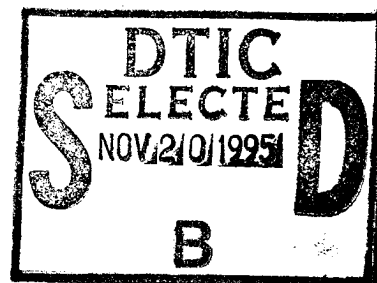
## NEODYMIUM LASER GLASS IMPROVEMENT PROGRAM

1 MAY 1962 - 1 MARCH 1971

RICHARD F. WOODCOCK, PROJECT SCIENTIST  
*American Optical Corporation*  
*Research Division*  
Southbridge, Massachusetts 01550

prepared for

Physics Branch  
Office of Naval Research  
Department of the Navy  
Arlington, Virginia 22217



Contract No. Nonr. 2885 (60)  
ARPA Order No. 306

*BD 20,548*  
Distribution of this document is unlimited.

Reproduction in whole or part is permitted for any purpose of the  
United States Government

This research is part of Project DEFENDER under the joint sponsorship of the  
Advanced Research Projects Agency, Department of Defense and the  
Office of Naval Research.

DTIC QUALITY INSPECTED 5

FINAL REPORT

July 1973

NEODYMIUM LASER GLASS IMPROVEMENT PROGRAM

1 May 1962 - 1 March 1971

Richard F. Woodcock - Project Scientist

American Optical Corporation  
Research Division  
Southbridge, Massachusetts 01550

prepared for  
Physics Branch  
Office of Naval Research  
Department of the Navy  
Arlington, Virginia 22217

Contract No. Nonr 3835(00)

Project Code 7300

ARPA Order No. 306

Distribution of this document is unlimited.

Reproduction in whole or part is permitted for any purpose of the  
United States Government

This research is part of Project DEFENDER under the joint sponsorship of the Advanced Research Projects Agency, Department of Defense and the Office of Naval Research.

*Rec'd 1-25-74  
American  
Optical  
Corp.*

## ABSTRACT

This final report describes work carried out over a nine-year period to improve the properties and performance of Nd-laser glass. One of the first tasks was the reduction of absorption at  $1.06\text{ }\mu\text{m}$  to a  $0.1\text{-}0.2\%/ \text{cm}$  level by the identification and elimination of such impurities as iron.

Fluorescent lifetime was investigated; (1) as a function of host glass composition to provide data on the range of values attainable for this important parameter, and (2) as a function of time, temperature and  $\text{Nd}_2\text{O}_3$  concentration to provide insight into the nature of the  $\text{Nd}^{3+}$ -ion site and its effect on emission.

The degree of discoloration due to solarization by the pump source and its effect on laser performance was investigated as a function of glass composition.

Theory was evolved for the design of an "athermal" laser material based on the hypothesis that thermally induced optical distortion resulting from thermal expansion and associated stress-optical effects can be counterbalanced by direct thermally induced index changes if proper glass composition and cavity design are chosen. Descriptions are given of the measuring techniques, which are unique in many cases, for determining coefficients of the above temperature and pressure effects as a function of glass composition. Several compositions showed theoretically predicted and experimentally verified marked improvement over our commercial laser material.

Accession For	
NTIS GRA&I	<input checked="checked" type="checkbox"/>
DTIC TAB	<input type="checkbox"/>
Unannounced	<input type="checkbox"/>
Justification	
By	
Distribution/	
Availability Codes	
Dist	Avail and/or Special
A-1	

## FOREWORD

This report was prepared by the Research Division of American Optical Corporation, Southbridge, Massachusetts under Contract Nonr 3835(00) entitled "Neodymium Laser Glass Improvement Program." The contract has been under the sponsorship of the Office of Naval Research.

This is the Final Report of this program and covers the period beginning 1 May 1962 and ending 31 March 1971. The original contract, scheduled to terminate 30 April 1963, was followed by six (6) contract modifications extending the scope of the effort and changing the final termination date to 31 January 1971.

Project managers of this contract have been Drs. Walter P. Siegmund, William R. Prindle and Richard F. Woodcock, consecutively. R. F. Woodcock was author of the majority of the technical reports. Luther Smith was responsible for measuring stress-optical coefficients and carried out efforts involved in the design and testing of the interferometer used for those measurements. He also was author of the section describing that work. Dr. H. Osterberg authored the appendices covering theoretical work which he and Luther Smith performed.

This program is part of project DEFENDER.

This report is unclassified.

# CONTENTS

	PAGE
1. INTRODUCTION. . . . .	1
2. TECHNICAL APPROACH. . . . .	4
2.1 OPTICAL TRANSMISSION STUDIES . . . . .	4
2.2 FLUORESCENT LIFETIME . . . . .	8
2.2.1 Effect of Host Composition on Fluorescent Lifetime . . . . .	9
2.2.2 Effect of $\text{Nd}_2\text{O}_3$ Concentration on Fluorescent Lifetime . . . . .	13
2.2.3 Fluorescent Decay as a Function of Time. . . . .	16
2.2.4 Effect of Temperature on Fluorescent Lifetime . . . . .	21
2.3 SOLARIZATION. . . . .	23
2.3.1 Transmission Studies of Solarization. . . . .	23
2.3.2 Laser Performance vs Solarization. . . . .	31
2.4 THERMAL PROPERTIES. . . . .	36
2.5 ATHERMALIZATION . . . . .	37
2.5.1 Athermalization Theory and Procedure. . . . .	37
2.5.2 Stress-Birefringence Coefficient . . . . .	43
2.5.3 Thermal Coefficient of Refractive Index. . . . .	44
2.5.4 Coefficient of Thermal Expansion . . . . .	52
2.5.5 Stress-Optical Coefficients. . . . .	56
2.5.5.1 <u>Interferometer Design</u> . . . . .	57
2.5.5.2 <u>Test of Interferometer Design</u> . . . . .	59
2.5.5.3 <u>Apparatus</u> . . . . .	63

# CONTENTS

	PAGE
2.5.5.4 <u>Experimental Procedure</u> . . . . .	67
2.5.5.5 <u>Stress-Optical Coefficient Values</u> . . . . .	72
2.5.6 Elastic Properties . . . . .	74
2.5.7 Athermalization Results . . . . .	75
3. SUMMARY. . . . .	81
APPENDIX I THEORETICAL CONSIDERATIONS OF ZERNIKE'S THREE PINHOLE INTERFEROMETER AS APPLIED TO THE MEASUREMENT OF STRESS OPTICAL COEFFICIENTS IN STRIATED GLASSES. . . . .	85
APPENDIX II TOLERANCE STUDIES ON THE INTERFEROMETER . .	105
REFERENCES . . . . .	123

# ILLUSTRATIONS

FIGURE		PAGE
1	Transmittance of a 20 mm thickness of a barium crown glass containing 5 wt % $\text{Nd}_2\text{O}_3$ made with standard purity ingredients. . . . .	7
2	Transmittance of a 20 mm thickness of the same composition used in Figure 1, but made with high purity ingredients . . . . .	7
3	Schematic diagram of the apparatus used in fluorescent decay studies . . . . .	8
4	Lifetime vs concentration curves for several oxides . . . . .	14
5	Effect of host composition on concentration quenching . . . . .	15
6	Interactions between energy levels of adjacent $\text{Nd}^{3+}$ ions. . . . .	16
7	$\text{Nd}^{3+}$ fluorescence vs time . . . . .	18
8	Fluorescent lifetime vs $\text{Nd}_2\text{O}_3$ concentration as measured at 300K and 77K. . . . .	21
9.	Spectral transmittance of Na-Ca-silica glass containing 1 wt% $\text{Sb}_2\text{O}_3$ before and after solarization. . . . .	25
10	Spectral transmittance of Na-Ca-silica glass free of $\text{Sb}_2\text{O}_3$ before and after solarization . . . . .	25
11	Spectral transmittance of K-Ba-silica glass containing 1 wt% $\text{Sb}_2\text{O}_3$ before and after solarization. . . . .	26
12	Spectral transmittance of K-Ba-silica glass free of $\text{Sb}_2\text{O}_3$ before and after solarization . . . . .	26
13	The effect of $\text{Sb}_2\text{O}_3$ , $\text{TiO}_2$ and $\text{CeO}_2$ on the solarization of a potassium-barium-silicate glass . . . . .	28

# ILLUSTRATIONS

FIGURE		PAGE
14	The effect on solarization of $\text{Sb}_2\text{O}_3$ and $\text{TiO}_2$ combined plus increased $\text{TiO}_2$ . . . . .	29
15	The effect on solarization of other combinations of $\text{TiO}_2$ , $\text{Sb}_2\text{O}_3$ and $\text{CeO}_2$ . . . . .	30
16	Change in laser characteristics due to solarization treatment . . . . .	32
17	Schematic diagrams of lasers with compensating Faraday rotators . . . . .	41
18	Schematic diagram of apparatus for measuring thermal coefficient of the index of refraction . . . . .	47
19	Spectral output of a glass laser with a thin plate acting as a reflection filter for various temperatures of the plate . . . . .	48
20	Effect of temperature on the parameter X where X may be length (L), emission wavelength ( $\lambda$ ) or refractive index (n) . . . . .	49
21	The basic three pinhole interferometer . . . . .	58
22	Illustration of the fringe system near focus in the Zernike interferometer . . . . .	59
23	Diagram of the three-pinhole interferometer for measuring the stress-optical effect in glass samples . . . . .	63
24	Autocollimator and pinhole subassembly . . . . .	64
25	Photograph of the strain frame. . . . .	65
26	Schematic drawing of the strain frame . . . . .	66
27	Experimental setup used for complete measurement of stress induced pathlength changes . . . . .	67
28	Apparatus for measuring pump-induced thermal distortion. . . . .	78

# LIST OF TABLES

NUMBER		PAGE
I	Effect of Purity on 1.06 $\mu\text{m}$ Absorption. . . . .	6
II	Composition vs Fluorescent Lifetime. . . . .	10
III	Correlation Coefficient for Composition vs Fluorescent Lifetime . . . . .	12
IV	Time Dependence of Lifetime vs $\text{Nd}_2\text{O}_3$ Concentration . . . . .	19
V	Time Dependence of Lifetime vs Glass Composition . . . . .	20
VI	Effect of Temperature on Fluorescent Lifetime . . .	23
VII	Effects of Solarization Treatment on Laser Characteristics . . . . .	33
VIII	Thermal Conductivity and Specific Heat. . . . .	36
IX	Glass Compositions for Athermalization Study. . .	42
X	Regression Coefficients ( $b_i$ ) of the Stress-Birefringence Coefficient ( $\Delta B$ ) . . . . .	45
XI	Comparison of Measured and Calculated Values of Stress-Birefringence . . . . .	46
XII	Thermal Coefficient of Refractive Index, $\alpha_n$ , and Preliminary Athermalization Figure of Merit $\alpha_n/\alpha$ . . . . .	50
XIII	Correlation Coefficient for Composition vs Thermal Coefficient of Refractive Index . . . . .	51
XIV	Regression Coefficients of the Coefficient of Expansion . . . . .	53
XV	Supplementary Glass Compositions for Athermalization Study . . . . .	54
XVI	Thermal Coefficient of Supplementary Series of Compositions . . . . .	55

# LIST OF TABLES

NUMBER		PAGE
XVII	Pathlength Changes $\Delta\phi$ , Induced by Repeated Stressing of a Glass Sample. . . . .	71
XVIII	Stress-Optical Coefficient Values. . . . .	73
XIX	Elastic Constants . . . . .	76
XX	Change in Optical Pathlength During Pumping . . .	77
XXI	Pump Induced Thermal Distortion . . . . .	79
XXII	Revised Values of Elastic Constants in Selected Glasses . . . . .	81

## NEODYMIUM LASER GLASS IMPROVEMENT PROGRAM

### 1. INTRODUCTION

This final report describes the work performed under Contract Nonr-3835(00). The research was part of project DEFENDER under the joint sponsorship of Advanced Research Projects Agency, the Office of Naval Research and the Department of Defense. The contract was initiated 1 May 1962 and terminated on 1 March 1971, following six modifications to the original contract. The level of effort has varied at times due to the nature of the work and during unfunded periods while contract modifications were being negotiated.

Prior to this contract, research and development work in the field of glass lasers had been carried out at American Optical Corporation's Research Division over a two and one-half year period under a company sponsored program. This work resulted in the development of the first neodymium glass laser<sup>1</sup> and included a material study program to improve the properties of neodymium glass which are pertinent to its laser performance. Among these were: dopant concentration, host composition, lifetime dependencies, material purity, optical quality, thermal and physical properties, core and cladding compatibility and glass making processes.

In the course of this program, dopant concentrations ranging from 0.1% to 13% by weight were added to various glass lasers. The base, or host glasses tested included crown, barium crown, high lead-content flint, borosilicate, phosphate and germanate glasses. In general, the crown glasses appeared to work best, and several satisfactory varieties of crown compositions were found.

The natural fluorescent decay lifetime of the Nd-ion was found to be concentration-dependent. It remains constant as the Nd<sup>3+</sup> concentration is increased to about  $1 \times 10^{20}$  ions/cm<sup>3</sup> but above this concentration the lifetime decreases. This concentration corresponds to 2 weight percent (wt%) of Nd<sub>2</sub>O<sub>3</sub> in a barium crown glass.

The threshold energy for onset of laser action is a function of the product of ion concentration and lifetime. A Nd<sup>3+</sup> concentration of  $6 \times 10^{20}$  ions/cm<sup>3</sup>, corresponding to

6 wt%  $\text{Nd}_2\text{O}_3$  in a barium crown base, was found to yield a minimum threshold for that base glass. The minimum threshold obtained prior to the contract was in a flint base glass containing about  $3 \times 10^{20}$  Nd ions/cm<sup>3</sup>.

In general, glass laser materials appeared to be divided into three categories according to their end use:

- (1) Those which possess long lifetimes for use in Q-switching applications,
- (2) those with high conversion efficiencies for high energy output, and
- (3) those with low thresholds.

Since these requirements are not compatible, different glass bases and  $\text{Nd}^{3+}$  concentrations were anticipated for different applications.

The flint glasses appeared to be best suited for low power threshold applications. They also showed high conversion efficiency, but were not durable enough to be used for high power applications. In the latter case, either a regular crown or barium crown would be used. Either of these might also be used in Q-switching applications, the barium crowns having the larger decay lifetime.

Variations of the relative amounts of the major constituents of the crown and barium crown glasses had been investigated for optimization of laser properties. In addition, the influence on durability of small concentrations of such elements as zinc, titanium, antimony and aluminum had been investigated. Since both iron and samarium produce an absorption at 1.06  $\mu\text{m}$ , freedom from these elements and other impurities in both host and dopant must be attained in the glass batch. The manufacturing techniques, such as the type of pot used in melting the glass, were also found to have an effect on the laser properties.

The initial objectives of this contractual effort represented a natural extension of the company sponsored work, namely to optimize the doping concentrations of the most promising base glass compositions and to perfect the optical quality of the laser glass. This was to include; (a) the identification of the attributes of the laser material which affect its laser properties, and determination of the relative magnitude of these effects so the results of dopant studies are not masked by unknown factors,

(b) the formulation and preparation of experimental glasses and  
(c) the performance of all necessary measurements of optical, mechanical, thermal and laser properties, and the evaluation of overall material performance.

As work on the contract progressed, the objectives were modified to include an investigation of the causes and prevention of solarization and an attempt to determine its effect on laser performance, and an investigation of optical inhomogeneities induced in the laser rod during the pumping process. The latter prompted both theoretical and experimental studies on the possibilities of developing an athermalized laser material in which the various pumplight-induced changes in optical properties of a given laser rod cancel each other. This included an investigation of the following properties as a function of base glass composition and in some cases the development of a technique for measuring these desired properties; (1) the thermal coefficient of refractive index ( $\alpha_n = 1/n \times dn/dT$ ) measured at the laser emission wavelength,  $1.06 \mu\text{m}$ , since this property is strongly wavelength dependent, (2) the thermal coefficient of expansion ( $\alpha = 1/L \times dL \times dL/dT$ ), (3) the stress birefringence or relative stress-optical coefficient ( $B = B_{\parallel} - B_{\perp}$ ) and (4) the stress-optical coefficients for light polarized both parallel to and perpendicular to the direction of applied stress,  $B_{\parallel}$  and  $B_{\perp}$  respectively.

Studies on optical quality of the glass led to the conclusion that marked improvement in the process for melting and annealing were needed in order to meet the requirements for use as a laser material. Preliminary experiments with the manufacture of laser glasses in a continuous tank, carried out in an ophthalmic crown continuous glass tank, just prior to the end of its "campaign" indicated that this would be an acceptable method of producing a glass with acceptable optical quality. A proposal to this effect was made by the American Optical Corporation, but was considered to be beyond the scope of this contract at the time.

In lieu of the above, two alternate approaches were taken for the procurement of suitable optical quality glass. The first was a company sponsored research and development effort to produce glass of acceptable optical quality in a platinum crucible capable of melting 50 pounds (22.7 kg) of glass at a time and discharging it by means of extrusion through a bottom orifice. The second approach, while our own development program was in progress, was to have glass melted for us by outside concerns which had continuous furnace facilities.

This work was initially performed for us by Sovirel using our glass composition MG-915, which they also designate as 915. This glass had satisfactory optical quality, but damaged easily in laser use due to the presence of platinum inclusions in the glass. Sovirel was not responsive at that time to our requests to produce this glass in a ceramic continuous tank (although they followed this approach a few years later) and as a result, a separate ONR-sponsored contract was established at American Optical Corporation, Contract No. Nonr 4656(00), for the development of a small, 40-50 lb, (18.1-22.7 kg) platinum-free laser glass melting facility. Negotiations were also carried out with the Schott Company in Germany to have them make laser glass in ceramic crucibles. In this case, part of the raw ingredients were supplied or the batch was completely pre-mixed at AO and shipped to Schott for melting in order to provide control over the purity of the batch ingredients. The problem encountered with all of the earlier work was that glasses made in platinum systems contained platinum inclusions and those made in all-ceramic systems had a higher level of  $\text{Fe}^{2+}$ -ion contamination than was desirable.

A study of the damage mechanism was initiated under one of the last contract modifications. This work was terminated at the request of the contracting agency when it became evident that there were not sufficient funds to complete both the athermalization study and the damage study. Termination occurred before any data were obtained.

## 2. TECHNICAL APPROACH

### 2.1 OPTICAL TRANSMISSION STUDIES

The attenuation of laser material at the laser output wavelength is a critical factor in laser performance. To obtain optimum laser operation it is desirable to reduce this attenuation to an absolute minimum. For this reason, one of the initial studies undertaken was the optical absorption of neodymium laser glass at  $1.06\text{ }\mu\text{m}$  as a function of composition and melting conditions and more specifically of certain impurities in the batch components, from the crucible in which the glass was melted, or both.

Preliminary studies were carried out on a barium crown laser glass made from the standard quality of batch ingredients used in the ophthalmic glass industry. Melts made in good quality

mullite crucibles showed about 10 percent higher absorption than those made in platinum crucibles (2.0 vs 1.8%/cm) indicating that the crucible was not the major source of contamination at this stage. Attempts to remove water vapor from the batch, which may have been contributing to the absorption at 1.06  $\mu$ m, and to provide an oxidizing atmosphere in the melt to shift any iron contamination present from an  $\text{Fe}^{2+}$ - to an  $\text{Fe}^{3+}$ -valence showed very little improvement.

The problem of excessive absorption at 1.06  $\mu$ m is now believed to be well understood. This absorption was caused by the presence of iron contaminants in the form of ferrous ions. Since silica is the predominant constituent in most of these glasses, a search was made to find a source of silica which is free of iron. The silica used in the production of ophthalmic crown glass contains about 0.02 wt%  $\text{Fe}_2\text{O}_3$ . The high purity silica presently being used contains only three parts per million of iron. Raw materials with comparable purities have also been located for the other glass batch components. An extensive study has been carried out on the effect of this impurity on transmittance. The glass used in this study was a barium crown composition containing 6.25 wt% of  $\text{Nd}_2\text{O}_3$ . The effect of using high purity chemicals is shown in Table I in which the above glass is referred to as "Standard Barium Crown." The improvement in transmittance with the use of pure ingredients in a variety of other crown and flint glass compositions is also shown in Table I.

The absorption data for this table were obtained from transmittance curves produced by a General Electric Recording Spectrophotometer. The accuracy of the transmission data obtained from this instrument is taken, conservatively, as  $\pm 0.5\%$  which yields accuracies of  $\pm 0.25$  and  $\pm 0.05\%$ /cm for the 2 cm and 10 cm length samples respectively. As may be seen from typical curves shown in Figures 1 and 2, the transmission was actually measured at 1  $\mu$ m instead of 1.060  $\mu$ m. Any error introduced by making the measurement at 1  $\mu$ m should be negligible and in such a direction as to make the absorption appear greater than it actually is. Glass samples of reasonable optical quality were required for the measurement, particularly on the 10 cm length samples, or the absorption would again appear greater than the true value.

Although the solution to the problem of absorption at 1.06  $\mu$ m was obtained early in the contract, the search for high purity raw ingredients and high purity crucible materials continued throughout the contract.

TABLE I. Effect of Purity on 1.06  $\mu$ m Absorption

Glass	Absorption ( $\%$ /cm)	
	2 cm	10 cm <sup>d</sup>
Std. Ba crown (6.25 wt% $\text{Nd}_2\text{O}_3$ ) Std. purity <sup>a</sup> in Frenchtown <sup>b</sup>	1.4 $\pm$ 0.25	-----
Std. Ba crown Std. purity in Pt <sup>c</sup>	1.35 $\pm$ 0.25	1.55 $\pm$ 0.05
Std. Ba crown Pure $\text{SiO}_2$ in Pt	0.0 $\pm$ 0.25	-----
Improved Ba crown <sup>e</sup> A (5 wt% $\text{Nd}_2\text{O}_3$ ) Std. purity in Frenchtown	1.8 $\pm$ 0.25	-----
Improved Ba crown A Pure chemicals in Pt	0.05 $\pm$ 0.25	0.12 $\pm$ 0.05
Improved Ba crown B (5 wt% $\text{Nd}_2\text{O}_3$ ) Pure chemicals in Pt	0.1 $\pm$ 0.25	0.11 $\pm$ 0.05
Dense flint (2 wt% $\text{Nd}_2\text{O}_3$ ) Std. purity	up to 1.75 $\pm$ 0.25	-----
Dense flint Pure chemicals in Pt	0.0 $\pm$ 0.25	-----
Flint (2 wt% $\text{Nd}_2\text{O}_3$ ) Std. purity in Pt	1.45 $\pm$ 0.25	-----
Flint Pure chemicals in Pt	0.05 $\pm$ 0.25	-----
Soda lime crown A (6 wt% $\text{Nd}_2\text{O}_3$ ) Std. purity in Pt	1.5 $\pm$ 0.25	-----
Soda lime crown A Pure chemicals in Pt	0.2 $\pm$ 0.25	-----
Soda lime crown B (2 wt% $\text{Nd}_2\text{O}_3$ ) Std. purity in Pt	1.55 $\pm$ 0.25	-----
Soda lime crown B Pure chemicals in Pt	0.2 $\pm$ 0.25	-----

<sup>a</sup>Standard purity refers to the grade of chemicals used in the manufacturing of optical quality glass.

<sup>b</sup>Frenchtown indicates the use of a high purity ceramic melting crucible.

<sup>c</sup>Pt indicates the use of a platinum crucible for melting.

<sup>d</sup>Some of the glasses were made only in a 1-pound (0.45 kg) melt which does not provide enough glass for the 10 cm pathlength required for the higher accuracy transmittance measurements.

<sup>e</sup>Glasses "A" and "B" differ in the relative amounts of alkali and alkaline earth oxides.

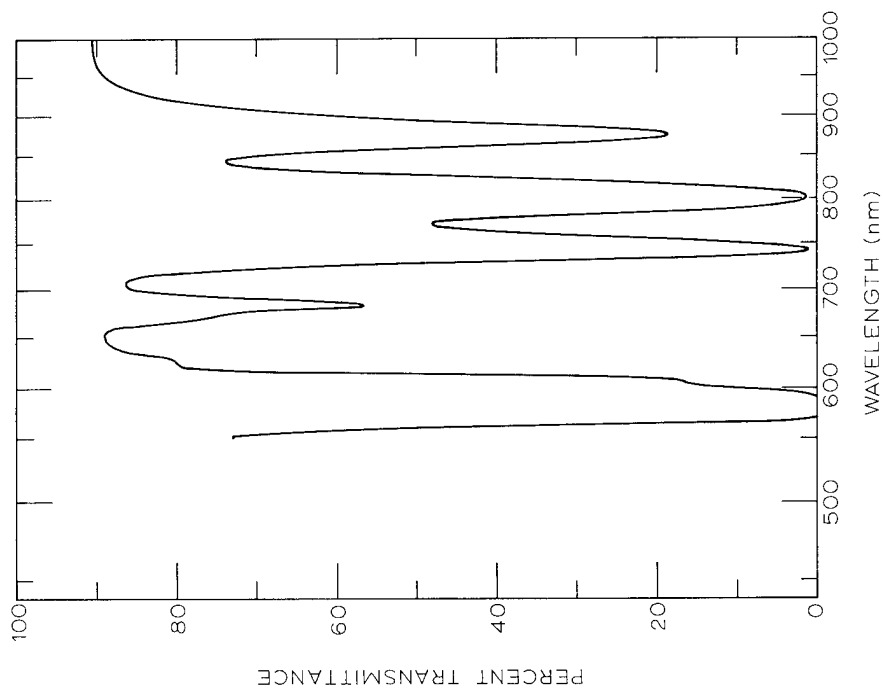


Figure 1. Transmittance of a 20 mm thickness of a barium crown glass containing 5 wt%  $\text{Nd}_2\text{O}_3$  made with standard purity ingredients.

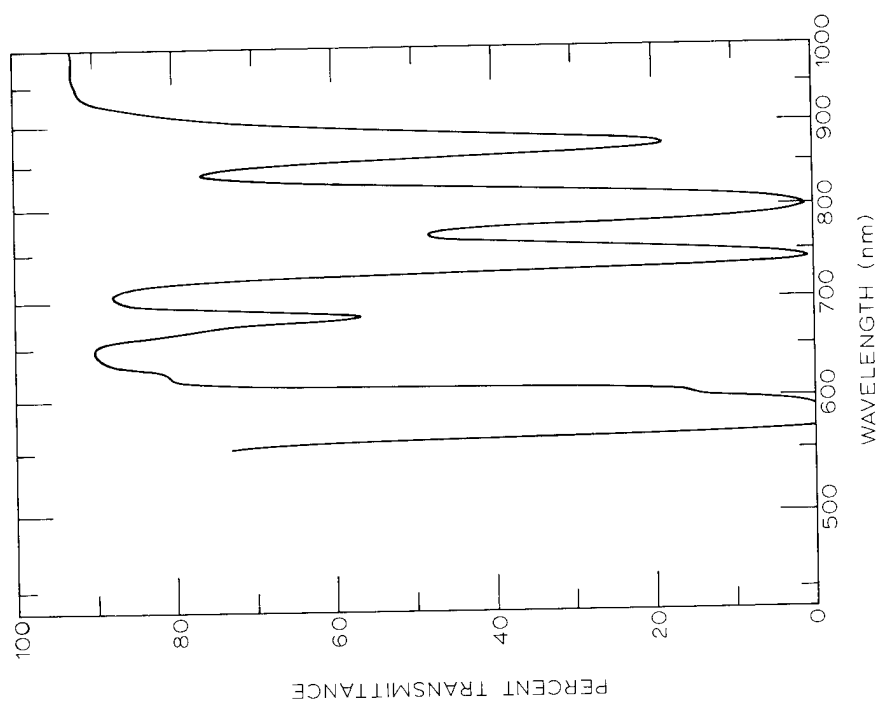


Figure 2. Transmittance of a 20 mm thickness of the same composition used in Figure 1 but made with high purity ingredients.

## 2.2 FLUORESCENT LIFETIME

The transition probability between the metastable state of an excited laser ion and its terminal state is one of the fundamental parameters by which laser materials are characterized. The transition probability is not measured directly, but rather, its reciprocal, fluorescent lifetime is measured. In the early stages of this work materials were sought which had high energy storage capabilities and long fluorescent lifetimes, i.e., low transition probabilities for high energy Q-switched applications.

The procedure for measuring fluorescent lifetime is shown schematically in Figure 3.

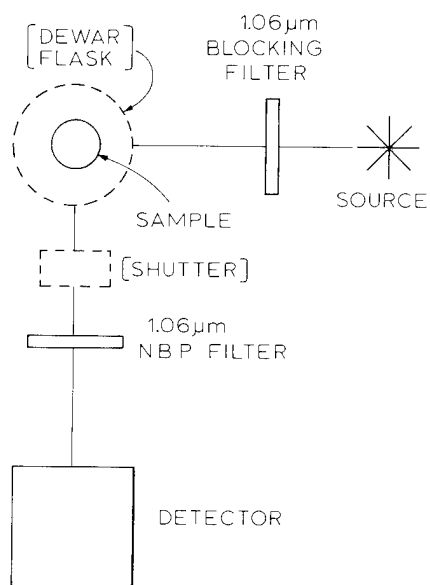


Figure 3. Schematic diagram of the apparatus used in fluorescent decay studies

The excitation source consists of a xenon flashlamp with a power supply and electronic circuitry to provide a pump pulse of about 10 microseconds pulse width at half peak intensity. The sample is excited by radiation from this source after it has passed through a filter which transmits the excitation wavelengths, but absorbs strongly at the fluorescent emission wavelength of

the sample, 1.06  $\mu\text{m}$ . Fluorescent emission from the sample is observed with a photomultiplier tube with an S-1 surface. Direct illumination of the photomultiplier tube by the excitation source is prevented by observing the fluorescent emission at right angles to the direction of irradiation from the flashlamp, and by using a filter on the detector with transmission characteristics complementary to those of the above filter, i.e., which transmits the 1.06  $\mu\text{m}$  wavelength and absorbs at all other wavelengths. A curve of fluorescent intensity as a function of time is displayed on an oscilloscope where it is recorded photographically.

If the fluorescent decay process was a truly exponential one, it would be possible to determine fluorescent lifetime by measuring the fluorescent intensity at any two points in time on the curve,  $(I_1, t_1)$  and  $(I_2, t_2)$ , and calculating the fluorescent lifetime ( $\tau$ ) from equation 1:

$$\tau = \frac{t_2 - t_1}{\ln(I_1/I_2)} \quad . \quad (1)$$

Since the fluorescent decay is not a true exponential, as will be discussed later, all fluorescent intensity measurements are made at arbitrary time intervals of 0.3 milliseconds and 0.6 milliseconds after the flashlamp is fired in order that valid comparisons of fluorescent lifetime for different glass compositions can be made. Fluorescent lifetime values made in this manner are reproducible to about  $\pm 3$  percent.

### 2.2.1 Effect of Host Composition on Fluorescent Lifetime

One of the first relationships to be investigated was the effect of host glass composition on fluorescent lifetime. The initial work was carried out on crown and flint type glasses in which the species of ingredients which serve as glass network modifiers or their concentrations were varied. Typical composition investigations and their results are given in Table II.

The results in Table II suggest that the crown type glasses have higher fluorescent lifetime values than the flint type glasses. It would also suggest that the network modifier ions of larger ionic radius yield higher fluorescent lifetimes. This is not an unreasonable conclusion based on the following arguments. The transition between the  $^4F_{3/2}$  and  $^4I_{9/2}$  levels of the  $\text{Nd}^{3+}$ -ion is a forbidden transition in the free state. This transition occurs for neodymium ions in a glass host only because of the

TABLE II. Composition vs. Fluorescent Lifetime

Test Variable	Composition (wt%)							Life-time (ms)			
<u>R<sub>2</sub>O vs. RO</u>											
	<u>SiO<sub>2</sub></u>	<u>Na<sub>2</sub>O</u>	<u>K<sub>2</sub>O</u>	<u>CaO</u>	<u>BaO</u>	<u>Sb<sub>2</sub>O<sub>3</sub></u>	<u>Nd<sub>2</sub>O<sub>3</sub></u>				
	68.0	15.5	-	-	13.0	1	2.5	0.43			
	68.0	15.5	-	13.0	-	1	2.5	0.32			
	68.0	-	15.5	-	13.0	1	2.5	0.64			
	68.0	-	15.5	13.0	-	1	2.5	0.39			
<u>R<sub>2</sub>O</u>											
	<u>SiO<sub>2</sub></u>	<u>K<sub>2</sub>O</u>	<u>Rb<sub>2</sub>O</u>	<u>Cs<sub>2</sub>O</u>	<u>BaO</u>	<u>Sb<sub>2</sub>O<sub>3</sub></u>	<u>Nd<sub>2</sub>O<sub>3</sub></u>				
	71.5	20	-	-	5	1	2.5	0.60			
	71.5	10	10	-	5	1	2.5	0.65			
	71.5	10	-	10	5	1	2.5	0.73			
<u>K<sub>2</sub>O vs. Rb<sub>2</sub>O</u>											
	<u>SiO<sub>2</sub></u>	<u>K<sub>2</sub>O</u>	<u>Rb<sub>2</sub>O</u>	<u>BaO</u>	<u>Sb<sub>2</sub>O<sub>3</sub></u>	<u>Nd<sub>2</sub>O<sub>3</sub></u>					
	69.1	21.7	-	3.3	1.2	4.7	0.59				
	66.2	15.6	10.3	3.1	1.2	3.6	0.63				
	62.9	9.9	19.6	3.0	1.1	3.5	0.65				
	60.0	4.7	28.1	2.8	1.1	3.3	0.68				
	57.4	-	35.8	2.7	1.0	3.2	0.66				
<u>K<sub>2</sub>O vs. BaO</u>											
	<u>SiO<sub>2</sub></u>	<u>K<sub>2</sub>O</u>	<u>BaO</u>	<u>Sb<sub>2</sub>O<sub>3</sub></u>	<u>Nd<sub>2</sub>O<sub>3</sub></u>						
	66.5	5	25	1	2.5	(did not make glass)					
	66.5	10	20	1	2.5	0.52					
	66.5	15	15	1	2.5	0.59					
	66.5	20	10	1	2.5	0.71					
	66.5	25	5	1	2.5	0.70					
	66.5	30	0	1	2.5	0.70					
	71.5	5	20	1	2.5	(did not make glass)					
	71.5	10	15	1	2.5	0.56					
	71.5	15	10	1	2.5	0.73					
	71.5	20	5	1	2.5	0.73					
<u>RO in flint glass</u>											
	<u>SiO<sub>2</sub></u>	<u>ZnO</u>	<u>MgO</u>	<u>SrO</u>	<u>CdO</u>	<u>BaO</u>	<u>PbO</u>	<u>Al<sub>2</sub>O<sub>3</sub></u>	<u>Sb<sub>2</sub>O<sub>3</sub></u>	<u>Nd<sub>2</sub>O<sub>3</sub></u>	
	43	-	-	-	-	-	52.5	2.0	0.5	2.0	0.22
	42	1	-	-	-	-	"	"	"	"	0.20
	41	2	-	-	-	-	"	"	"	"	0.16
	39	4	-	-	-	-	"	"	"	"	0.18
	37	6	-	-	-	-	"	"	"	"	0.16
	41	-	2	-	-	-	"	"	"	"	0.19
	41	-	-	2	-	-	"	"	"	"	0.21
	41	-	-	-	2	-	"	"	"	"	0.20
	41	-	-	-	-	2	"	"	"	"	0.20

perturbation of the energy levels of the  $\text{Nd}^{3+}$ -ions by the host material. One would expect the network modifier ions of larger ionic radius to cause less perturbation of the energy levels of the neodymium ions and thus produce lower transition probabilities and higher fluorescent lifetimes.

These initial studies led to two separate approaches in the investigation of fluorescent lifetime as a function of host glass composition. In the first, a general survey of fluorescent lifetime data was made in search of correlations between lifetime values and the commonly used glass ingredients. The second was a more detailed study of the effect of the concentration of an individual glass component on fluorescent lifetime since the broad survey above was based on the unverified assumption that a linear relationship existed between concentration and fluorescent lifetime for a given glass ingredient.

For the general investigation of the correlation between fluorescent lifetime and composition, 300 existing glass compositions containing 16 of the more commonly used glass ingredients were subjected to a regression analysis with the aid of a small IBM 1620 computer. The best agreement between calculated and experimental values of fluorescent lifetime was obtained when the following relationship was used;

$$\tau = 0.461 + A_{\text{SiO}_2} C_{\text{SiO}_2} + \sum_n \frac{A_n C_n}{C_{\text{SiO}_2}} \quad (2)$$

where  $\tau$  is the lifetime in milliseconds,  $C_n$  is the concentration of a given oxide (n) in weight percent and  $A_n$  is the correlation coefficient which establishes the relationship between composition and lifetime. The oxides included in the study, their coefficients ( $A_n$ ) and computer calculated standard deviations of these coefficients ( $\sigma_n$ ) are given in Table III. The coefficients for  $\text{K}_2\text{O}$ ,  $\text{ZrO}_2$  and  $\text{Sb}_2\text{O}_3$  have small absolute values which are less than the standard deviation and therefore they were considered to be zero in this analysis.

Using the above expression for  $\tau$  and the  $A_n$  values of Table III, calculated values of  $\tau$  were computed for the 300 compositions used in the analysis. The standard (rms) deviation between experimental and calculated values of  $\tau$  was  $\pm 0.08$  ms. A small amount of this error may be attributed to the experimental data itself which is reproducible to about  $\pm 0.01$  ms. The main cause of this deviation, however, is due to the limited accuracy

of the correlation coefficients. The standard deviations of these coefficients have values that are 10 to 30% of the value of the coefficients themselves.

TABLE III. Correlation Coefficient for  
Composition vs Fluorescent Lifetime

Periodic Group	n (oxide)	$A_n$ (correlation coefficient)	$\sigma_n$ (standard deviation)	ionic radii $\text{\AA}$
I A	Li <sub>2</sub> O	- 1.288	0.291	0.78
	Na <sub>2</sub> O	- 0.619	0.074	0.98
	K <sub>2</sub> O	~ 0		1.33
	Rb <sub>2</sub> O	0.167	0.036	1.49
	Cs <sub>2</sub>	0.138	0.040	1.65
II A	CaO	- 1.025	0.109	1.06
	BaO	- 0.259	0.046	1.43
II B	MgO	- 1.054	0.215	0.78
	ZnO	- 1.555	0.100	0.83
III A	Nd <sub>2</sub> O <sub>3</sub>	- 1.567	0.422	1.15
III B	B <sub>2</sub> O <sub>3</sub>	- 0.980	0.308	0.2
	Al <sub>2</sub> O <sub>3</sub>	- 1.223	0.378	0.57
IV A	TiO <sub>2</sub>	- 0.452	0.158	0.64
	ZrO <sub>2</sub>	~ 0		0.87
IV B	SiO <sub>2</sub>	0.592	0.136	0.39
	PbO	- 0.115	0.032	1.32
V B	Sb <sub>2</sub> O <sub>3</sub>	~ 0		0.62

Despite the fact that these coefficients leave something to be desired in the way of accuracy, the data in Table III show a definite trend in the correlation between composition and lifetime: namely, the correlation coefficient becomes more positive (lifetime increases) as the atomic number increases (more specifically as this ionic radius increases) in any given periodic group, i.e., Li to Cs.

Notable exceptions are the cases of  $\text{SiO}_2$  and  $\text{B}_2\text{O}_3$  which are more positive than the trend would predict. This may be due in part to the fact that these are network forming elements and as such may have less interaction with the  $\text{Nd}^{3+}$ -ions than do the network modifying ions.

The results of a study of the relationship between fluorescent lifetime and the concentration of specific glass ingredients are shown graphically in Figure 4. Each curve represents a series of glasses in which the oxide being studied was substituted for silica only and the concentration of the other ingredients was kept constant.

The curves for the heavier oxides in Group IA, which are of most interest because they have some areas of positive slope, i.e., positive regression coefficients, are unfortunately the least linear. At higher concentrations, they either level off or go through a maximum. These data suggest that the optimum concentration of these oxides would be about 10, 12 or greater, and 15 Mol % for  $\text{Cs}_2\text{O}$ ,  $\text{Rb}_2\text{O}$ , and  $\text{K}_2\text{O}$  respectively. These values may change as a function of the host glass composition. In general, the glass compositions used for the analysis in Table III contained concentrations in the lower range where the relationship with fluorescent lifetime is more nearly linear.

#### 2.2.2 Effect of $\text{Nd}_2\text{O}_3$ Concentration on Fluorescent Lifetime

In association with the study of fluorescent lifetime as a function of host glass composition, the fluorescent lifetime was investigated as a function of  $\text{Nd}_2\text{O}_3$  concentration. For most of the glass types examined, as the neodymium concentration was gradually increased, the fluorescent lifetime remained relatively constant for low concentrations of  $\text{Nd}_2\text{O}_3$  and then decreased with increasing  $\text{Nd}_2\text{O}_3$  concentration, as shown in Figure 5. The point at which this "concentration quenching" is first observed varies with the host glass composition.

In the crown type glasses, changing the alkali component from low atomic number to high atomic number not only increased

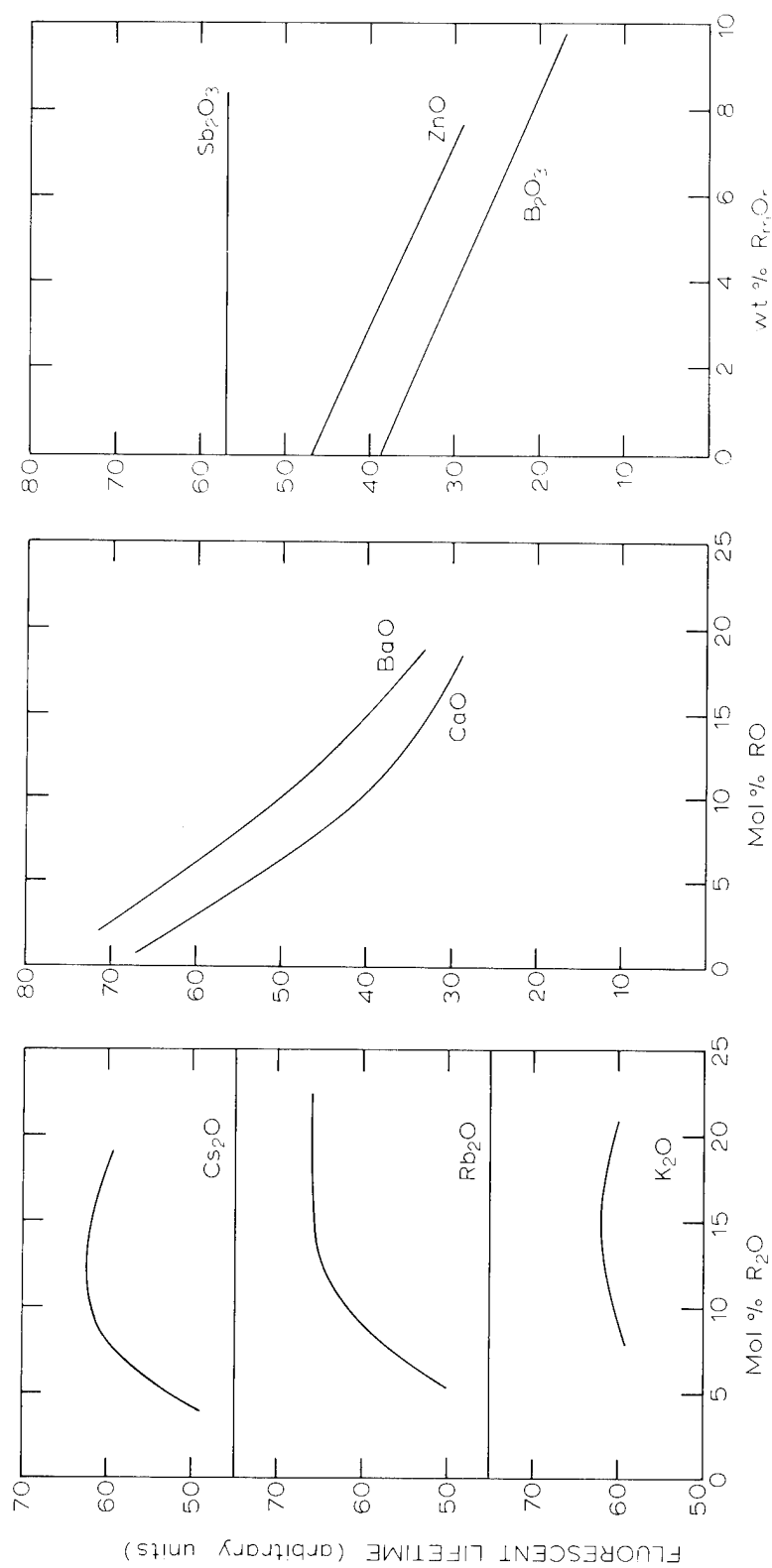


Figure 4. Lifetime vs concentration curves for several oxides.  
All substitutions are at the expense of silica.

the fluorescent lifetime as indicated in Section 2.2.1, but also increased the amount of  $\text{Nd}_2\text{O}_3$  which may be incorporated in the glass before concentration quenching is observed. As indicated in Figure 5, quenching takes place in the 5 to 7 wt%  $\text{Nd}_2\text{O}_3$  region for a K, Rb-crown glass, but in the 2 to 3 wt% region in an Na, K-crown glass. The ability of the host material to accept increased amounts of  $\text{Nd}_2\text{O}_3$  without showing effects of concentration quenching can be as important as the lifetime value itself in some applications. For example, both fluorescent lifetime and neodymium ion concentration should be considered for the energy storage capabilities of a material or for a material in which minimum laser threshold energy is desired.

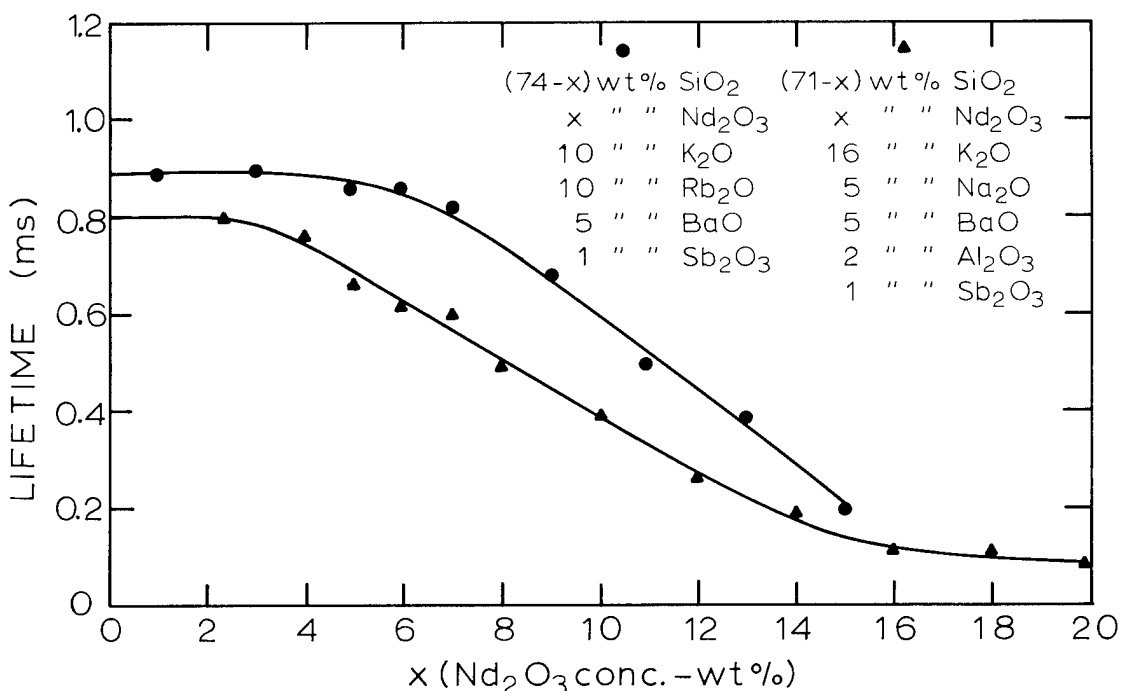


Figure 5. Effect of host composition on concentration quenching

### 2.2.3 Fluorescent Decay as a Function of Time

As previously stated, the fluorescent decay curves are not simple exponentials. Further analysis of these curves was made in an effort to gain some insight regarding the nature of the neodymium ion site in the host material, i.e. does the site vary with composition or does the interaction between like sites vary. The first step was an attempt to resolve the observed decay curves into two or more pure exponential curves, which might represent fluorescent emission from neodymium ions having sites with two or more different decay transition probabilities. Typical curves of fluorescent intensity as a function of time following a 10  $\mu$ s excitation pulse are shown in Figure 7 for a silicate glass base with varying amounts of neodymium concentration.

In order for a decay process such as fluorescent emission to give rise to a "composite" decay curve composed of two or more true exponential processes, two or more types of  $\text{Nd}^{3+}$ -ion sites must exist which are completely independent of each other. Figure 6 shows two types of interaction which may take place between  $\text{Nd}^{3+}$ -ion sites if proper conditions exist.

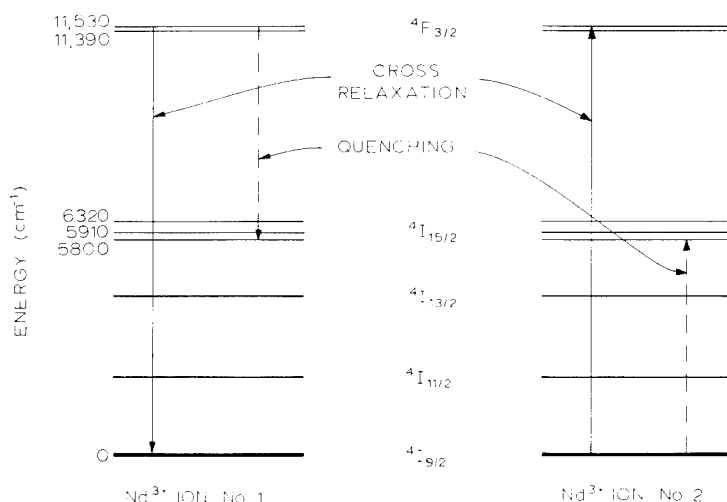


Figure 6. Interactions between energy levels of adjacent  $\text{Nd}^{3+}$  ions. Cross relaxation process (—). Quenching by non-radiative resonant energy exchange process (----)

The solid lines represent cross-relaxation processes which regulate the degree to which hole burning occurs. Hole burning data indicate that the cross-relaxation process is quite rapid and highly efficient. With this degree of interaction between neodymium sites, one would not expect to be able to detect site variations, for example, due to the presence of  $K^+$ -ions vs  $Rb^+$ -ions, in the host material by this type of analysis of the fluorescent decay curve.

The dotted lines in Figure 6 represent the concentration quenching process as proposed by Peterson and Bridenbaugh.<sup>2</sup> It was assumed that the concentration quenching process would lead to a time-dependent curve of fluorescent intensity due to the fact that the neodymium ions are randomly distributed within the glass. The relatively isolated ions would emit as if no concentration quenching occurred, but closely spaced ions, between which resonant energy transfer is probable, would show a shortened lifetime.

The decay curve analysis was carried out as shown in Figure 7 for a series of potassium-barium-silicate based glasses containing 0.5, 2.5, 5, and 7.5 wt %  $Nd_2O_3$ . The solid curves on the left of Figure 7 are plots of the experimental data. The straight portion at the end of the curve is attributed to emission from the long lifetime component only, since it is assumed that the short lifetime sites have been emptied by this time. The slope of this straight portion provides a value of  $\tau_1$  for the long lifetime sites. The dotted curves are an extrapolation of this straight portion back to  $t_0$  and represents the fluorescent light intensity due to long lifetime sites, assuming a true exponential process. The intensity difference between the experimental curve and this extrapolated curve represents the light intensity emitted from the short lifetime sites. These intensity values are replotted on the right-hand side of Figure 7 as a function of time. The lifetime values,  $\tau_2$ , and the initial intensity,  $I_{20}$ , of the short lifetime sites are obtained from the slope and intercept of the ordinate axis, respectively, of these generated curves. These results are summarized in Table IV.

We assume that the longer lifetimes,  $\tau_1$ , are associated with isolated neodymium sites and observe that the fluorescent lifetime of these sites decreases with increased  $Nd_2O_3$  concentration.

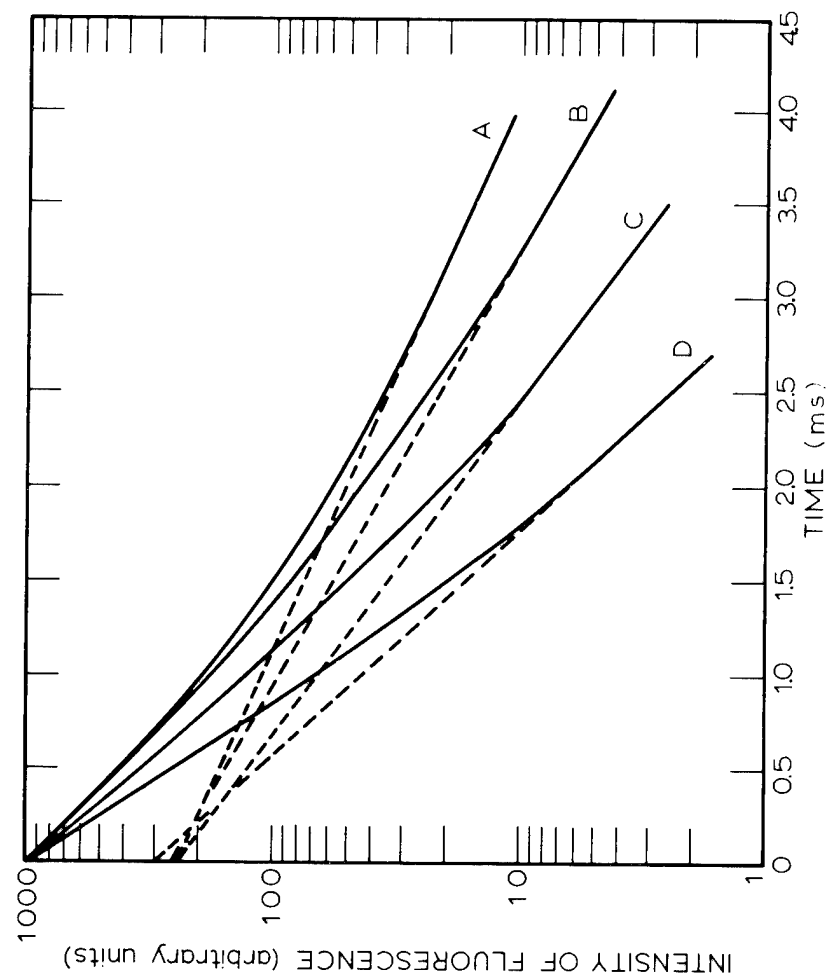
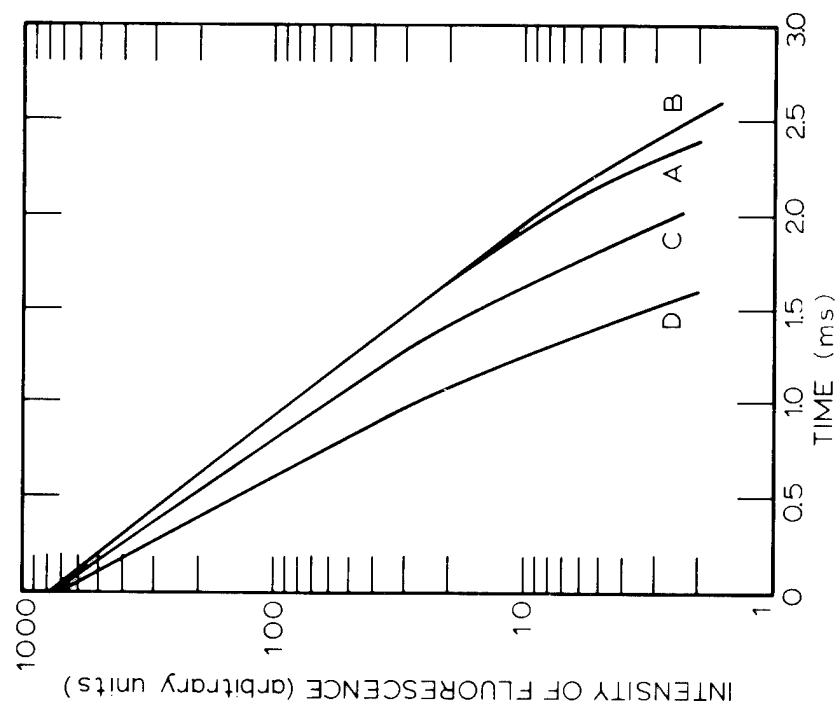


Figure 7. Nd<sup>3+</sup> fluorescence vs time.

TABLE IV. Time Dependence of Lifetime vs  $\text{Nd}_2\text{O}_3$  Concentration

Curve	$\text{Nd}_2\text{O}_3$ (wt %)	$\tau_1$	$\tau_2$	$\tau_1/\tau_2$	$I_{10}/I_{20}$
A	0.5	1.37	0.48	2.85	0.293
B	2.5	1.09	0.48	2.27	0.325
C	5.0	0.83	0.43	1.93	0.329
D	7.5	0.57	0.33	1.73	0.43

If these sites were truly isolated, one would not expect the observed decrease in fluorescent lifetime with increased  $\text{Nd}_2\text{O}_3$  concentration. This would suggest that these sites are not truly isolated (at least for concentrations greater than 0.5 wt %  $\text{Nd}_2\text{O}_3$ ) and that the probability of a concentration quenching event rather than the probability of a radiative transition event is the rate controlling step in the depletion of excited ions in these isolated sites. This is further suggested by the fact that the ratio of  $\tau_1/\tau_2$  moves toward unity as the  $\text{Nd}_2\text{O}_3$  concentration is increased. Values of fluorescent lifetime for coupled sites,  $\tau_2$ , also decrease with an increase in  $\text{Nd}_2\text{O}_3$  concentration, but to a lesser extent.

The ratio of fluorescent intensities from the two different sites,  $I_{10}/I_{20}$ , indicates that there are fewer isolated sites than coupled sites at low  $\text{Nd}_2\text{O}_3$  concentrations, and that the relative number of isolated sites increases with  $\text{Nd}_2\text{O}_3$  concentration. This appears to be contrary to what one would expect, but may be due to the fact that the number of radiative transitions from the coupled sites actually decreases relative to radiation from isolated sites, due to the increased number of nonradiative transitions occurring from the coupled sites. One might expect this to be comparable to the lifetime shortening of the coupled sites,  $\tau_2$ , and the data in Table III appear to support this.

It should be emphasized that the accuracy of these values is dependent on one's ability to define the straight portion of the curve and extrapolate back to time zero ( $t_0$ ). This is complicated by the fact that the light intensities at this end of the scale are very low, making it difficult to accurately determine the shape of the curve in this region.

This type of analysis was also carried out on three glasses in which the neodymium concentration was held constant and the glass composition was varied to replace part of the  $K_2O$  by  $Rb_2O$  and  $Cs_2O$ . Results on these three glasses, given in Table V, indicate that there is no correlation between the different lifetimes ( $\tau_1$  and  $\tau_2$ ) and the species of alkali substituted for the  $K_2O$ , e.g., the individual  $\tau$  values are not associated with a specific component such as  $K_2O$ ,  $Rb_2O$ , or  $Cs_2O$  such that the composite curve becomes a function of glass composition. On the contrary, both  $\tau_1$  and  $\tau_2$  tend to increase proportionately as  $Rb_2O$  and  $Cs_2O$  are added to the composition, in general agreement with the above suggestion that the  $\tau_1$  and  $\tau_2$  result from coupled vs isolated sites in the glass.

TABLE V. Time Dependence of Lifetime vs Glass Composition

Composition (Mol %)							$\tau_1$	$\tau_2$	$\tau_1/\tau_2$
$SiO_2$	$K_2O$	$Rb_2O$	$Cs_2O$	$BaO$	$Sb_2O_3$	$Nd_2O_3$			
74.4	12.3	-	-	12.4	0.3	0.6	0.57	0.20	2.85
83.6	11.3	2.0	-	2.3	0.2	0.6	0.89	0.37	2.41
86.5	7.7	-	2.5	2.4	0.3	0.6	0.97	0.42	2.31

The apparatus used in the latter studies is shown in Figure 3, but with the shutter added between the sample and the detector. At the longer time values, the light intensity becomes quite low and rather high gain on the detector is required. As previously described, the decay curve is made up of a series of exposures. In this case, the shutter passes fluorescent light only during the time interval being displayed on the oscilloscope, so that the detector is not saturated at the higher gain settings by the initial portions of the fluorescent curve which may have intensities 100 to 1000 times greater than the recorded portion.

#### 2.2.4 Effect of Temperature on Fluorescent Lifetime

The effects of temperature on fluorescent lifetime have been investigated as a function of neodymium concentration for several different types of host glass.<sup>3</sup> Lifetime measurements were made at 300K and 77K for flint glasses containing 0.25 to 4.5 wt% neodymium, crown glasses containing 0.5 to 9 wt%  $\text{Nd}_2\text{O}_3$ , and barium crown glasses containing 0.5 to 12.0 wt%  $\text{Nd}_2\text{O}_3$ . The curves in Figure 8 for the flint glass series are typical of the results obtained, namely, in regions where concentration quenching exists, the fluorescent lifetime is higher at the lower temperature, while in regions where the  $\text{Nd}_2\text{O}_3$  concentration is below the quenching level, fluorescent lifetime is lower at the lower temperature.

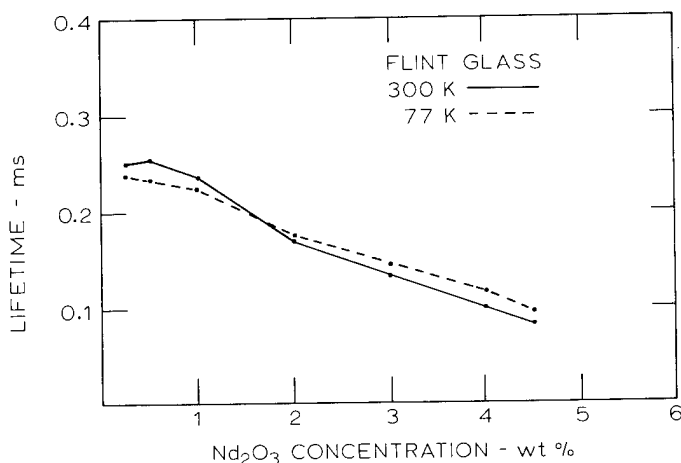


Figure 8. Fluorescent lifetime vs  $\text{Nd}_2\text{O}_3$  concentration as measured at 300K and 77 K

At the lower concentration end of the series, the lifetime behavior may be explained in the following manner. The  $^4\text{F}_{3/2}$  level of the  $\text{Nd}^{3+}$ -ion consists of a doublet as shown in Figure 6. Absorption spectra indicate that the transition probability to and from the lower level of this doublet is much greater than the upper level. At the lower temperature, the population in the upper level is decreased, thus, the average transition probability from these two levels is greater and the fluorescent lifetime is shortened.

At the higher  $\text{Nd}_2\text{O}_3$  concentration end of the series, we are well within the region where concentration quenching occurs. In the concentration mechanism proposed by Peterson and Brindenbaugh<sup>2</sup> the energy of an electron in the excited  $^4\text{F}_{3/2}$  level of a given  $\text{Nd}^{3+}$ -ion is divided to provide two adjacent ions with electrons excited to the  $^4\text{I}_{15/2}$  level from which nonradiative decay occurs as shown schematically in Figure 6. This requires that the energy gap between the  $^4\text{F}_{3/2}$  and the  $^4\text{I}_{15/2}$  levels must nearly match that of the energy gap between the  $^4\text{I}_{15/2}$  and the  $^4\text{I}_{9/2}$  energy levels of the neodymium ions.

As may be seen in Figure 6, this is most nearly achieved for transitions from the upper level of the  $^4\text{F}_{3/2}$  band to the lower level of the  $^4\text{I}_{15/2}$  band. The energy level diagram in Figure 6 was obtained on a barium-rubidium silicate glass by Robinson.<sup>4</sup> Decreasing temperature from 300K to 77K would significantly depopulate the upper  $^4\text{F}_{3/2}$  level thus "detuning" the resonance exchange and decreasing the probability of concentration taking place. This decrease in the degree of concentration quenching as temperature is decreased will result in an increase in the fluorescent lifetime.

To check the hypothesis evoked in the case of low  $\text{Nd}_2\text{O}_3$  concentration, a theoretical calculation was made of the ratio of the total emission transition probability from the  $^4\text{F}_{3/2}$  doublet at 300K vs 77K. The calculation of this ratio was based on the relative areas under the absorption curves of the two levels in this doublet and their separation. In Table VI the measured lifetimes at 300K and 77K for the three types of glass are tabulated with the calculated values of lifetime at 77K. The calculated value was arrived at by multiplying the measured value at 300K by the calculated ratio of transition probabilities. The accuracy of these measured lifetime values is about  $\pm 0.010$  ms, thus the magnitude of the effect in some cases is about the same as the limit of error. The shift, however, appears to be consistently in the proper direction according to the calculated values of lifetime at 77K.

TABLE VI. Effect of Temperature on  
Fluorescent Lifetime

Glass Type	Nd <sub>2</sub> O <sub>3</sub> Core (wt%)	Lifetime (ms)		Calc. 77K
		Meas. 300K	Meas. 77K	
Crown	0.5	0.37	0.36	0.34
	1.0	0.38	0.34	0.33
	2.0	0.35	0.34	0.32
Flint	0.25	0.25	0.24	0.23
	0.5	0.25	0.23	0.24
	1.0	0.24	0.22	0.22
Barium Crown	1.0	0.43	0.41	0.39
	2.0	0.43	0.40	0.38
	4.0	0.36	0.33	0.32

### 2.3 SOLARIZATION

The xenon flashlamps used as laser cavity pump sources have emission spectra which are rich in the blue and ultraviolet end of the spectrum. This ultraviolet light tends to create color centers in the laser rod which absorb in the blue and visible regions of the spectrum. These solarization effects are of interest because (1) the absorption may extend into the IR region and increase cavity losses at 1.06  $\mu\text{m}$ , (2) the absorption in the visible region tends to decrease the efficiency of the pump source, and, (3) because absorption at wavelengths other than the pump band generate undesirable thermal gradients in the laser rod.

#### 2.3.1 Transmission Studies of Solarization

A cursory investigation was made of the effect of glass composition on solarization, plus a slightly more detailed investigation of the effect of glass ingredients which serve as

"antisolarizing" agents. The latter either introduce absorption in the glass near the blue cut-off of the visible region to screen out the undesirable ultraviolet wavelengths, or are ions which readily exist in a glassy matrix in more than one valence state to minimize the formation of color centers.

The  $\text{Nd}_2\text{O}_3$  was eliminated from the glasses used in this study so that the  $\text{Nd}^{3+}$ -ion absorption bands would not mask any changes in transmission due to solarization. The solarization samples were approximately 20 mm square with a thickness of  $2.0 \pm 0.002$  mm. The test was performed by suspending the sample inside the helix of an FT-524 xenon flashlamp where it was subjected to 10 flashes of 3200 J each at 3 minute intervals. The energy was delivered to the lamp from a 320  $\mu\text{F}$  condenser charged to 4.5 kV with an inductance of 0 to 150  $\mu\text{H}$ . This is near the upper operating limit of the flashlamp where the UV content of the emission is relatively high.

Transmission curves were obtained before and after the solarizing process using a Hardy type General Electric spectrophotometer equipped with an integrating sphere for the visible and near IR and a Cary 14 spectrophotometer for wavelengths below 400 nm with the intensity normalized at 400 nm to the GE curves. The spectra in Figures 9, 10, 11 and 12 show the effects of solarization on Na-Ca-silica glasses vs K-Ba-silica glasses, with and without the presence of  $\text{Sb}_2\text{O}_3$ . These very limited results suggest that the glasses containing lighter alkali and alkaline earth elements tend to solarize worse, both with and without the presence of  $\text{Sb}_2\text{O}_3$ . The  $\text{Sb}_2\text{O}_3$  (or  $\text{As}_2\text{O}_3$ ) is commonly added to the glass as a fining agent because they are able to exist in multiple valent states and, therefore, aid in the reabsorption of absorbed oxygen in the glass during the fining process.

It should be noted in the samples free of  $\text{Sb}_2\text{O}_3$  that the general shape of the solarization absorption consists of a broad band at approximately 400 nm, and a second band at approximately 550 nm, followed by a tail which extends out to about 1000 nm. For glasses in which the solarization has been suppressed, it is not unreasonable to expect absorption in the same general wavelength regions, thus, even though the effects of solarization have been reduced the data on these 2 mm thick samples suggest that absorption at 1.06  $\mu\text{m}$  in a meter long rod may still be a serious problem.

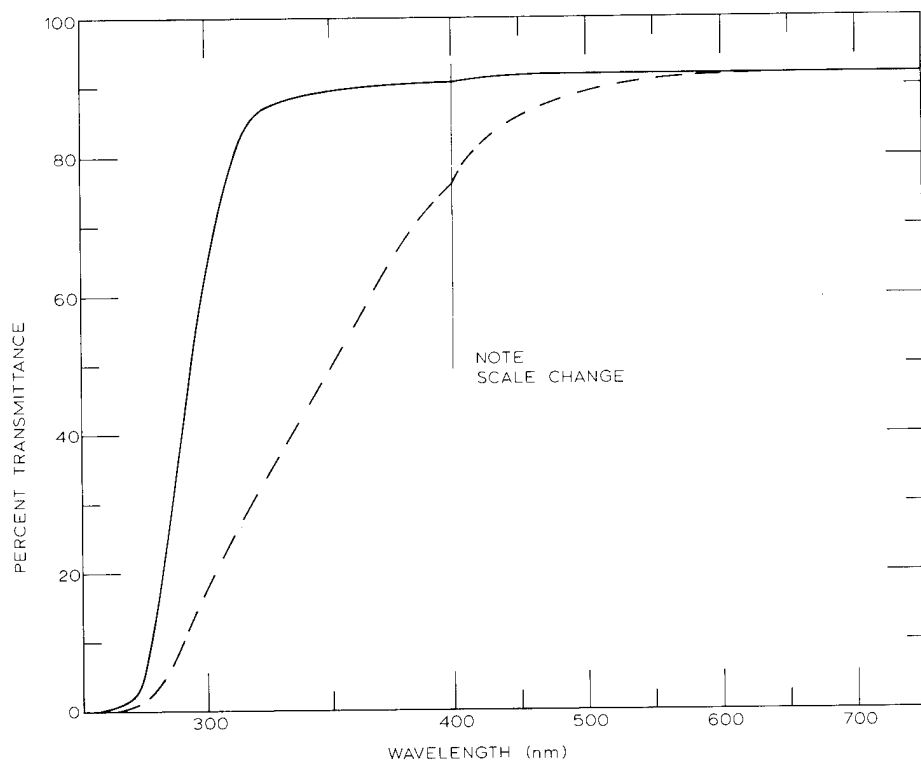


Figure 9. Spectral transmittance of Na-Ca-Silica glass containing 1 wt%  $\text{Sb}_2\text{O}_3$  before (—) and after (---) solarization

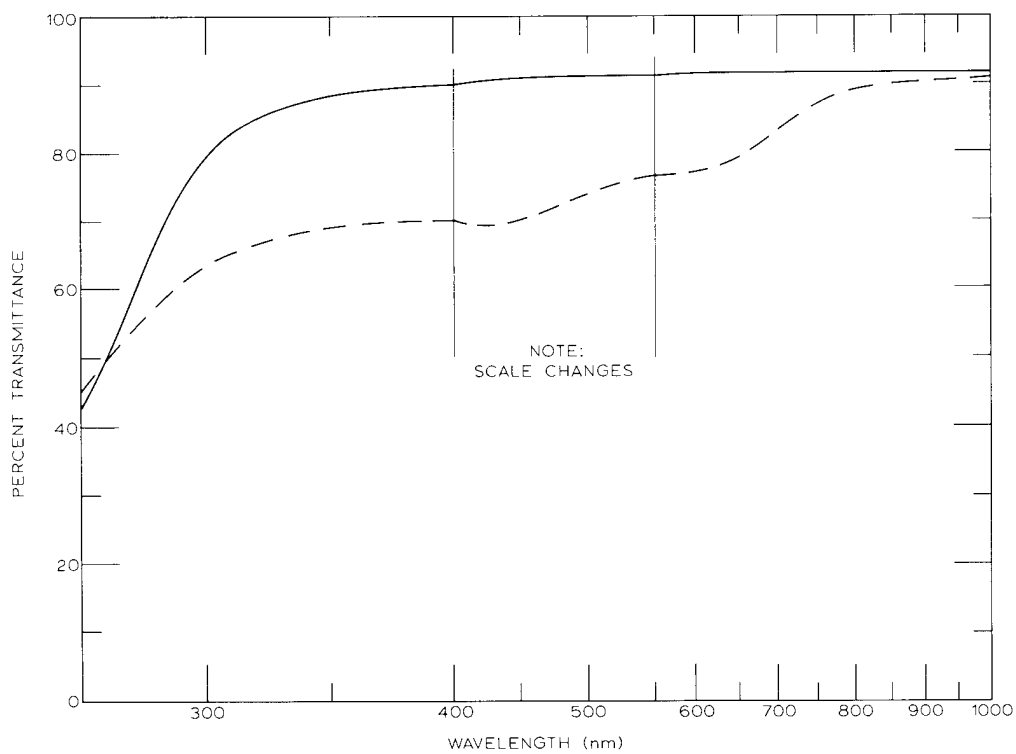


Figure 10. Spectral transmittance of Na-Ca-Silica glass free of  $\text{Sb}_2\text{O}_3$  before (—) and after (----) solarization

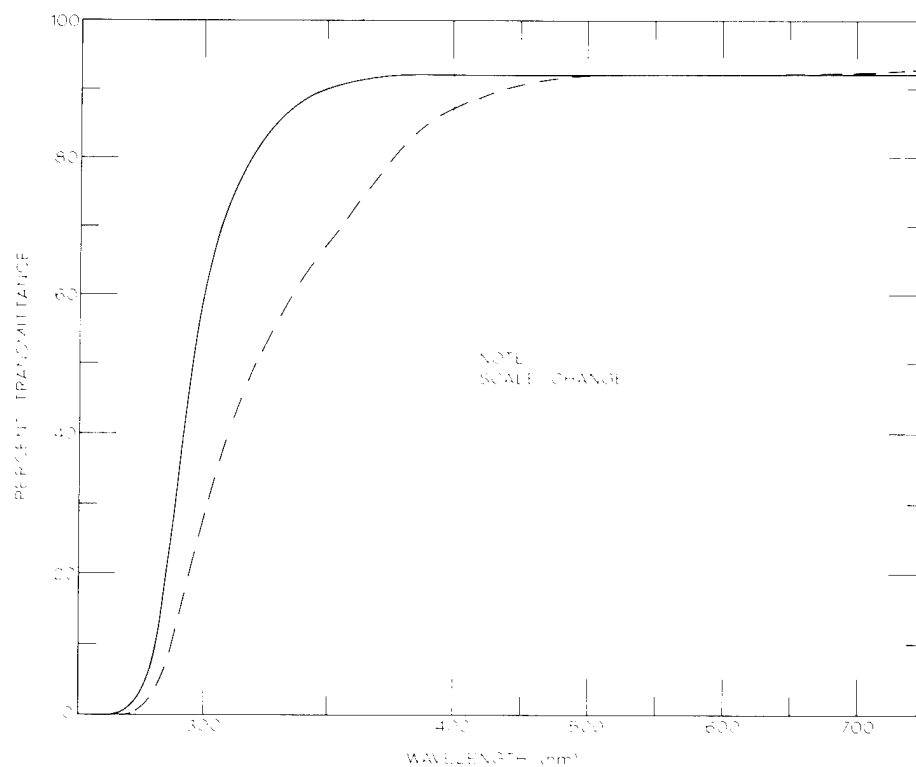


Figure 11. Spectral transmittance of K-Ba-silica glass containing 1 wt%  $\text{Sb}_2\text{O}_3$  before (—) and after (---) solarization

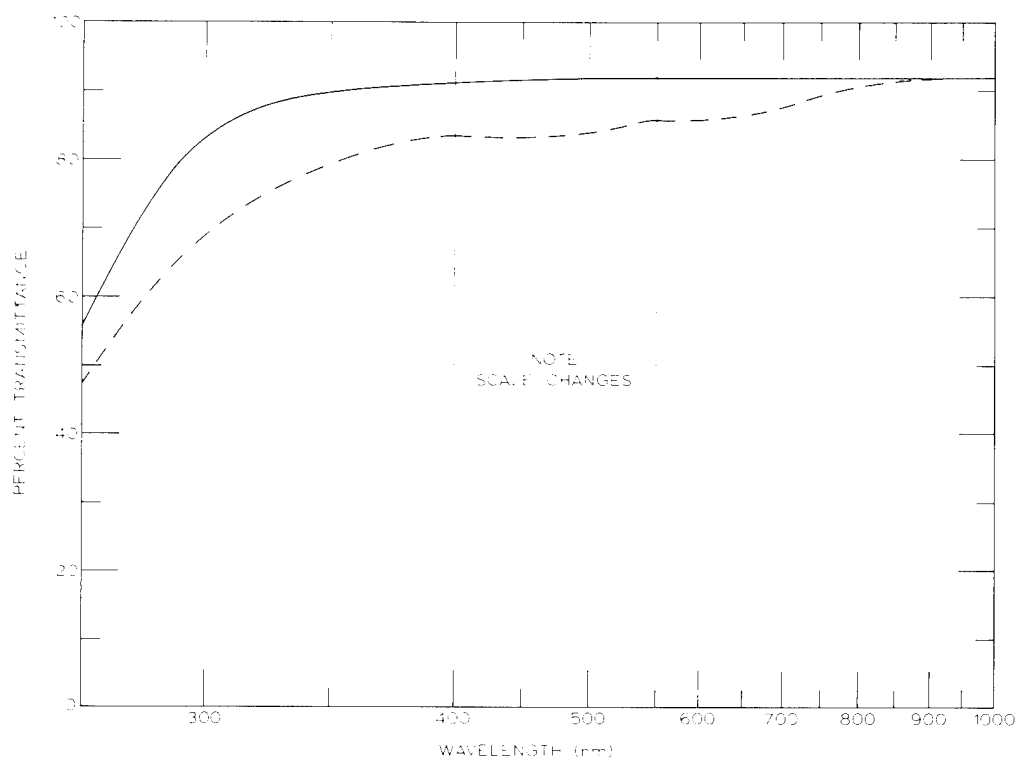


Figure 12. Spectral transmittance of K-Ba-silica glass free of  $\text{Sb}_2\text{O}_3$  before (—) and after (---) solarization

The curves in Figures 13, 14 and 15 were made using a Cary 14 spectrophotometer (normalized at 700 nm to the above GE instrument). They show the effects of the addition of potential antisolarizing agents  $\text{Sb}_2\text{O}_3$ ,  $\text{TiO}_2$  and  $\text{CeO}_2$  in varying amounts and varying combinations. The base glass in this case was a barium-crown of slightly different composition from the above K-Ba-silica glass.

Figure 13 suggests that the addition of elements which absorb in the UV but are not able to change valence easily, such as  $\text{TiO}_2$  in silica glasses, still produce solarization throughout the visible region, but at a slightly lower degree. The addition of  $\text{Sb}_2\text{O}_3$  to the glass which provides a multivalent ion, but only slight UV absorption characteristics, results in a solarized spectrum which absorbs strongly in the UV and the blue end of the region, but transmits reasonably well at 500 nm and longer wavelengths. The addition of  $\text{CeO}_2$  to the glass which provides both a multivalent ion and a good UV absorber appears to combine the advantages of both types of antisolarization agent. Increasing the concentration of  $\text{TiO}_2$  to 3 wt%, Figure 14, uniformly reduces the degree of solarization throughout the visible region. Attempts to add the UV absorption characteristic and the multivalent ion characteristic via separate agents by combining  $\text{Sb}_2\text{O}_3$  and  $\text{TiO}_2$  in the glass met with reasonable success when the  $\text{TiO}_2$  concentration was 3 wt%. This resulted in a glass which has antisolarization characteristics similar to the  $\text{CeO}_2$  glass in Figure 13, but with better transmission in the ultraviolet region. The addition of  $\text{Sb}_2\text{O}_3$  and  $\text{CeO}_2$ , Figure 15, forms a solarization couple similar to the  $\text{As}_2\text{O}_3$ - $\text{CeO}_2$  solarization couple reported in the literature.<sup>5</sup> The combination of 1 wt%  $\text{TiO}_2$  and 1 wt%  $\text{CeO}_2$  in the glass gives essentially the same result as  $\text{CeO}_2$  alone. The addition of 1 wt% each of  $\text{Sb}_2\text{O}_3$ ,  $\text{TiO}_2$  and  $\text{CeO}_2$  shows fairly good resistance to solarization in contrast to what might be expected based on reviews in the literature<sup>5</sup> in which a combination of  $\text{CeO}_2$ ,  $\text{TiO}_2$  and  $\text{As}_2\text{O}_3$  resulted in a highly sensitized solarization couple.

These results suggest that two types of antisolarization protection are possible within the glass, each with a characteristic absorption spectrum. The active agent in one case consists of a UV absorbing ingredient. Any changes in transmission resulting from solarization of these glasses are similar to those of unprotected glasses, but to a much lesser degree, depending on the amount of UV absorber present. The active agent in the second case is an element which readily exists in multiple valence states, such as the fining agents. In this case, changes in transmission resulting from solarization occur mainly in the shorter wavelength region.

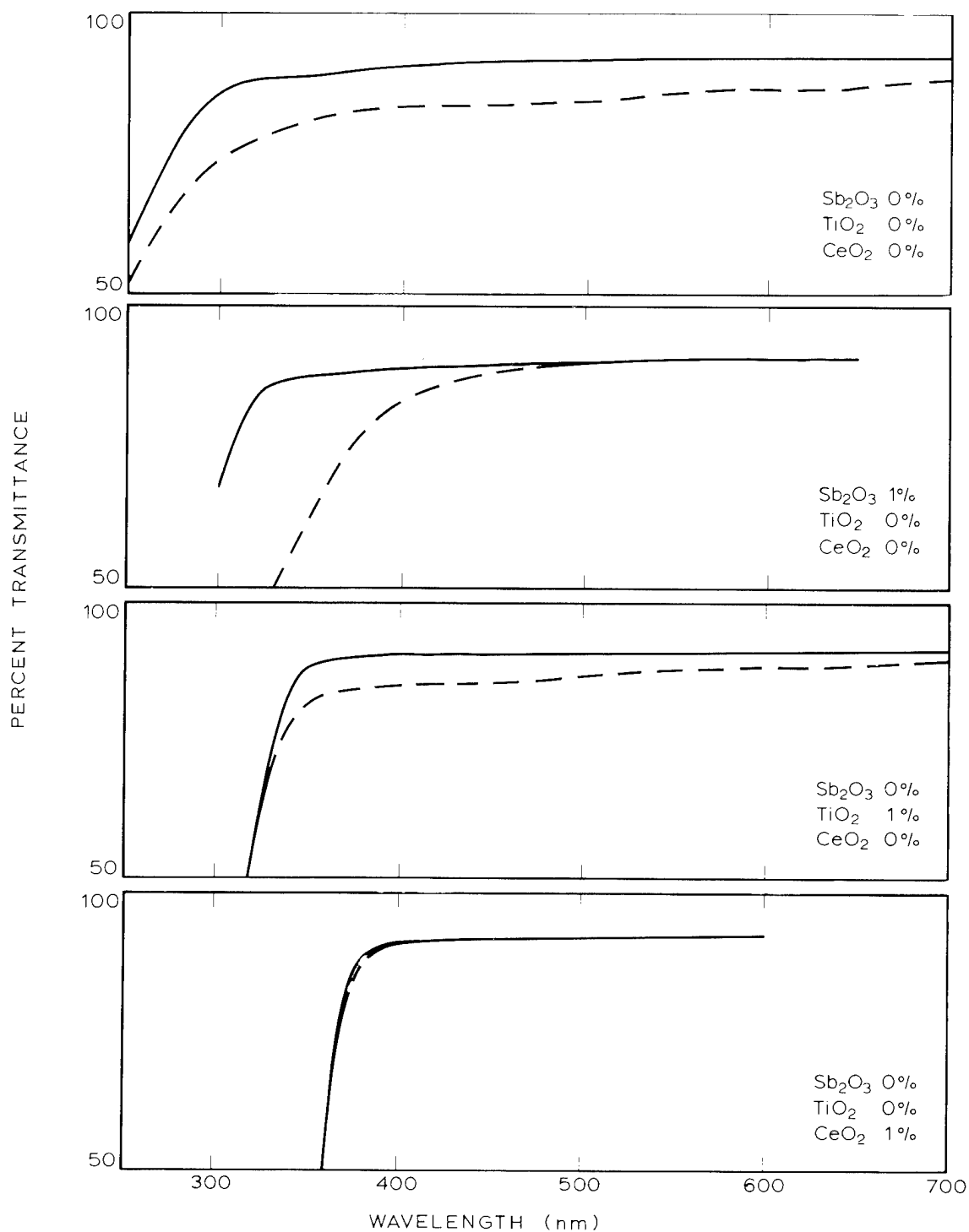


Figure 13. The effect of  $\text{Sb}_2\text{O}_3$ ,  $\text{TiO}_2$  and  $\text{CeO}_2$  on the solarization of a potassium-barium-silicate glass. Transmission before (—) and after (---) solarization of 2 mm thick samples.

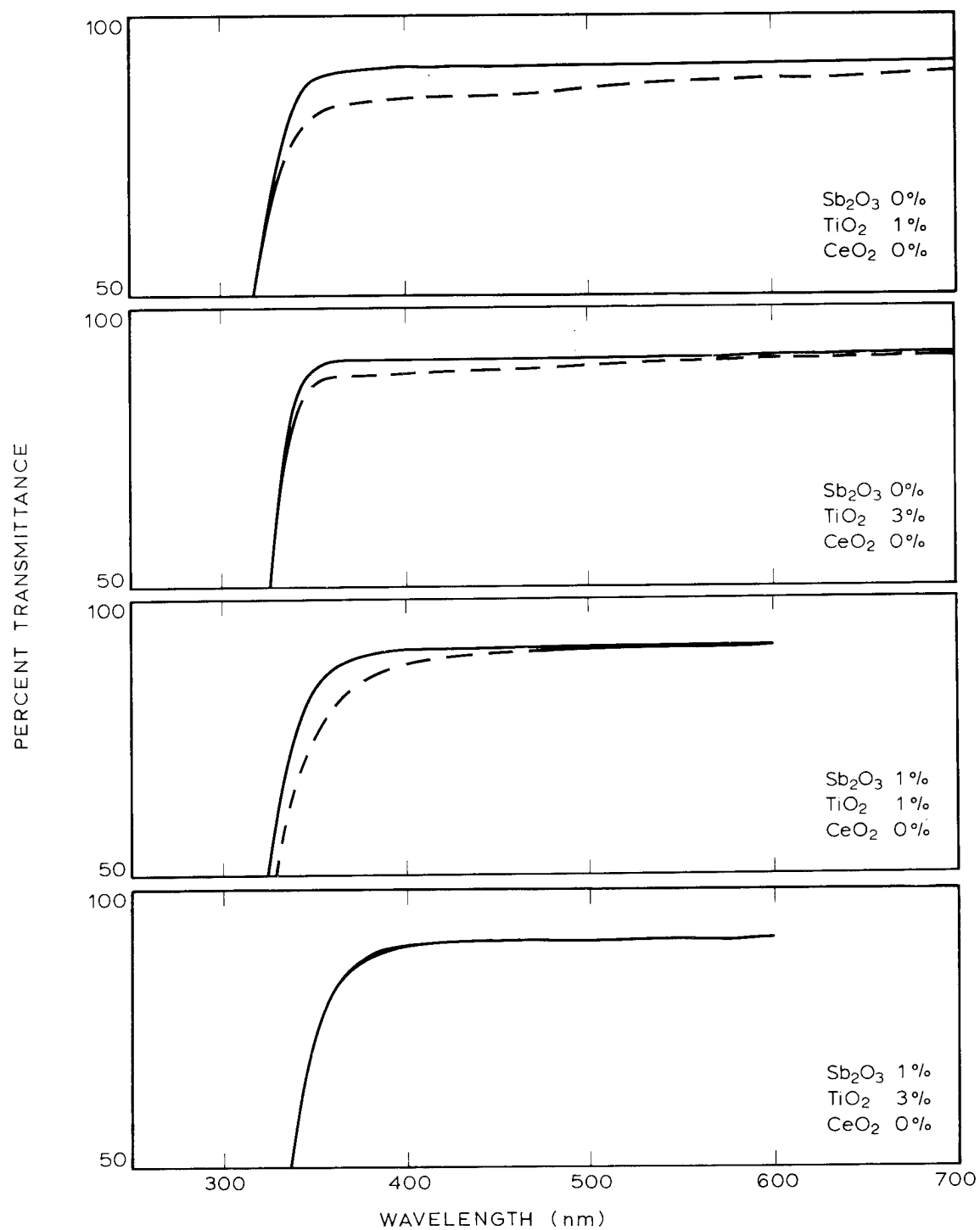


Figure 14. The effect on solarization of  $\text{Sb}_2\text{O}_3$  and  $\text{TiO}_2$  combined plus increased  $\text{TiO}_2$  transmission before (—) and after (---) solarization of 2 mm thick samples.

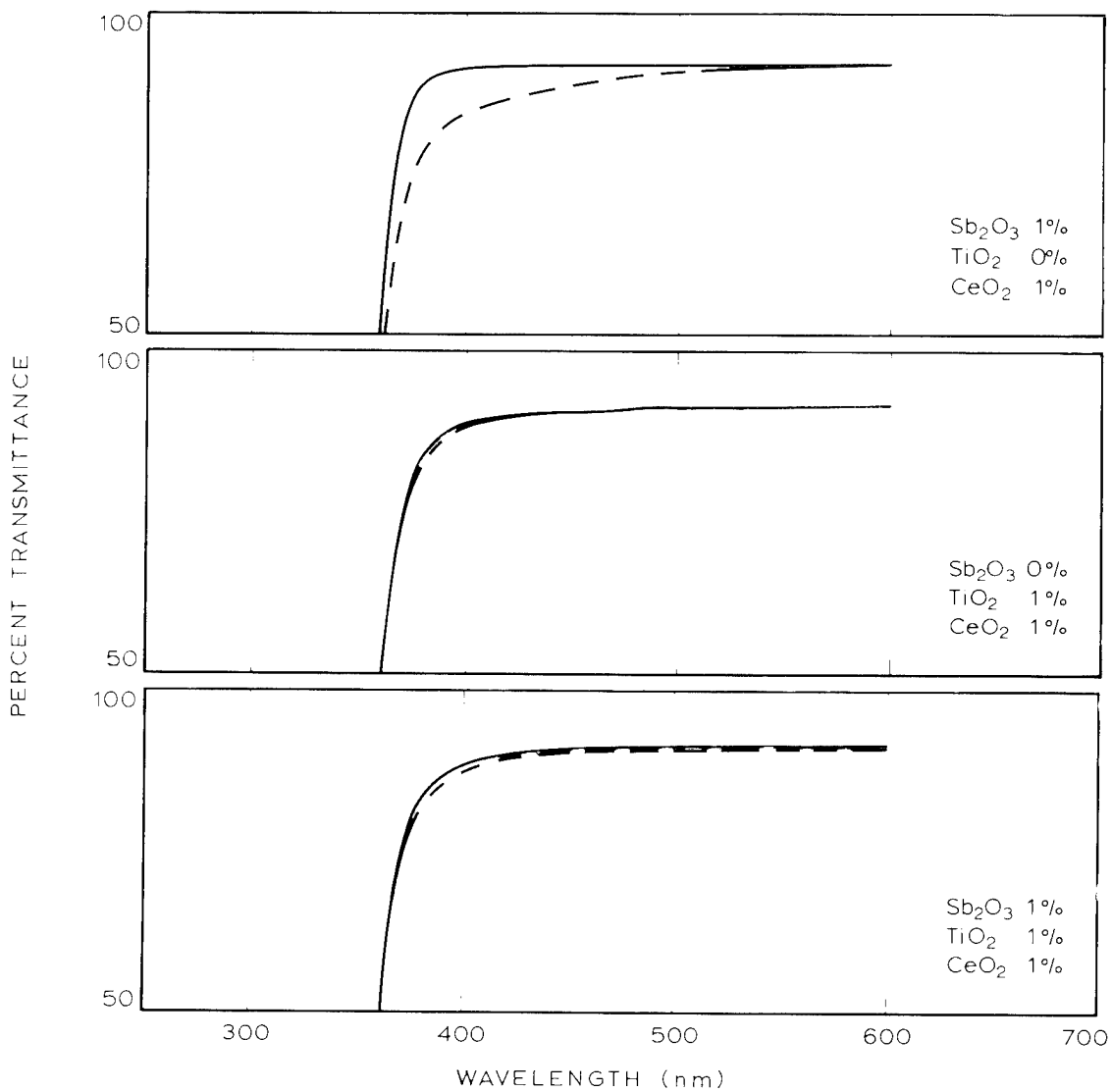


Figure 15. The effect on solarization of other combinations of  $\text{TiO}_2$ ,  $\text{Sb}_2\text{O}_3$  and  $\text{CeO}_2$ . Transmission before (—) and after (---) solarization of 2 mm thick samples.

### 2.3.2 Laser Performance vs Solarization

In addition to the study on the optical changes produced by solarization, a study was made of the effect of solarization on laser threshold and slope efficiency. The latter study is probably more pertinent than the former and should indicate to what extent solarization is a cosmetic defect and to what extent it actually degrades laser performance.

This investigation was carried out on a series of glasses containing various antisolarization agents as well as a variety of host glass compositions. The laser cavity in this study contained a laser rod 6 mm in diameter by 30 cm in length with a TIR roof on one end and an uncoated flat normal to the rod axis on the other end. These end reflectors were chosen instead of the more conventional removed dielectric mirrors in order to minimize possible variations in results which might be introduced by lack of optical homogeneity in the rods. Ten pound (4.5 kg) melts of glass were made for this study and the laser rods drawn from them were of fair optical quality but were not, in general, completely stria-free.

A single linear flashlamp with a 25.4 cm arc length was used as a pump source. This was optically coupled to the laser rod with a tight wrap of silver foil. The flashlamp was energized from a power supply with a 240  $\mu$ F storage capacitance equipped with a 600  $\mu$ H inductor. The laser cavity, with the exception of the ends of the laser rod, was totally immersed in a liquid which served as a thermal bath in all cases and in some cases as ultraviolet protection in addition. Laser output energy was measured with a Model 101 TRG thermopile with the output end of the laser rod actually placed inside the input aperture of the thermopile to insure that all the output laser light was collected.

The general procedure for evaluating the effect of solarization was as follows. First, the laser cavity was filled with a 15 percent solution of sodium nitrite to prevent solarization and data were taken to determine an unsolarized value of slope efficiency and threshold. The input energies ranged from approximately laser threshold energy to about three times this value; i.e., 300 to 1000 joules input. Readings were taken at three minute intervals so that the degree of cooling of the laser rod by the surrounding bath would be approximately the same in each case.

The sodium nitrite was then removed from the cavity, the cavity was flushed and filled with distilled water. The laser was fired 10 times at three minute intervals at an energy input

of 1075 joules. With the circuit parameters given above, this results in a current density of about 1000 amperes per square centimeter in the flashlamp. The distilled water was added to provide a thermal bath as previously stated. Since the spacing between the laser rod and the flashlamp was about one millimeter and the two were closely wrapped with silver foil it was not expected that the presence of water would provide any protection against solarization from the flashlamps.

Finally, the distilled water was removed from the cavity and replaced with sodium nitrite solution again. The slope efficiency measurement was then repeated. The latter procedure was followed to prevent solarization from occurring while the slope efficiency measurement was being made. Curves illustrating the most drastic change in laser threshold and slope efficiency as a result of this solarization procedure are shown in Figure 16.

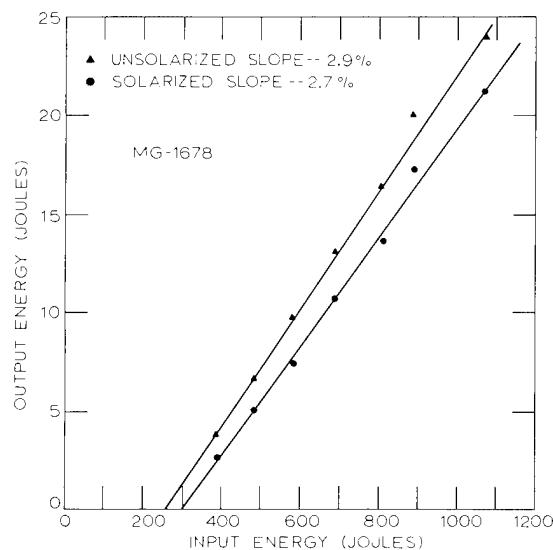


Figure 16. Change in laser characteristics due to solarization treatment

The observed changes in slope efficiency and laser threshold, expressed as the ratio of the solarized to unsolarized values are given in Table VII for several different glass compositions. The degree of solarization is indicated by the decrease in transmission at 400 nm produced by our standard solarization test on a 2 mm thick glass sample. The 400 nm region is chosen

TABLE VII. Effects of Solarization Treatment on Laser Characteristics

Glass Number	Solarization at 400 nm <sup>a</sup>	Slope		Laser		Composition				
		Efficiency (%)		Threshold (J)		Base Type	Antisolarization Agent			
		Unsolar.	Solar.	Unsolar.	Solar.		PbO	Sb <sub>2</sub> O <sub>3</sub>	TiO <sub>2</sub>	Cr <sub>2</sub> O <sub>3</sub>
MG-1670	0	3.1	3.1	285	300	A	-	-	-	1.0
MG-1677	0.8	3.3	3.0	270	300	A	-	-	1.0	1.0
MG-1678	1.2	2.9	2.7	260	300	A	-	1.0	1.0	1.0
MG-1681	0.6	3.1	3.2	310	310	B	7.1	1.0	3.0	-
MG-1713	0	2.0	2.0	410	420	C	-	-	-	0.6
MG-1720	5.0	3.8	3.8	290	305	B	-	1.0	-	-
MG-1723	4.5	3.4	3.3	300	315	A	-	1.0	-	0.1
MG-3835	7.0	3.3	3.1	310	300	A	-	1.0	-	-

<sup>a</sup>Decrease in percent transmittance of a 2 mm thick sample due to solarization.

<sup>b</sup>Base A is [Li, Na, K]-Ba-silicate, Base B is [Na, K, Rb]-Ba-silicate, and Base C is [Na, K]-Ba-silicate glass.

because the effect is large in this region. Also included in the table is compositional information on the base glass type, plus specific ingredients which might effect solarization of the glass. As may be seen from Table VII, the change in values of transmission at 400 nm, slope efficiency and laser threshold varies from 0% to 10% as a result of this "solarization" treatment. However, there appears to be no correlation between the degree of solarization as indicated by the change of transmission at 400 nm and the laser properties of slope efficiency and threshold. There is good correlation for a given composition between the transmission data on 2 mm thick samples at 400 nm and the observed discoloration of a laser rod made following the solarization treatment. For example, the rod made from glass composition 1723 had a distinct reddish discoloration following the testing procedure whereas the laser rod fabricated from glass MG-1681 showed no discoloration when viewed by eye.

Because of the lack of correlation between the degree of solarization as evidenced by transmission changes at 400 nm and the changes which occurred in the lasing characteristics of the glass, a more detailed investigation was made of the factors affecting laser characteristics. Glass composition MG-3835 was chosen for this purpose because it was available in good optical quality, thus decreasing the possibility of spurious results due to stria, and because the optical study showed that this glass had the largest change in transmission at 400 nm of any of the materials shown in Table VII.

In order to determine whether the decrease in laser slope efficiency and the increase in laser threshold energy is associated with solarization of the laser rod or with some other deleterious process taking place in the laser cavity, the following test was performed on a "fresh" laser rod. The slope efficiency was determined as described previously using sodium nitrite in the cavity to prevent solarization. This was followed by 60 shots on the laser rod instead of the 10 shots used in the previous procedure but in this case the sodium nitrite solution was left in the cavity to prevent solarization of the rod. Following this, the slope efficiency was again determined in the usual manner. No color change was observed in the laser rod following this procedure indicating that no solarization had taken place; however, the slope efficiency had decreased from 3.1 percent to 2.9 percent and the laser threshold had increased from 320 joules to 340 joules between the initial and final measurements, comparable to the results on MG-3835 in Table VII. During the "exposure" process in which the laser rod was fired at 1075 joules input, the output energy was measured on every fifth shot and was found to

decrease from 23.2 joules output to about 21 joules output. Most of the decrease appeared to occur during the first 40 shots. The temperature of the water bath was maintained at  $100^{\circ} \pm 1^{\circ}\text{F}$  ( $37.8^{\circ}\text{C}$ ) during these measurements to eliminate the possibility of variations in output due to temperature changes. As a check to insure that the change in laser characteristics was not due to a thermal gradient established within the laser rod during the solarizing process, the system was allowed to set overnight and slope efficiency and laser threshold remained unchanged at 2.9 percent and 340 joules, respectively.

The laser rod, which then had a total of 81 shots on it including 21 shots acquired during the three efficiency measurements, was then subjected to the normal solarization procedure, namely: (1) the slope efficiency was determined using sodium nitrite solution to prevent solarization, (2) the sodium nitrite solution was replaced with distilled water and the laser was fired 10 times at 1075 joules input, and (3) the water was replaced with sodium nitrite and the slope efficiency was again determined.

By visual inspection, the laser rod exhibited a reddish discoloration after the first shot with distilled water in the cavity. This discoloration was even more strongly evident after the third shot. The measured slope efficiency appeared to improve slightly from 2.9 to 3.0 percent and the laser threshold remained constant at 325 joules between the "before" and "after" measurements of this last series. The temperature of the bath was monitored, but not regulated during this test and was found to be slightly higher at the end of the run. It is not clear whether the slight apparent increase in slope efficiency is; (1) due to this temperature change, (2) is in fact a true increase in slope efficiency, or (3) represents the limit of error of the measurement.

These latter tests strongly suggest that the changes in laser characteristics reported in Table VII were due to some kind of an aging process since these changes were also observed in the latter tests when no visible solarization occurred in the rod. Furthermore, once this "aging" had taken place, the laser rod could be "solarized" as indicated by a visual reddening of the rod without changing the laser characteristics of the rod. Actual data are restricted to just this one case in which  $\text{Sb}_2\text{O}_3$  was used as the antisolarizing agent.

An attempt to repeat the initial phase of the work at a higher level of solarization by increasing the peak current density in the flashlamp to  $2500 \text{ A/cm}^2$  was unsuccessful due to flashlamp failure at this current density.

## 2.4 THERMAL PROPERTIES

The thermal conductivity and specific heat were measured under a subcontract to Battelle Memorial Institute to characterize the glass more completely. A temperature range from 100°C to -180°C was used in the measurements. The results of these measurements are given in Table VIII. Two quite different glass compositions, a flint and crown glass, were chosen for the measurement. The values in the table are in fair agreement with published data in the literature<sup>6</sup> for a third composition, "white plate glass." These data suggest that for silicate based glasses thermal conductivity and specific heat values do not change greatly as a function of composition.

TABLE VIII. Thermal Conductivity and Specific Heat

Temperature (°C)	Thermal Conductivity (watt cm <sup>-2</sup> cm° C <sup>-1</sup> )		Specific Heat (cal g <sup>-1</sup> °C <sup>-1</sup> )	
	Flint	Crown	Flint	Crown
-194	---	---	0.045	0.060
-180	0.0049	0.0049	0.051	0.070
-150	0.0058	0.0058	0.060	0.080
-100	0.0069	0.0069	0.077	0.109
- 50	0.0073	0.0074	0.096	0.127
0	0.0077	0.0080	0.107	0.140
50	0.0080	0.0085	0.115	0.156
100	0.0084	0.0091	0.128	0.169

## 2.5 ATHERMALIZATION

To obtain diffraction limited beams from laser devices it is not only necessary to have good optical quality glass initially, but also to have no distortion generated in the laser cavity during the pumping process. Optical distortion usually occurs, however, due to a pump induced non-uniform temperature distribution in the laser rod. With a proper resonant cavity design and a properly chosen glass composition athermalized laser systems, i.e. those which are free of thermally induced distortion, appear to be feasible.

### 2.5.1 Athermalization Theory and Procedure

For optically pumped laser rods, changes in the optical pathlength of the cavity may arise from three factors. First, pump induced non-uniform changes in temperature lead to an elongation of the rod as governed by the coefficient of thermal expansion,  $\alpha$ , of the glass. Second, this non-uniform temperature distribution will also cause a non-uniform change in the index of refraction due to the thermal coefficient of the index of refraction,  $\alpha_n$ . Finally, thermal gradients in the glass produce stresses, which result in index changes and birefringence due to the stress-optical coefficient of the glass,  $B$ .

Morey<sup>7</sup> points out that the parameter commonly referred to as the stress-optical coefficient is actually the difference, at any given point, between the stress-optical coefficients for light polarized at right angles to, and the light polarized parallel to the force producing the stress as viewed from a mutually perpendicular direction. This parameter more accurately describes the birefringence produced by stress and it will therefore be referred to here as the "stress birefringence" coefficient,  $\Delta B$ . Following Morey's notation, the term stress-optical coefficient will be reserved for the change in refractive index between the stressed and unstressed states as indicated below,

$$n_z - n = B_{\perp} P_y \quad , \quad n_y - n = B_{\parallel} P_y \quad \text{and} \quad B_{\parallel} - B_{\perp} = \Delta B \quad (3)$$

where  $P_y$  is a thrust in the  $y$  direction  $B_{\perp}$  and  $B_{\parallel}$  are the stress-optical coefficients in directions perpendicular to, and parallel to the direction of thrust respectively.

The general approach to the problem of athermalizing laser glass is to derive an expression for the change in the optical

pathlength for various rays and polarizations in the cavity in terms of temperature dependent parameters, which may be set equal to zero. Since the stress-optical coefficient is a function of the plane of polarization of the light, expressions must be derived for the changes in pathlength in both the radial and tangential planes of polarization. Unlike the coefficients of index and expansion which are functions of temperature at the point under consideration, the stress-optical coefficient is a function of stress which may arise from temperature changes in adjacent areas and therefore the physical shape of the laser rod and its overall temperature distribution must be considered.

In the original analysis of this problem by Snitzer<sup>8</sup> of American Optical Corporation, the effects of expansion, index changes and stress on the optical pathlength were considered for two extreme physical configurations. In one case the ratio of length,  $L$ , to radius,  $a$ , is much greater than unity and the condition of plane stress exists, i.e., the stress exists only in a plane perpendicular to the axis of the rod. In the other case, the ratio  $L/a$  is much less than unity and the condition of plane strain exists. Assuming a radial temperature distribution and choosing an appropriate value of the stress-optical coefficient from the literature (that is, the stress birefringence as defined above) the range of values for  $\alpha$  and  $\alpha_n$ , which produce zero path difference between the center and the edge of the rod, were determined for these extreme configurations. All other configurations would fall between these extremes and require intermediate values of these parameters.

Subsequently, a more rigorous analysis was carried out by Quelle<sup>9</sup> of ONR for the case of  $L/a > 1$  with a cylindrical temperature distribution. It includes the distinction between stress birefringence,  $\Delta B$ , and the stress-optical coefficients  $B_{\perp}$  and  $B_{\parallel}$ . From these analyses, one obtains the following equations for the radially polarized and tangential polarized differences in pathlengths,  $\Delta P_r(r)$  and  $\Delta P_{\theta}(r)$ , for beams of light a distance  $r$  from the axis as compared with the ray through the axis where  $E$  is Young's modulus,  $\sigma$  is Poisson's ratio and  $T(r)$  is the temperature distribution.

$$\begin{aligned} \Delta P_r(r) = L \left\{ \left[ n\alpha_n + \frac{\alpha E}{1-\sigma} (2B_{\perp}) \right] T(r) \right. \\ \left. + \frac{\alpha E}{1-\sigma} [B_{\parallel} - B_{\perp}] \frac{1}{r^2} \int_0^r T(r) r dr \right. \\ \left. + \left[ 2\alpha(n-1) - \frac{\alpha E}{1-\sigma} (3B_{\perp} + B_{\parallel}) \right] \frac{1}{A^2} \int_0^A T(r) r dr \right\} \end{aligned} \quad (4)$$

$$\begin{aligned}
\Delta P_{\theta}(r) = L \left\{ \left[ n\alpha_n + \frac{\alpha E}{1-\sigma} (B_{\parallel} + B_{\perp}) \right] T(r) \right. \\
+ \frac{\alpha E}{1-\sigma} [B_{\perp} - B_{\parallel}] \frac{1}{r^2} \int_0^r T(r) r dr \\
\left. + \left[ 2\alpha(n-1) - \frac{\alpha E}{1-\sigma} (3B_{\perp} + B_{\parallel}) \right] \frac{1}{A^2} \int_0^A T(r) r dr \right\}
\end{aligned} \tag{5}$$

In both Eqs. (4) and (5) only the first two terms are radius dependent. The third term is therefore only capable of introducing changes in pathlength which will result in a change in the wavelength of the laser radiation and will not distort a plane wave passing through the laser system. The athermalization of the glass is feasible because the value of the thermal coefficient of the index of refraction at 1.06  $\mu\text{m}$  may be varied, as a function of glass composition, from about  $-40 \times 10^{-7}/^{\circ}\text{C}$  to about  $+40 \times 10^{-7}/^{\circ}\text{C}$ .

The conditions necessary for athermalization, i.e.,  $\Delta P = 0$ , are thus determined by the first two terms of Eqs. (4) and (5). In general, to make  $\Delta P$  equal zero the quantities in the square brackets must be made equal to zero. Two general cases exist; Case I in which  $B_{\perp} = B_{\parallel}$ , that is stress-birefringence ( $\Delta B$ ) is zero and Case II in which  $B_{\perp} \neq B_{\parallel}$ .

#### CASE I

If  $B_{\perp} = B_{\parallel}$  the second terms in Eqs. (4) and (5) vanish since the quantity within the square bracket,  $\Delta B$ , equals zero. In addition, the first terms become identical and the change in pathlength is the same for both directions of polarization as prescribed for the case of zero birefringence. In order to make the  $\Delta P$ 's equal zero the quantity within the square brackets in the first terms must equal zero, i.e.

$$n\alpha_n + \frac{\alpha E}{1-\sigma} (2B) = 0 \quad . \tag{6}$$

To satisfy this equation, the value of  $\alpha_n$  must be a negative quantity since the other parameters in the equation are positive and  $\sigma$  is less than unity.

At the present time the only glass known to have zero stress-birefringence is one introduced by Pockels<sup>10</sup> containing about 76 wt% lead oxide. Unfortunately, this glass has a positive value of  $\alpha_n$  at room temperature and above and therefore Eq. (4) will not be satisfied. Lowering the temperature shifts  $\alpha_n$  toward more negative values, but there are insufficient data at the present time to tell if the shift would be sufficient in this case. One of our goals therefore was to determine the effect of glass composition on  $\Delta B$ , so that the feasibility of developing other zero stress-birefringence glasses may be determined.

## CASE II

When  $B_{\perp}$  and  $B_{\parallel}$  are not equal the glass exhibits stress-birefringence and the values of  $\Delta P_r(r)$  and  $\Delta P_{\theta}(r)$  are never equal as may be seen from Eqs. (4) and (5). It is no longer possible to choose a set of parameters for Eqs. (4) and (5) such that  $\Delta P_r$  and  $\Delta P_{\theta}$  are both zero. Two alternative methods of athermalization were therefore considered in which the pathlength for a ray near the edge of the laser is made equal to the pathlength along the center of the rod.

The first method is to choose the parameters such that the average pathlength for the two directions of polarization near the edge of the rod is equal to the pathlength at the center as shown in Eq. (7).

$$\frac{\Delta P_r(r) + \Delta P_{\theta}(r)}{2} = \frac{L}{2} \left[ 2n\alpha_n + \frac{\alpha E}{1-\sigma} (B_{\parallel} + 3B_{\perp}) \right] T(r) = 0 \quad (7)$$

$$\text{or} \quad 2n\alpha_n + \frac{\alpha E}{1-\sigma} (B_{\parallel} + 3B_{\perp}) = 0 \quad (8)$$

A cavity design is chosen such that the direction of polarization, for a ray oscillating within the cavity, alternates between radial and tangential for each successive passage through the active laser element. Two such systems are shown in Figure 17 (a and b). In Figure 17a, a 45° Faraday rotator is interposed between the laser rod and the totally reflecting end mirror. Thus, a tangentially polarized ray will become a radially polarized ray in the process of being totally reflected at this end of the cavity and vice versa. This results in a pathlength at the edge of the rod which is the average of the optical pathlengths of these two planes of polarization as the light passes back and forth between end reflectors. A similar result can be achieved

in a cascaded system as shown in Figure 17b by introducing a  $90^\circ$  Faraday rotator between the laser components.

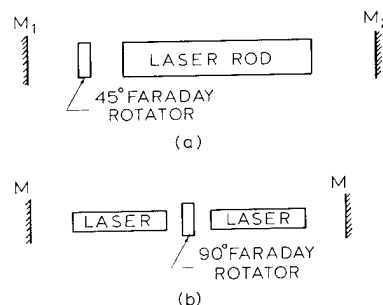


Figure 17. Schematic diagrams of lasers with compensating Faraday rotators

The second method of making the pathlength at the edge of the rod equal to that of the center, for the case where  $B_\perp$  and  $B_\parallel$  are not equal, is as follows. The edge and center pathlengths are made equal either for rays which are tangentially polarized or for those which are radially polarized, but not both. The cavity is then operated only in that mode for which the pathlengths are equal, i.e., if the pathlengths are equal for radially polarized light then the radially polarized  $TM_{01}$  mode is excited and if tangentially polarized paths are of equal length, the  $TE_{01}$  mode is excited.

To develop a material which will satisfy the conditions of either Case I or Case II above, a knowledge of the compositional dependence is required for the various parameters involved. For this purpose a series of glass compositions was designed to provide maximum information, but not necessarily useable laser compositions. Each of the more commonly used glass ingredients was included in at least four different concentrations which covered a range equalling or exceeding that normally encountered in glass technology. Individual glasses contained from six to nine oxides. Since the resulting data were to be submitted to a regression analysis, care was taken to be sure that no cross-correlation in composition existed between glasses, that is, that the ratio of concentrations of any two ingredients in one glass is not repeated in any other glass. The series also contained some of the less commonly used ingredients. These compositions are given in Table IX.

TABLE IX. Glass Compositions for Athermalization Study

Glass Code	SiO <sub>2</sub>	Li <sub>2</sub> O	Na <sub>2</sub> O	K <sub>2</sub> O	Rb <sub>2</sub> O	CaO	BaO	ZnO	La <sub>2</sub> O <sub>3</sub>	CeO <sub>2</sub>	B <sub>2</sub> O <sub>3</sub>	Al <sub>2</sub> O <sub>3</sub>	TiO <sub>2</sub>	SnO	PbO	Nb <sub>2</sub> O <sub>5</sub>	Ta <sub>2</sub> O <sub>5</sub>	Sb <sub>2</sub> O <sub>3</sub>	Bi <sub>2</sub> O <sub>3</sub>	Nd <sub>2</sub> O <sub>3</sub>
1191	58.8		9.6	4.8		19.0		3.8				1.9	1.4					0.23		0.47
1192	71.0			5.0			15.0		6.0			1.0						1.0		1
1193	74.2				5.0		5.0	1.0							12.0			0.8		0.1
1194	49.2	15.0	10.0			15.0		4.0				1.0	3.0					0.8		0.1
1195	75.0		15.0			5.0		2.0		2.0								1.0		1.0
1196	69.2			10.0			15.0	1.0				4.0						0.3		0.5
1197	64.2				10.0		20.0		3.0			2.0						0.5		0.3
1199	48.0						20.0	1.0				4.0			6.0			0.75		0.25
1200	70.0			15.0				2.0		0.5								0.5		0.1
1201	58.2					10.0		4.0				1.0						0.3		1.0
1202	63.1	16.6	6.7			10.0		0.7							2.0			0.2		0.7
1203	66.5											1.0						0.5		0.1
1204	57.0			20.0			5.0					2.0	6.0					0.75		0.25
1233	52.8	18.6	12.8				10.0	4.0	5.3											0.2
1248	69.8						10.3	2.0		1.0		1.2						1.0		0.5
1260	73.0		10.0	5.0			10.0					1.0		0.25				0.5		0.25
1261	75.0					5.0						1.0		2.0				1.0		1.0
1262	71.9						15.0					2.0		0.5				0.5		0.1
1263	68.2			20.0		10.0								1.0				0.3		0.5
1264	75.8			15.0		5.0												0.7	2.5	1.0
1266	74.0			10.0			10.0					0.5						0.25	5.0	0.25
1267	67.7						10.0											0.8	1.0	0.5
1268	53.9		15.0			20.0						0.5						0.5	10.0	0.1
1269	75.0					10.0						0.5					2.5	1.0		1.0
1270	72.0			20.0			5.0										1.0	0.75		0.25
1271	58.5		10.0	5.0		20.0											5.0	1.0		0.5
1272	68.9					15.0											0.5	0.5		0.1
1273	65.8			10.0			20.0					2.0				1.0		0.7		0.5
1274	65.1			15.0		15.0						2.0				2.5		0.3		0.1
1275	77.5						15.0									0.5		1.0		1.0
1276	59.5						15.0											0.7		0.5
1465	63.5						14.4	1.9				1.0						0.3		0.1
1466	63.7											4.8	1.0					0.25		0.25
1467	57.4					9.8						14.7	0.5					0.7		0.9
1468	60.2					20.1		0.5				10.1						0.5		1.0
1474	51.0			2.0				1.0				20.1	2.0		46.2			0.25		0.8

A knowledge of the effect of these glass ingredients on the above parameters should provide the flexibility required for the athermalization schemes suggested. To acquire this information the general procedure is to collect enough data to make the results significant and then subject it to a regression analysis. Accuracy in the present case may suffer from the limited number of glasses involved in this analysis. It should also be borne in mind that some parameters may not have a simple dependence upon composition, i.e., that the regression equation may be complex and thus more difficult to determine. Our experience, however, suggests that this technique is a useful tool for determining trends which are composition dependent.

### 2.5.2 Stress-Birefringence Coefficient

Stress-birefringence measurements were made to provide data for an analysis of  $\Delta B$  as a function of composition in an attempt to develop glasses, other than the present Pockels glass, which would have zero birefringence. The stress-birefringence is measured by a system originally described by Cornu<sup>11</sup> in which a rod of glass with rectangular cross section is flexed over a double fulcrum system. The measurement of retardation due to stress from a known applied force is made between the two inner fulcrum points using a quartz wedge.

In addition to the above series of compositions, a variety of different types of glass were measured including some non-silicate glasses. The range of  $\Delta B$  values for non-lead containing glasses varied from -0.69 to -2.8 Brewsters for the series and from -0.5 to -4.7 Brewsters for all glasses measured. The highest value was for a germanate glass, the two lowest values were obtained with a phosphate glass and a Bi containing glass.

A regression analysis of the stress-birefringence coefficient as a function of glass composition was made resulting in the regression coefficients  $b_1$  listed in Table X for the glass ingredients listed therein. These results show some general trend in the effects of composition on stress-birefringence, but the accuracy of the regression coefficients in general are too poor to give any strong indications of new compositions which might lead to glasses with zero stress-birefringence. Lead oxide glasses were not included in this analysis study because glasses of the Pockels type are not particularly good laser materials and have the disadvantage that their thermal coefficient of refractive index is a positive value whereas a negative value is required to satisfy the conditions of athermalization as previously stated. The 51 glasses included in this analysis, their measured stress-

birefringence coefficients  $\Delta B$  and the values of stress-birefringence calculated from the regression coefficients listed in Table X are tabulated in Table XI.

The comparison between measured and calculated values in Table XI was made in an attempt to provide some insight into the reasons for the poor  $\sigma$ -values in Table X. Considering these  $\sigma$ -values, the agreement between measured and calculated values of  $\Delta B$  was surprisingly good. It is assumed that the uncertainty in the regression coefficient values is probably due to the fact that for some of these values only a few glasses containing the glass ingredient in question were available for analysis or that the range of concentration in some cases may have exceeded the region of linear dependence.

From these results it would appear that the chances were rather remote for obtaining a satisfactory laser glass material in which the stress-birefringence was zero and the conditions for athermalization in Case I could be satisfied. Future efforts to obtain an athermalized material would therefore be confined to Case II in which the stress-optical coefficients differ for rays polarized parallel to and perpendicular to the direction of thrust.

### 2.5.3 Thermal Coefficient of Refractive Index

The technique used for the measurement of the thermal coefficient of refractive index,  $\alpha_n$ , is based on the fact that the output spectrum of a laser rod in a laser cavity which uses a thin plate of transparent material as the output reflector is controlled by the optical thickness of that thin plate. This occurs because the reflectivity of the plate increases from the normal Fresnel reflectance of 4% per surface, in the case of crown glass, to about 16% at those wavelengths for which the optical thickness of the plate,  $nL$ , is equal to an odd number of  $1/4$  wavelengths, i.e.

$$nL = (2N + 1) \lambda/4 \quad , \quad (9)$$

where  $n$  is the index of refraction,  $L$  is the physical thickness of the plate,  $N$  is an integer and the resulting  $\lambda$ 's are possible laser emission wavelengths if located within the fluorescent emission bandwidth. When the temperature is changed, both the physical thickness and the index of refraction of the glass plate will change and thus the wavelength at which laser action may take place will shift. This shift is governed by the following

TABLE X. Regression Coefficients ( $b_i$ ) of the Stress-Birefringence Coefficient ( $\Delta B$ )

PERIODIC GROUP	GLASS COMPONENT	REGRESSION COEFFICIENT	$\sigma$ (rms DEVIATION)	RANGE OF $X_i$ VALUES (wt%)
IA	$\text{Li}_2\text{O}$	0.007	0.047	0-7.7
	$\text{Na}_2\text{O}$	-0.007	0.020	0-24.1
	$\text{K}_2\text{O}$	-0.003	0.020	0-30.1
	$\text{Rb}_2\text{O}$	-0.012	0.011	0-40.6
IIA	$\text{CaO}$	-0.001	0.047	0-34.2
	$\text{BaO}$	0.002	0.006	0-51.4
IIB	$\text{ZnO}$	-0.051	0.060	0-9.0
IIIA	$\text{La}_2\text{O}_3$	-0.012	0.020	0-22.0
	$\text{CeO}_2$	-0.030	0.109	0-5.0
	$\text{Nd}_2\text{O}_3$	-0.063	0.048	0-7.0
IIIB	$\text{B}_2\text{O}_3$	-0.012	0.019	0-15.0
	$\text{Al}_2\text{O}_3$	-0.068	0.031	0-22.0
IVA	$\text{TiO}_2$	-0.046	0.015	0-42.0
IVB	$\text{SiO}_2$	-0.033	0.007	0-70.4
	$\text{SnO}$	-0.040	0.140	0-3.1
VA	$\text{Nb}_2\text{O}_5$	-0.034	0.030	0-15.4
	$\text{Ta}_2\text{O}_5$	-0.042	0.022	0-26.3
VB	$\text{P}_2\text{O}_5$	-0.013	0.009	0-73.1
	$\text{Sb}_2\text{O}_3$	0.086	0.088	0-4.2
	$\text{Bi}_2\text{O}_3$	-0.009	0.006	0-85.0

TABLE XI. Comparison of Measured and Calculated  
Values of Stress-Birefringence

COMPOSITION NUMBER	$\Delta B$ (BREWSTERS)		COMPOSITION NUMBER	$\Delta B$ (BREWSTERS)	
	MEASURED	CALCULATED		MEASURED	CALCULATED
MG-256	-2.6	-2.3	MG-1267A	-1.2	-1.7
MG-372	-0.5	-0.6	MG-1268C	-2.0	-1.4
MG-467	-2.6	-2.6	MG-1269A	-2.5	-2.3
MG-702D	-2.9	-2.7	MG-1270A	-2.2	-2.1
MG-1015A	-1.2	-1.2	MG-1271B	-2.2	-2.4
MG-1050A	-3.1	-3.0	MG-1272A	-2.3	-2.1
MG-1191A	-2.2	-2.27	MG-1273A	-1.4	-1.6
MG-1192B	-1.9	-1.7	MG-1274B	-2.2	-2.3
MG-1194A	-2.1	-2.0	MG-1275A	-2.3	-2.2
MG-1195A	-2.4	-2.5	MG-1276A	-2.0	-1.2
MG-1196A	-2.2	-2.1	MG-1465A	-1.9	-1.2
MG-1197A	-1.3	-1.6	MG-1466B	-2.5	-2.3
MG-1200A	-2.3	-2.2	MG-1467A	-2.4	-2.2
MG-1201A	-1.6	-2.3	MG-1468A	-2.3	-2.3
MG-1203A	-2.2	-2.1	MG-1479B	-2.1	-2.2
MG-1204A	-2.2	-1.9	MG-1480B	-0.6	-0.9
MG-1217A	-2.0	-2.3	MG-1482A	2.3	-2.4
MG-1233B	-1.5	-1.6	MG-1489A	-2.2	-2.0
MG-1248B	-2.2	-2.1	MG-1504A	-1.5	-1.2
MG-1260A	-0.9	-2.0	MG-1514A	-1.5	-1.3
MG-1261B	-2.6	-2.3	3255	-2.5	-1.9
MG-1262B	-1.6	-1.8	3403	-2.8	-2.2
MG-1263A	-1.6	-2.2	3669	-2.6	-2.6
MG-1264A	-0.7	-2.1	3832	-2.6	-2.4
MG-1266B	-2.8	-1.8	3835	-2.4	-2.7
			EB-20B	-2.6	-2.5

expression which is obtained from Eq. (9), namely

$$\frac{dL}{LdT} + \frac{dn}{ndT} = \frac{d\lambda}{\lambda dt} \quad (10)$$

or

$$\alpha + \alpha_n = \alpha_T, \quad (11)$$

where  $\alpha$  is the conventional expansion coefficient,  $\alpha_n$  is the thermal coefficient of refractive index and  $\alpha_T$  is the coefficient of the shift in wavelength of the laser emission as a function of temperature.

The apparatus for measuring  $\alpha_T$  is shown schematically in Figure 18.

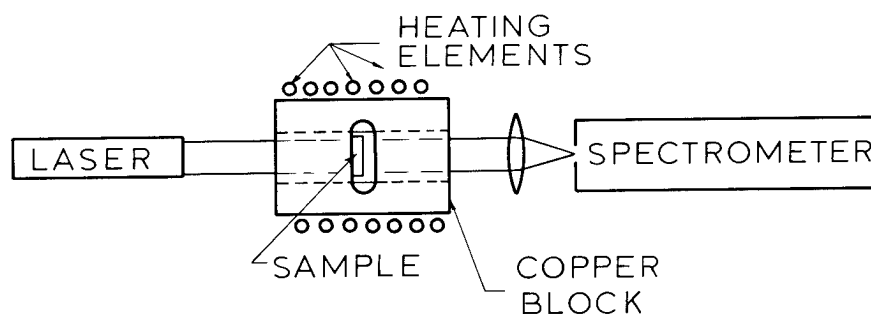


Figure 18. Schematic diagram of apparatus for measuring thermal coefficient of the index of refraction

A neodymium laser was used in the experiment because we wished to measure  $\alpha_n$  at the  $1.06 \mu\text{m}$  wavelength. The material to be measured is fabricated into a plate about 0.5 mm thick with the surfaces of the plate polished to an optical parallelism of about 5 fringes or less per centimeter. This plate which serves as the front reflector of the laser rod is placed in a furnace fabricated from a solid block of copper to provide thermal stability. Light from this laser system is focused upon the slits of a Model No. 70-32 Jarrell-Ash grating spectrometer and the resulting spectra are recorded on infrared sensitive Kodak type 1-Z spectroscopic plates. Exposures are made at several different temperatures in

the range from room temperature to 100°C. The plate is moved vertically for successive exposures.

Spectra of a typical glass sample as a function of temperature are shown in Figure 19. As may be seen, the width of the fluorescent envelope increases slightly with temperature and the position of individual emission lines within the envelope shifts slightly with each change in temperature.

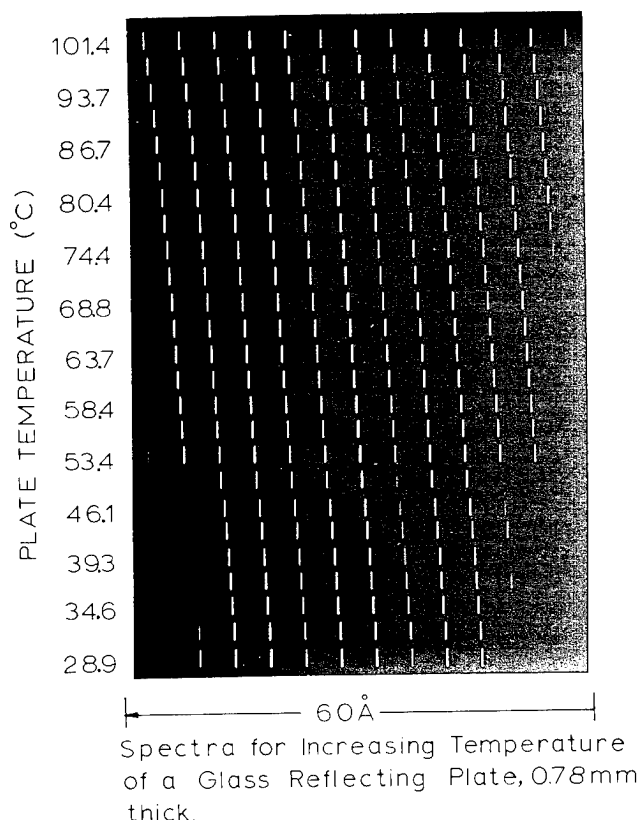


Figure 19. Spectral output of a glass laser with a thin plate acting as a reflection filter for various temperatures of the plate.

This shift in emission wavelengths is measured on the 1-Z plates and from this data a curve of  $\Delta\lambda/\lambda$  vs  $T$  is plotted, the slope of which is  $\alpha_T$ . These plots are not necessarily straight lines, since the expansion coefficient,  $\alpha$ , is not a true constant with respect to temperature. Careful expansion measurements by Kishii<sup>1,2</sup> show that the curve over the range 25 to 125°C usually shows a very slight increase in rate of expansion as temperature increases. By making

a separate measurement (cf. Section 2.5.4) of the thermal expansion coefficient ( $\alpha$ ) and plotting  $\Delta L/L$  vs temperature on this same graph with the  $\alpha_T$ , as shown in Figure 20, it is possible to take the difference between these two curves on a point by point basis and plot these difference values to determine the curve for  $\Delta n/n$  as a function of temperature, the slope of which is  $\alpha_n$ .

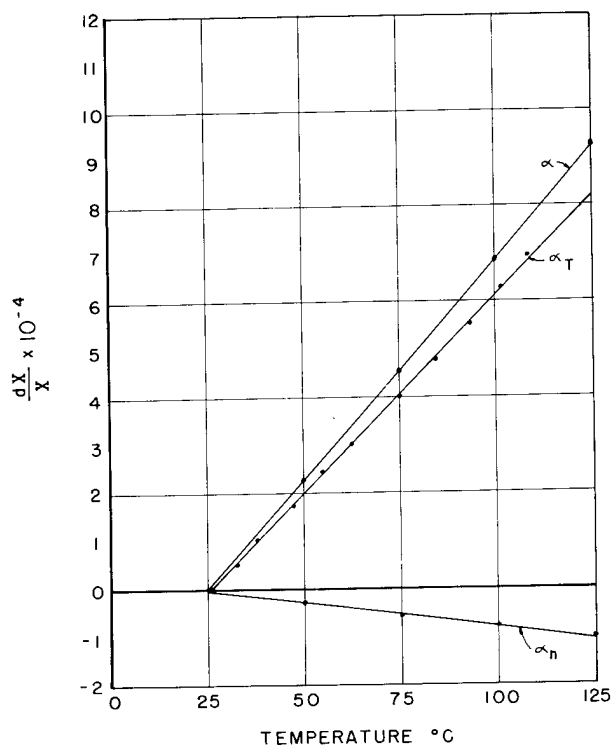


Figure 20. Effect of temperature on the parameter X where X may be length (L), emission wavelength ( $\lambda$ ) or refractive index (n). The slopes of the curve are  $\alpha$ ,  $\alpha_T$  and  $\alpha_n$  respectively. The curve for  $\alpha_n$  is derived from the other two curves.

Results of this measurement for the compositions in Table IX are given in Table XII. In order to satisfy the conditions for athermalization set forth in either Eqs. (6) or (8),  $\alpha_n$  must be a negative value, as previously stated. If all other parameters were constant this would suggest that the ratio of  $\alpha_n/\alpha$  should be as large a negative value as possible. Regression coefficients of  $\alpha_n$  are given in Table XIII. Values of this preliminary figure of merit are also included in Table XII.

---

TABLE XII. Thermal Coefficient of Refractive Index,  $\alpha_n$ ,  
and Preliminary Athermalization Figure-of-Merit  $\alpha_n/\alpha$

---

GLASS NUMBER	$\alpha_n$ ( $\times 10^{-7}$ )	$\alpha_n/\alpha$
1175	35	0.42
1191	- 5	-0.05
1192	3	0.04
1193	13	0.19
1194	5	0.04
1195	8	0.09
1196	- 9	-0.10
1197	-15	-0.16
1199	-16	-0.13
1200	-13	-0.13
1201	-16	-0.16
1202	0	0
1203	-15	-0.12
1204	-29	-0.24
1233	-20	-0.15
1260	-16	-0.15
1261	-11	-0.13
1262	-11.5	-0.14
1263	-24.5	-0.22
1264	- 9	-0.09
1266	- 4	-0.04
1267	-12.5	-0.11
1268	10	0.09
1269	8	0.12
1270	-28	-0.24
1271	0	0
1273	-18	-0.18
1274	-12.5	-0.13
1275	0	0
1276	-21	-0.19
1465	- 5.7	-0.06
1467	7	0.08
1468	11	0.15
3835	-11	-0.11

---

TABLE XIII. Correlation Coefficient for Composition vs Thermal Coefficient of Refractive Index

Periodic Group	Glass Ingredient, n	Correlation Coefficient, $A_n$	Standard Deviation, $\alpha_n$
I A	$\text{Li}_2\text{O}$	-1.88	0.49
	$\text{Na}_2\text{O}$	-2.33	0.21
	$\text{K}_2\text{O}$	-2.30	0.19
	$\text{Rb}_2\text{O}$	-1.20	0.11
II A	$\text{CaO}$	-0.16	0.21
	$\text{BaO}$	-0.70	0.10
II B	$\text{ZnO}$	0.58	0.97
III A	$\text{Nd}_2\text{O}_3$	0.26	0.54
III B	$\text{B}_2\text{O}_3$	0.44	0.2
	$\text{Al}_2\text{O}_3$	1.66	0.7
IV A	$\text{TiO}_2$	0.67	0.9
	$\text{ZrO}_2$	--	--
IV B	$\text{SiO}_2$	0.36	0.08
	$\text{PbO}$	0.30	0.06
V B	$\text{Sb}_2\text{O}_3$	2.14	0.8

#### 2.5.4 Coefficient of Thermal Expansion

Expansion coefficient measurements required for the determination of  $\alpha_n$  (Section 2.5.3) were made on the series of glasses in Table IX. A Chevenard dilatometer was used to make these measurements. This instrument detects changes in length by means of an optical lever which has one leg on the unknown sample and one of the other legs on a known standard which serves as a temperature monitor.

A regression analysis of these results was made using the expression

$$\alpha = \sum b_i x_i \quad , \quad (12)$$

where  $x_i$  is the concentration of the  $i$ th ingredient expressed in weight percent and  $b_i$  is the regression coefficient or weighting factor for that ingredient. Values of  $b_i$  obtained in this manner are shown in Table XIV. The values of  $\sigma$  are the root-mean-square (rms) deviations of  $b_i$  predicted by the analysis. The equation used in the analysis is undoubtedly an oversimplification of the actual situations; in particular, the coefficient for  $\text{SiO}_2$  is not a linear function of composition as noted in the literature.<sup>13,14</sup> Error introduced by this non-linearity will show up as an increase in the values of  $\sigma$ . Despite this oversimplification, the trends appear to be in general agreement with the available published data. The present study covers a wider variety of glass ingredients and provides continuity with the other parameters being studied.

For the sake of comparison, Table XIV also includes values of  $b_i$  obtained by Hall<sup>13</sup> which he arrived at by "inspection and trial," plus values of  $b_i$  obtained using Hall's data and the above regression analysis technique. As shown in the table, the agreement is fairly good.

Although the rationale for choosing the glass compositions given in Table IX was to provide maximum variation in composition, the preliminary figure of merit in Table XII would indicate that a significant improvement in the athermal properties of the glass, with respect to MG-3835, had already been achieved. Based on these results and on preliminary tests of pump induced distortion (Section 2.5.7) in MG-1204 type glass containing 2.5 wt%  $\text{Nd}_2\text{O}_3$  (MG-1750), a second series of athermal glass compositions was prepared. These compositions, given in Table XV, were prepared in hopes of improving still further the athermal properties of

TABLE XIV. Regression Coefficients of the  
Coefficient of Expansion

Periodic Group	$x_i$	$b_i$	$\sigma$	Hall's $b_i$	$b_i$ from Hall's data
IA	Li <sub>2</sub> O	0.49	0.06	--	--
	Na <sub>2</sub> O	0.43	0.008	0.38	0.44
	K <sub>2</sub> O	0.35	0.008	0.30	0.34
	Rb <sub>2</sub> O	0.21	0.004	--	--
IIA	CaO	0.12	0.04	0.15	0.16
	BaO	0.15	0.02	0.12	0.13
IIB	ZnO	0.08	0.16	0.10	0.10
IIIA	La <sub>2</sub> O <sub>3</sub>	0.07	0.02	---	---
	CeO <sub>2</sub>	0.12	0.14	---	---
	Nd <sub>2</sub> O <sub>3</sub>	0.145	0.085	---	---
IIIB	Al <sub>2</sub> O <sub>3</sub>	-0.06	0.1	0.05	0.08
IVA	TiO <sub>2</sub>	-0.03	0.16	---	---
IVB	SiO <sub>2</sub>	0.02	0.01	*	0.02
	SnO	0.007	0.15	---	---
	PbO	0.10	0.002	0.075	0.09
VA	Nb <sub>2</sub> O <sub>3</sub>	0.02	0.04	---	---
	Ta <sub>2</sub> O <sub>5</sub>	0.06	0.03	---	---
VB	Sb <sub>2</sub> O <sub>3</sub>	-0.10	0.14	---	---
	Bi <sub>2</sub> O <sub>3</sub>	0.126	0.01	---	---

\*Non-linear

TABLE XV. Supplementary Glass Compositions for Athermalization Study

Glass Code	$\text{SiO}_2$	$\text{Na}_2\text{O}$	$\text{K}_2\text{O}$	$\text{Rb}_2\text{O}$	$\text{CaO}$	$\text{BaO}$	$\text{ZnO}$	$\text{Al}_2\text{O}_3$	$\text{TiO}_2$	$\text{Sb}_2\text{O}_3$	$\text{Nd}_2\text{O}_3$
1750	57.0		19.9			10.1	4.0	2.0	6.1	0.3	0.6
1855	56.7		19.8			10.0	4.0	2.0	6.0	0.3	1.2
1894	56.7		19.8		10.0		4.0	2.0	6.0	0.3	1.2
1897	60.6	16.0			10.0		3.0	3.0	6.0	0.2	1.2
1898	63.7		16.0			6.0	4.0	2.0	7.0	0.1	1.2
1899	64.4			16.0		12.0	5.0	1.0		0.4	1.2
1902	67.5	18.0				8.0			5.0	0.3	1.2
1903	60.5		18.0		12.0			1.0	7.0	0.3	1.2
1906	69.4			18.0			5.0		6.0	0.4	1.2
1907	54.7	20.0				12.0	4.0	3.0	5.0	0.1	1.2
1910	59.6		20.0			14.0	3.0	2.0		0.2	1.2
1911	64.4			20.0		8.0	4.0	2.0		0.4	1.2
1915	51.5	22.0				14.0	3.0	3.0	5.0	0.3	1.2
1917	55.6		22.0		10.0		5.0		6.0	0.2	1.2
1918	62.7			22.0		6.0	1.0		7.0	0.1	1.2
1919	51.7	24.0		12.0			5.0	1.0	5.0	0.1	1.2

MR-1750 and of producing a family of glasses which would provide some choice in the other physical and laser properties of an athermal material.

Measurements of the thermal expansion coefficient,  $\alpha$ , and the coefficient for the change in total optical thickness as a function of temperature,  $\alpha_T$ , were made on this second series of glass composition. Values of the thermal coefficient of refractive index,  $\alpha_n$ , were calculated from these measurements for the temperature range between 25° and 125°C. These values together with values of the preliminary athermalization figure of merit,  $\alpha_n/\alpha$ , for this second series of glasses, are listed in Table XVI. These results indicate that compositions are available which are equal to or better than the original MG-1204 (or MG-1750) composition. The MG-1855 glass is an MG-1204 composition with the  $\text{Nd}_2\text{O}_3$  concentration increased to 5 wt%.

TABLE XVI. Thermal Coefficient of Supplementary Series of Compositions

Glass Number	Refractive Index Coefficient ( $\alpha_n$ )	Expansion Coefficient ( $\alpha$ )	Optical Thickness Coefficient ( $\alpha_t$ )	Figure of Merit ( $\alpha_n/\alpha$ )
MG-1855	-48.5	128	79.5	-0.38
MG-1894	-46.3	125	78.7	-0.37
MG-1897	-17.5	106	88.5	-0.16
MG-1898	-24.7	100	75.3	-0.25
MG-1899	-43.3	112	68.7	-0.39
MG-1902	-29.2	114	84.8	-0.26
MG-1903	-40.0	119	79.5	-0.34
MG-1906	-33.6	104	70.4	-0.32
MG-1907	-33.6	122	88.4	-0.27
MG-1911	-44.5	120	75.5	-0.37
MG-1915	-42.5	131	88.5	-0.32
MG-1917	-59.3	141	81.7	-0.42
MG-1918	-68.0	138	70.0	-0.49
MG-1919	-29.0	128	99.0	-0.22

## 2.5.5 Stress-Optical Coefficients

It is well known that a block of glass acted upon by non-uniform pressure resulting from a thrust or tension normally becomes doubly refracting, behaving as a uniaxial, optically negative crystal with the optic axis parallel to the local direction of the stress, and with a birefringence proportional to the intensity of the stress. This phenomenon is analyzed theoretically<sup>15,16</sup> [also, Appendix I] in terms of two coefficients,  $p$  and  $q$ , which relate the changes in the propagation of light through a medium to the elastic deformations of that medium due to an applied pressure. These will be referred to here as "strain-optical" coefficients. The stress-optical coefficients  $B_{\perp}$  and  $B_{\parallel}$  defined in Eq. (3) are related to the strain-optical coefficients by the following expressions:

$$B_{\perp} \simeq \frac{n}{E} \left[ (1-\sigma) \frac{p}{\nu} - \frac{q}{\nu} \right] \text{ and } B_{\parallel} \simeq \frac{n}{E} \left( -2\sigma \frac{p}{\nu} + \frac{q}{\nu} \right) , \quad (13)$$

where  $\nu$  is the velocity of light in the unstressed material.

The experience of a previous investigator<sup>17</sup> indicates that an interferometric method with a sensitivity of 1/100 wavelength of phase change will be necessary in order to determine the stress-optical coefficients with a precision of 5 to 10%. Initial experimental work on the measurement of stress-optical coefficients for both homogeneous and inhomogeneous test specimens indicated that a better method of measurement was required in the latter case.

The above accuracy requirement, together with the fact that the test specimens would undoubtedly contain some degree of inhomogeneity, led to the choice of a Zernike type interferometer for this measurement. Theoretical analysis and experimental evaluation of the tolerances required in this instrument and related components were carried out prior to finalizing the detailed design of the apparatus.

The interferometer will measure the change in optical thickness which is due to the combined effects of the change in refractive index and the change in sample dimensions as a function of applied stress. Since the stress-optical coefficients are related only to the index changes, factors containing the change in sample dimensions [cf. Appendix I] must be subtracted from the observed change in pathlength. Dimensional changes

of the specimen were calculated from measured values of the applied pressure (P), young's Modulus (E) and Poisson's Ratio ( $\sigma$ ). The elasticity constants were determined from an independent measurement of the velocity of sound on samples taken from the same glass melt as the stress-optic coefficient samples. Preparation of additional melts of suitable quality glass were required in many cases to provide for the fabrication of test specimens for the above measurements.

2.5.5.1 Interferometer Design---Whereas many interferometers can be used to measure the changes in optical pathlength for homogeneous samples of high quality, most of them are eliminated when glass containing striae is to be measured with precision. Thus, the Jamin interferometer used by Pockels, and indeed any wavefront shearing interferometer cannot be used because of the irregular fringes that appear with optically inhomogeneous samples. One way out of this difficulty is to arrange to measure the average optical path through a small area of the specimen, which suggests the use of a pinhole interferometer. The three-pinhole method due to Zernike<sup>18,19,20</sup> operates in this fashion and produces fringe patterns with excellent regularity of spacing even when the glass specimen is quite non-uniform optically. The method also appears to have the necessary sensitivity and is, therefore, the method chosen for modification to make the present measurements.

Figure 21 is a plan view of the basic three-pinhole interferometer. The glass sample is strained by compression along an axis perpendicular to the plane of the figure, while the light passing through the system is linearly polarized. The cross section of the glass samples is nominally 10 mm x 10 mm, so the pinholes are separated by some 7 mm center-to-center. Because the radiation coming through them must interfere at and near the back focal plane of the telescope lens they must be illuminated by light with good spatial and temporal coherence. The need for coherence, the need for polarized light and the need for sufficient intensity to make visual observations on the interference fringes have led to the use of a He-Ne cw laser (0.1 milliwatt single mode output) to illuminate the collimator pinhole O.

It can be shown [cf. Appendix I] that if the three pinholes are of equal size, are equally spaced in a straight line, are small compared to their separation and are placed in the front focal plane of the telescope lens, then the interference pattern in a small neighborhood of the back focal point of the lens is periodic along the optic axis as well as along a direction parallel to the line joining the centers of the pinholes. If the

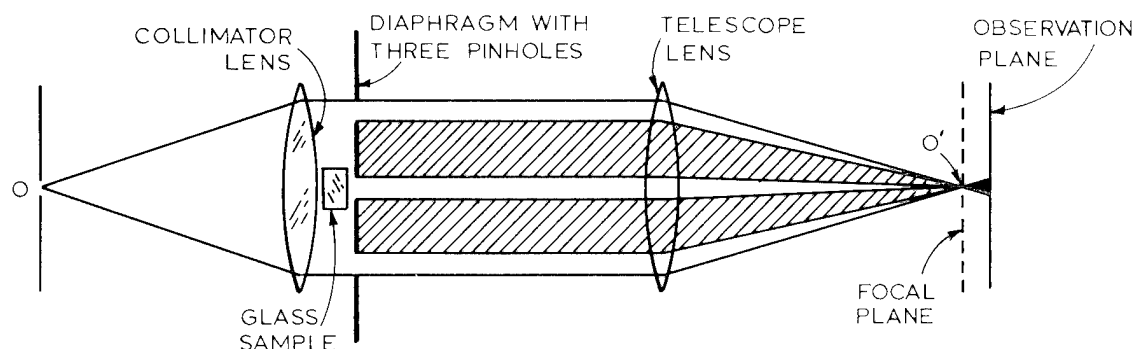


Figure 21. The basic three pinhole interferometer. Light from a laser is focused upon the pinhole O. The interference pattern in the observation plane is examined through a microscope ( $\sim 100\times$  mag.).

coherent light beams from the three pinholes are all in phase, the back focal plane itself will contain a set of fringes that are equally spaced and alternate in intensity, with the strong fringes nine times as intense as the weak ones. This pattern is repeated in planes parallel to the back focal plane and spaced at equal intervals from it both inside and outside of focus. However, in adjacent planes, the strong fringes have exchanged places with the weak fringes. See Figure 22. Half way between these planes are planes in which the fringes are equally spaced and all of the same intensity. The eye is very good at judging the intensity match between adjacent fringes, so it is one of these latter planes that is followed during measurements because it is so accurately identifiable visually.

The entire family of fringes will shift in or out along the optic axis as the phase of the beam from the central pinhole is changed relative to that for the two side pinholes. Furthermore, the amount of shift is directly proportional to the amount of phase shift, so if a microscope is arranged to focus on one of the fringe patterns and can be moved in and out along the optic axis in a controlled and measurable way, a phase shift in the central beam can be translated into motion of the microscope and can be measured thereby. The constant of proportionality is obtained by considering the geometry of the three converging beams. For example, to maintain a chosen phase relation between the light from the three beams arriving at an axial point as the phase of the central beam is retarded more and more, the point must be moved in along the axis since such a motion shortens the

geometrical path from the central hole to the point more than it shortens the paths from the side holes to the point.

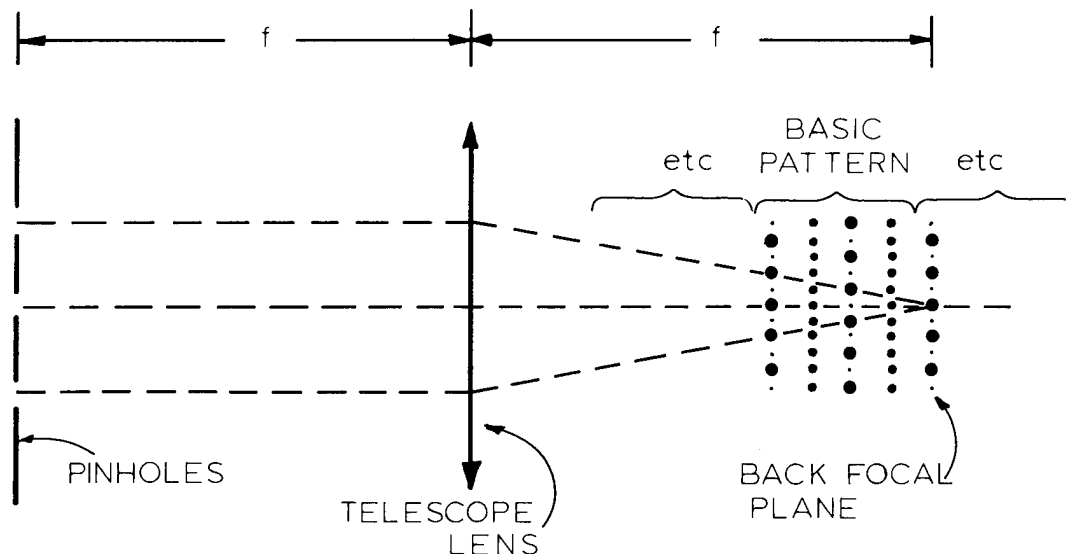


Figure 22. Illustration of the fringe system near focus in the Zernike interferometer. The fringes extend in and out of the plane of the figure. Their relative intensities are indicated by the size of the dots. Fringe spacing is not to scale.

This geometrical effect also exists in the three-dimensional stationary fringe pattern of the undisturbed beams; the distance the microscope must be moved to focus first on one plane where the fringes are all of equal intensity and then on an adjacent plane containing an identical pattern corresponds to a one-half wavelength phase change in the light from the central hole relative to that from the side holes. The interferometer is "self calibrating" in this manner and the size and spacing of the pinholes need not be known at all while the focal length of the telescope lens need be known only approximately.

**2.5.5.2 Test of Interferometer Design---**Preliminary tests of various components of the system were carried out to establish the validity of the overall design of the system and to establish the tolerances required in specific components. In these tests stress was applied to the sample with the arbor press and sample fixtures used in the initial stress-optical coefficient measurement studies while an improved design of these components, dictated

by the results of the original study was being formulated.

(a) Fringe Formation and Stability---It has been established that illumination of sufficient intensity, coherence and degree of polarization to produce clear interference fringes in this system can be obtained by passing light from a Spectra-Physics Mod. 130 He-Ne laser through a 20x microscope objective to focus it down on an 8  $\mu$ m diameter pinhole (pinhole 0 in Figure 21) after which it diverges to a 38 cm focal length doublet serving as collimator lens. Various combinations of the three pinholes that mask out all but three small pencils of light in the collimated beam illuminating the sample have been tried. Consistent with the theory, the use of a central pinhole of larger diameter than the two outer holes is not necessary. In our application, it is preferable to let the three pinholes have the same diameter. Also, it is preferable to keep the central pinhole as small as practically possible in order to obtain the measurement of the average optical path over the selected area of a glass sample with striae. Three pinholes having the diameter of about 0.34 mm and separated by 7 mm provide enough light in the fringes. The use of even smaller pinholes may be possible, but pinholes having diameters of 0.50 mm or more produce a fringe system that has too small lateral extent in this application.

In these early experiments it was found that good fringe settings could be obtained whether the central pinhole was uncovered or covered with uniform or nonuniform blocks of glass. The fringe settings with glass in the central pencil of light, however, drifted rapidly with time whenever the temperature of the sample was changing. It was necessary to smooth out the effect of the 2 to 3°C temperature fluctuations within the air-conditioned measurement laboratory by surrounding the sample, or the entire interferometer, with a secondary isothermal enclosure.

(b) Interferometer Calibration vs Pinhole Location---With respect to the scheme of Figure 21, the collimator and telescope lenses are of about 38 cm focal length. Observation planes near the focal plane 0' are observed with a microscope having a 10x objective and a 10x eyepiece with reticle so that one can concentrate on a particular localized region of the fringe pattern when necessary. The microscope body tube is mounted on a small, sliding table actuated by a thimble micrometer so that the microscope can be moved along the optic axis of the interferometer in a controlled manner and the displacement be read to  $\pm 0.00254$  mm. A total motion of 2.54 cm is possible.

With the interferometer in adjustment, a sequence of 10 readings from the micrometer of repeated settings when the observer

judges that the magnified fringes seen in the microscope are all of the same intensity will have a standard deviation 0.01270 to 0.01524 mm. The distance between planes in which the fringes are all of the same intensity is about 1.854 mm for our choice of pinhole spacing and focal length of the telescope lens. As explained previously, this distance represents a pathlength change of  $1/2$  wavelength between the light coming from the center pinhole and that coming from the two outer pinholes in the interferometer, hence we have the sensitivity to detect changes as small as  $0.0127 \div 3.7 \approx 0.0034$  wavelength.

The displacement  $\delta z$  (approx. 1.854 mm in our case) that alters the phase by  $\pi$  (a pathlength change of  $1/2$  wavelength) is predicted by theory to be a constant no matter which two adjacent planes of equal-intensity fringes are examined near the back focal plane of the telescope lens provided the triplet of pinholes is located at the front focal plane. This has been found to be the case for a range of  $6-1/2$  wavelengths of path change both inside and outside the back focus, a range that exceeds by a healthy margin the pathlength changes expected from straining the glass samples. It is safe, therefore, to determine this "calibration" distance over one part of this range and apply it to phase change measurements in another part.

When the triplet of pinholes was positioned several centimeters nearer the telescope lens, the "calibration" distance  $\delta z$  became a function of the distance from the back focal plane at which the fringes were examined. The change was perceptible, but the tolerance on positioning the triplet of pinholes is judged to be  $\pm 2.54$  mm. That is, translations of  $\pm 2.54$  mm along the axis of the interferometer from the first focal plane of the telescope are not large enough to matter.

(c) Tolerance of Pinhole Spacing---The effect of unequal spacing of the pinholes, i.e. inaccurate positioning of the central pinhole between the two outer pinholes was studied theoretically. The conclusion is that the central hole must not be located off-center by any more than 0.0254 mm, a tolerance that can be met with relative ease.

(d) Tolerance on Sample Alignment---The most damaging effect of the tilt of the sample from perpendicularity to the incident collimated light is the change in tilt that may be produced upon changing the pressure applied to the sample. That is, a slight rotation of the sample, bodily, will introduce a change not related to the stress-optical effect in the pathlength for light passing through the sample and the central pinhole. The effect of change in tilt depends on the initial amount of tilt,

being a minimum when the nominally parallel faces of the sample are perpendicular to the incident light. Some simple geometrical optical calculations show that, for example, if the sample has an initial tilt of  $0.1^\circ$  then an additive change in tilt (assuming 10 mm of glass with a refractive index of 1.5) of  $0.05^\circ = 3$  min. will cause an error of 0.01 wavelength in the measurement of change in pathlength.

Accordingly, the head of an autocollimating device is placed just beyond the pinhole O, Figure 21, for the purpose of monitoring how nearly normal the surfaces of the glass sample are to the incident beam. During initial sample alignment motion of the return beam in two directions must be watched and the resultant not allowed to exceed about 7 minutes of arc (Appendix II.10). The change in tilt during the application of stress to the sample should not exceed about 20 seconds of arc.

(e) Tolerance on Lateral Pinhole Motion---During the measurement one can hardly expect to tolerate any relative motion between the glass sample and the central pinhole when the glass has striae or other inhomogeneities. A rough experimental check on this point using a glass block with striae visible to the unaided eye showed that relative motion as large as  $2.5 \mu\text{m}$  caused interferometric phase changes easily visible in the fringe pattern of the interferometer. It was necessary, then, to attach the triplet of pinholes to the glass sample (in a manner that will not interfere with the strain pattern) so that relative motion between the two is virtually eliminated. When this is done, the sample-plus-pin-holes can be translated by as much as 0.25 mm with no detectable effect on the fringe pattern.

(f) Non-Critical Tolerances---The study on component tolerances indicates that: (1) defocusing of the collimator lens in the arrangement of Figure 23 by relatively slight amounts will not alter the accuracy of the measurement of the induced change in pathlength (Appendix II.1), (2) the tolerances on the setting of the polarizer or analyzer, using either the "X-Y Method" or the " $45^\circ$  Method" are large enough so that no difficulty need be expected, (Appendix II.2 and II.3), (3) the presence of wedge in the test specimen does not affect the measurement of the change in optical pathlength as a function of applied pressure, but in order that the light diffracted from the three pinholes shall overlap properly in the plane of observation, the degree of wedge in the sample should not exceed about 2.7 minutes, (Appendix II.5, II.6 and II.8), and (4) surface flatness does not affect optical pathlength measurements, (Appendix II.7).

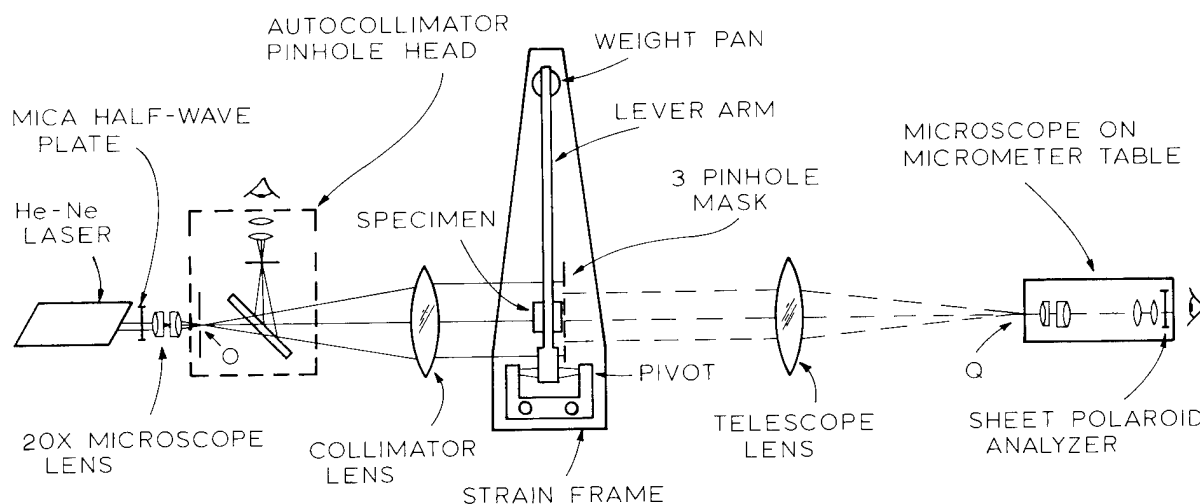


Figure 23. Diagram of the three-pin-hole interferometer for measuring the stress-optical effect in glass samples.

2.5.5.3 Apparatus---The final design of the system is shown in Figure 23. The apparatus includes an autocollimating device for aligning the He-Ne cw laser required (cf. Section 2.5.5.1) for the light source of the interferometer, an accurate lever type strain frame for applying stress to the sample, and a half wave plate for rotating the plane of polarization of light from the laser source, plus a rotatable linear polarizer on the eye piece of the microscope. The latter were added for greater convenience and reliability in making the measurements to obtain the separate stress-optical coefficients for light vibrating parallel to the direction of stress and for light vibrating perpendicular thereto.

The final design of the subassemblies and their necessity were determined in part by an investigation, both theoretical and experimental, of permissible tolerances in various components of the interferometer. This investigation indicates that the apparatus can measure pathlength changes induced by stress in the glass samples to an accuracy of  $\lambda/100$ ,  $\lambda = 6328$  Angstroms, but that nonuniformity of stress within the test specimen may limit the accuracy of the determination to somewhat less than this.

(a) Autocollimator and Pinhole Subassembly---The need for some form of autocollimating device to monitor the alignment of the sample with respect to the incident light was indicated in the tolerance study. The subassembly fabricated

for this purpose is shown in Figure 24. With this device, setting the sample to within the allotted seven minute tolerance mentioned above is an easy matter. This subassembly in addition contains the collimator pinhole, mounted on the left in Figure 24 (see also Figure 23), with its own fine X-Y adjustment. The beamsplitter plate is adjustable with respect to both the base and the Filar Micrometer Eyepiece which serves as the eyepiece of the autocollimator.

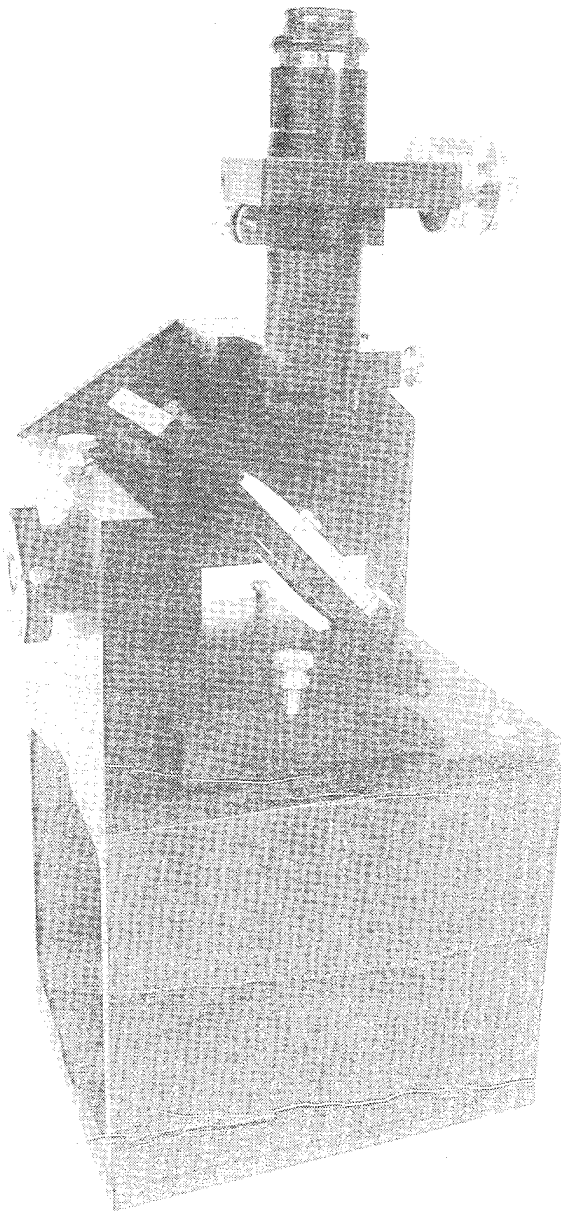


Figure 24. Autocollimator and pinhole subassembly.

(b) Precision Strain Frame---Results of initial tests, plus inquiries to manufacturers of laboratory presses, indicated that a weight-and-fulcrum device was the most expedient approach to provide constant vibration-free straining of the glass samples. The frame was designed so that the sample can be aligned to have its polished faces accurately perpendicular to the incoming beam of light from the interferometer collimator head and sturdy enough so that the sample does not move appreciably as the load is applied. It has a low profile so that it and the interferometer can all be covered with a secondary thermal shield built to cover the granite test block (1.2 x 2.4 m) which serves as a base.

A photograph of the complete strain frame is shown in Figure 25; a cutaway drawing to clarify the design is shown in Figure 26. In operation, the desired vertical downward force is applied to the specimen by means of a 1 meter long, tapered, lever arm that is counterweighted to avoid the task of determining the loading effect of the arm itself. Weights mounted on a sliding weight hanger allow for selection of the maximum force applied. The outer end of the lever is supported by an adjustable arm rest (N in Figure 26) when a sample is not being compressed. The fulcrum of the lever is at the center line (A) of a set of ball bearings, the mount for which (B) is supported on two vertical columns (C). The ball bearing mount may be raised or lowered along the support columns by means of a screw which couples the ball bearing mount to a fixed crosspiece (D) which is also clamped to the vertical support columns. In actual practice, this screw is used to lift the ball bearing mount and lever arm enough to allow the test specimen to be put in place and then to lower this assembly onto the test specimen until the outer end of the lever arm is lifted free from its arm rest, thus applying the full load to the test specimen.

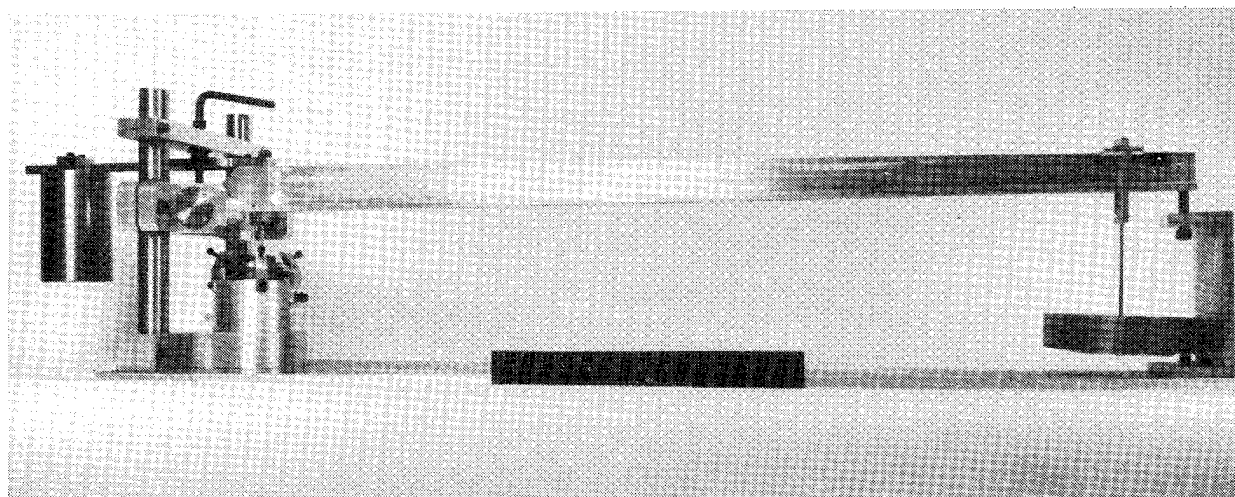


Figure 25. Photograph of the strain frame.

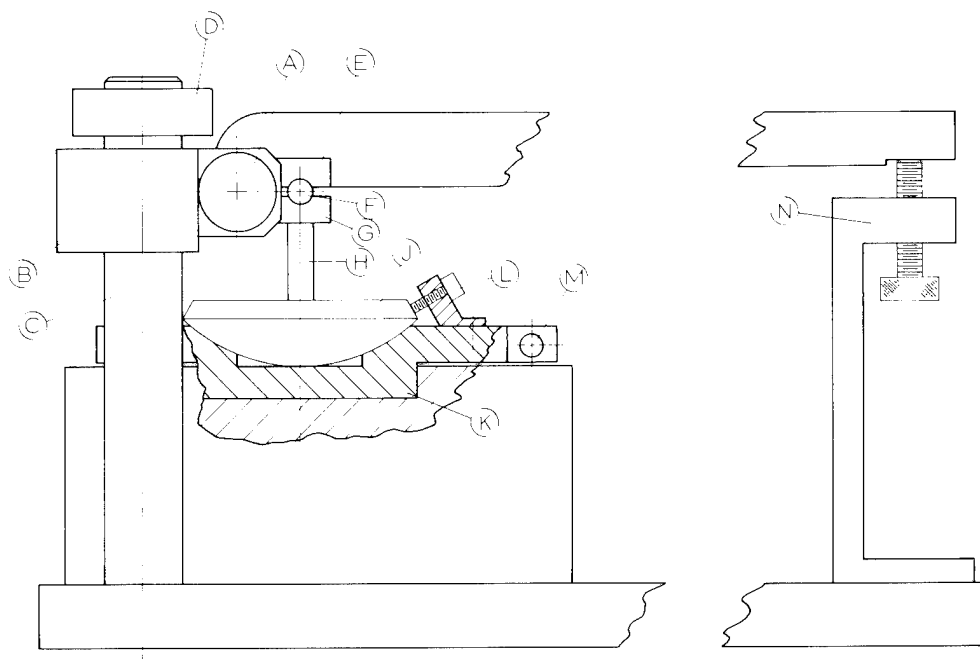


Figure 26. Schematic drawing of the strain frame.

The lever arm has a hardened steel socket in an anvil (E) on its lower side accurately centered 1.000 inch (2.540 cm) from the line of centers of the ball-bearings about which the lever arm pivots. The socket accepts a 1/2-inch steel ball (F) that transmits the load to a mating lower anvil (G) whose flat lower surface presses against the upper end of the test specimen (H). A 1/16 inch (1.59 mm) sheet of neoprene rubber is used to improve the load uniformity between G and H. The sample stands on a platform (J) that is held in a cup-shaped holder (K) with a system of screws for adjustment and locking of position. The mating surfaces between the holder and anvil are ground spherical with a radius of curvature of about 7 cm, a distance calculated to locate the ball (F) and socket of the upper anvils very nearly coincident with their center of curvature when a sample is in place. The sample platform can be moved and clamped in position by three screws (L) acting radially on it; the holder can be rotated in a horizontal plane by a tangent arm and screw (M). These motions are provided so that the glass sample can be adjusted to have its polished surfaces perpendicular to the optic axis of the interferometer prior to any strenuous compression.

The strain frame works satisfactorily to compress the 1 x 1 x 3 cm glass samples with loads of 175-250 kg-wts/cm<sup>2</sup> with little or no sample motion. Some tilt of the sample can be seen

when force is applied, but with a little patience the sample can be adjusted to reduce this motion to the recommended level of tolerance.

2.5.5.4 Experimental Procedure---The components needed for a complete measurement of pathlength changes induced by stress in  $1 \times 1 \times 3$  cm glass blocks are shown assembled in Figure 27.

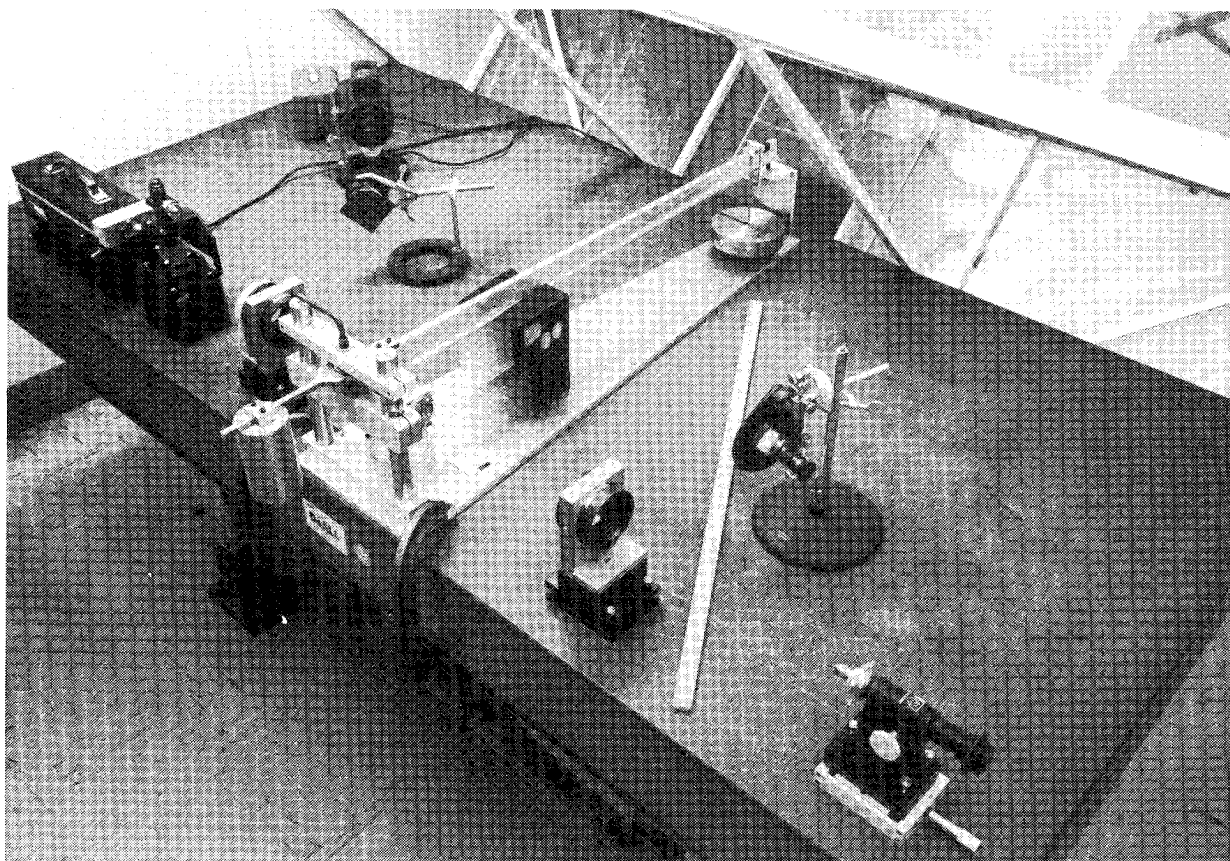


Figure 27. Experimental setup used for complete measurement of stress induced pathlength changes.

The main interferometer is shown lined up parallel to the near edge of the  $4 \times 8$  ft granite vibration isolation table. From upper left to lower right in the photograph they are; the He-Ne laser light source, the collimator-pinhole head assembly, the collimator lens, the strain frame clamped to the table, the telescope lens and the  $100\times$  microscope, with polarizing eyepiece, on its micrometer table. To the right of the collimator-pinhole head assembly are the mercury vapor lamp, 546 Angstrom filter, diffuser and sheet polarizer used to check on uniformity of

stress in the glass sample. To the right of the telescope lens in the Babinet-Soleil compensator and polarizing eyepiece used to check on the uniformity of stress in the sample and to measure the birefringence induced by the stress. The wood and sheet plastic framework in the background is placed over the apparatus during the measurements to provide a thermal shield. This framework has panels for access to the various parts of the interferometer.

(a) Method of Polarization---The laser in Figure 23 (see also, Figure 27) in its normal position, emits an E-vector that vibrates approximately along Z, the line of the applied pressure. A rotatable half-wave plate was mounted external to the laser cavity in order to obtain other planes of vibration easily. Two methods of choosing the plane of polarization of the sampling beam were considered which are designated herein as the "X-Z Method" and the "45° Method." Tolerances on the angles of orientation involved in these two methods are such that either method should yield satisfactory results.

In the X-Z method the  $\lambda/2$ -plate is oriented so that the vector E is incident on the glass sample with E vibrating along Z or X. With moderate force on the sample, the glass becomes birefringent; thus, only light polarized parallel to the direction of stress (Z-axis) or normal to it will emerge plane polarized. Alignment of the incident E-vector along the Z or X axis may thus be accomplished with the aid of a crossed analyzer. By aligning the combination for minimum transmission these scale settings can be determined to about  $\pm 0.1^\circ$ .

The pathlength changes,  $\Delta\phi_Z$  and  $\Delta\phi_X$ , are observed by setting the  $\lambda/2$  plate so that the incident E-vector vibrates along Z and X respectively and measuring the change in interference pattern with stress. The advantages of this method are that little laser light is wasted and that no analyzer is needed in observing the fringe settings. The main disadvantage is that the  $\lambda/2$ -plate adjustment is out of reach of the operator while the fringes are being viewed (see Figure 27).

In the 45° method the  $\lambda/2$  plate is set and left at a scale setting for which the incident E-vector at the strained glass sample vibrates near or at 45° with respect to Z and X. This setting is chosen to provide components of light in the Z and X directions of roughly equal intensities and need not be exact. The fringe patterns formed in the interferometer by each of these components coincide when the glass is stress-free, but as stress is applied they shift by different amounts and produce a

composite pattern of generally reduced contrast. A linear polarizer over the eyepiece of the microscope allows one to examine at will the fringe pattern from one of these components while eliminating the effect of the other simply by turning the polarizer to cross out the light of the unwanted direction of polarization.

In addition, the birefringence, which depends on the difference between the induced pathlength changes, can be measured directly by replacing the telescope lens with a Babinet-Soleil compensator followed by its own linear polarizer and adjusting it to remove and thus measure the relative phase difference between Z and X components of the light coming through the central pinhole and strained sample. This birefringence measurement is used as a cross-check on the measurements of the separate induced pathlength changes, since the difference calculated from the separate measurements made by using first the component vibrating in the Z direction, then that vibrating in the X direction should agree within experimental error with the difference measured directly using the compensator.

(b) Uniformity of Stress in the Glass Specimen---The Babinet-Soleil compensator also is used to check on the uniformity of stress across the central one-third of the 30 mm high glass test samples. The need for this method of determining stress uniformity rather than the use of simple crossed Polaroid sheets became evident in an early comparison of the Zernike three pin-hole system with a "Senarmont-with-one-pinhole" technique. Samples under stress which had been adjusted to look quite uniform in their central region when viewed between crossed Polaroid sheets showed a relative retardation,  $\delta$ , ranging from  $41^\circ$  on one side, to  $55^\circ$  at the center, to  $45^\circ$  on the other side when measured with the Senarmont Method. These limits of Polaroid sheets were corroborated in recent work on mica, which displays sharp steps in thickness and hence  $\delta$ , between crossed Polaroid where the limit of detectability of the steps occurred when  $\delta$  differs by  $5^\circ$  across the step. With continuous variations of  $\delta$ , as in the case of stressed glass, one cannot expect to do as well as  $5^\circ$ .

The following procedure is used to check stress uniformity in the test specimen under pressure. The filtered light from a mercury discharge lamp is aimed so as to illuminate a diffusely transmitting screen backed by a sheet polarizer placed between the collimator lens and the sample cf. Figure 23 (see also Figure 27). The laser light is blocked and the triplet of pinholes is removed. The substitute, diffuse, monochromatic ( $5461\text{\AA}$ ), linearly polarized light source (the plane of polarization is again at  $45^\circ$  to the Z

direction in the glass sample) is viewed through the sample, plus the Babinet-Soleil compensator, plus the linear polarizer on the compensator. If the glass is not stressed, and the compensator, is set on zero, the field of view can be made dark by crossing the compensator polarizer with that of the diffuse source. When the glass is stressed, the compensator must be adjusted to restore the polarization, whereupon the field through the sample can be made dark again. The more uniformly dark this field is, the more uniform is the stress on the glass block. The eye is rather limited in its ability to judge uniformity under these conditions; it is estimated that the variations in birefringence across the sample can be kept to less than  $10^\circ$  or  $10/360$ , 0.03 wavelength. On the average, the birefringence at the center of the block should not vary from one application of a given load to the next by more than this.

Unfortunately this method of checking uniformity of stress is not sensitive enough to guarantee a repeatability of pathlength change from one application of the load to the next of 0.01 wavelength. More sensitive methods for monitoring the uniformity of stress are available, but they are much more time consuming to use since they are not broad field in nature. It was decided that this limitation on the accuracy of the measurements would be accepted. The accuracy actually achieved was checked by duplicating measurements on some samples on the completed apparatus.

(c) Sample Measurement---After the laser has been turned on and thermal equilibrium has been reached, a measurement is carried out approximately as follows: The glass sample to be examined is positioned in the strain frame and oriented so that its polished faces return images of the illuminating pinhole onto the reticle of the auto-collimator eyepiece. The lever arm of the strain frame is raised and lowered and adjustments of sample orientations are made until the sample can be strained with little or no tilting. Then the uniformity of stress in the strained test specimen is checked using the procedure just described. The telescope lens is removed from the optical system during this check, but its base which remains in position has detents for accurate re-positioning.

When satisfactory stress uniformity has been obtained in the test specimen, the laser light and telescope lens are restored. The sample is stressed moderately, the polished faces are cleaned and the triplet of pinholes is attached to the side of the sample nearest the telescope lens with a minimum of soft wax. An inner thermal shield, the black cardboard box shown displaced to the right of the sample and under the lever arm in Figure 27, is

placed around the sample, the access panels on the large thermal shield are closed and observations can begin on the three pin-hole interference fringe system now in the field of view of the microscope.

The first step is to determine the no-load position of the fringes and their spacing along the optic axis. Then the motion of these fringes is followed with the microscope on its micrometer table as the sample is slowly stressed until the lever arm and weight on the strain frame rise from the arm rest. When those readings are completed for both directions of polarization, the triplet of pinholes is removed, the compensator is substituted for the telescope lens and a reading is taken of the birefringence induced in the sample by the stress. Then the stress is removed. If the relative pathlength change as measured by the compensator (line 5 of Table XVII) does not agree with that calculated by taking the difference between the absolute pathlength changes as measured by the three-pinhole interferometer for the X- and Z- polarizations (line 4 of Table XVII) the measurement is repeated.

A typical set of results for five separate measurements on one sample of glass is listed in Table XVII.

---

TABLE XVII. Pathlength Changes  $\Delta\phi$ , Induced by Repeated Stressing of a Glass Sample. The Changes are Expressed in Wave-Lengths of  $6328\text{\AA}$

---

Measurement	1	2	3	4	5
$\Delta\phi_Z$	0.703	0.698	0.696	0.709	0.693
$\Delta\phi_X$	1.436	1.408	1.432	1.453	1.455
$\Delta\phi_Z - \Delta\phi_X$	0.733	0.710	0.736	0.744	0.762
B-S <sup>(a)</sup>	0.733	0.712	0.739	0.698	0.737

---

(a) Result from the Babinet-Soleil compensator measurement.

---

As suggested in the discussion on "Uniformity of Stress in the Glass Specimen," the variation seen from one measurement to the next is attributed principally to nonuniform strain induced in the sample, i.e. the agreement between lines 3 and 4 is better for a given run than reproducibility between runs. It appears that, as a general figure of merit, the stress-optical coefficients will be determined by this method and apparatus to  $\pm 10\%$  assuming that correct values for Young's Modulus and Poisson's Ratio can be obtained for the glass samples.

2.5.5.5 Stress Optical Coefficient Values---Stress-optical measurements were made on both the original and supplementary series of athermal glass compositions.

The measurement described in Section 2.5.5.4 results in a change in optical pathlength,  $\Delta\phi$ , expressed in wavelengths of light (632.8 nm). The values of the change in optical pathlength, ( $\Delta P$ ) given in Columns 3 and 4 of Table XVIII are expressed as the change in pathlength (nm) per unit sample length (cm) per unit applied pressure to the sample ( $\text{kg}/\text{cm}^2$ ) obtained by the expression:

$$\Delta P = \lambda \Delta\phi / p d \quad , \quad (14)$$

where  $\lambda$  is the wavelength of the probe light in nm,  $p$  is the pressure and  $d$  is the sample thickness.

The portion of the change in optical thickness of the sample under pressure, which is due to the change in physical dimensions of the sample, must be subtracted from the above value of  $\Delta P$  to obtain the values of the stress-optical coefficients ( $B$ ), given in Columns 6 and 7, i.e.:

$$B = \Delta P - (n-1) \sigma / E \quad (15)$$

where  $B$  is expressed in Brewsters or  $(\text{nm}/\text{cm})/\text{Bar}$ .

Column 5 is the ratio of values of phase retardation due to birefringence measured directly using a Babinet-Soleil compensator vs values calculated from the above measurement. This comparison is used as an indication of the validity of the measurement as indicated in the discussion on Sample Measurement in Section 2.5.5.4.

TABLE XVIII. Stress-Optical Coefficient Values

Glass Melt No.	Refrac- tive Index $n_{632.8}$	Change in Optical Path (nm/cm)		Birefring- ence meas/calc.	Stress- Optical Coef. (Brewsters)	
		$\Delta P_{\parallel}$	$\Delta P_{\perp}$		$B_{\parallel}$	$B_{\perp}$
MG-1191C	1.568	2.01	4.39	.66/.66	-1.86*	0.57*
MG-1192E	1.615	3.22	5.30	.55/.57	0.39	2.51
MG-1193C	1.592	4.39	7.25	.78/.79	1.55	4.47
MG-1194	1.601	1.53	3.7	.57/.59	0.22	2.44
MG-1195C	1.543	2.36	5.19	.80/.78	1.47	4.36
MG-1196D	1.550	2.98	5.32	.64/.64	-0.76	1.63
MG-1197F	1.597	3.89	5.69	.50/.51	1.52	3.35
MG-1199C	1.636	3.51	5.26	.47/.48	1.04	2.83
MG-1200C	1.526	2.98	5.65	.74/.73	1.25	3.98
MG-1201B	1.564	3.22	5.49	.62/.63	1.03	3.34
MG-1202D	1.574	2.13	4.20	.59/.57	0	2.12
MG-1203C	1.528	3.41	5.80	.65/.66	1.87	4.31
MG-1204D	1.582	3.55	6.03	.67/.69	1.14	3.67
MG-1233	1.626	2.35	3.89	.43/.42	0.057	2.14
MG-1248	1.537	3.96	6.41	.67/.67	1.62	4.08
MG-1263B	1.528	3.25	5.70	.67/.67	1.05	3.55
MG-1264B	1.558	3.27	6.33	.84/.84	---	---
MG-1276B	1.631	3.01	5.12	.56/.58	0.49	2.64
MG-1467B	1.570	1.94	6.44	.74/.71	-0.38	1.98
MG-1474	1.855	10.44	10.16	.78/.77	6.56	6.28
MG-1855B	1.585	3.62	5.95	.66/.64	0.72	3.10
MG-1894	1.570	2.96	5.53	.71/.71	0.79*	3.41*
MG-1897	1.581	2.13	4.67	.73/.70	0.33	2.93
MG-1898B	1.570	3.13	5.76	.74/.71	1.04	3.73
MG-1899	1.566	3.85	6.15	.62/.63	1.04	3.73
MG-1902B	1.572	2.75	5.05	.63/.63	0.87	3.21
MG-1903B	1.568	3.06	5.58	.72/.69	1.08	3.65
MG-1906B	1.550	3.96	6.79	.78/.78	1.48	4.37
MG-1907	1.599	2.65	4.76	.65/.64	0.46*	2.82*
MG-1911	1.555	4.14	6.52	.65/.66	1.65*	4.08*
MG-1915B	1.573	3.13	5.55	.73/.73	1.25	3.72
MG-1917A	1.573	3.20	5.85	.71/.73	0.45*	3.15*
MG-1918	1.566	5.20	7.14	.61/.58	1.93	4.10
MG-1919B	1.589	1.96	4.46	.68/.68	-6.14	-3.59
MG-3835	1.517	2.56	5.23	.74/.74	0.90	3.63

\*c.f. Table XXI for corrected values

Determination of the values of  $\sigma$  and  $E$  for the above calculation of  $B$  are discussed in the next section (Section 2.5.6).

## 2.5.6 Elastic Properties

As stated in Section 2.5.5 the change in optical thickness of a test specimen as a function of applied pressure is a combination of a change in refractive index and a change in physical dimensions. The stress-optical coefficient relates only to the change in index and, therefore, the change in pathlength due to the change in sample dimension must be accounted for. The change in sample thickness can either be measured directly or calculated. The latter method was chosen since values of  $E$  and  $\sigma$  are also required in determining the conditions for athermalization ( $\Delta P = 0$ ) in Equations (6), (7) and (8). The change in sample thickness per unit length,  $\Delta L/L$ , along the optical axis of the interferometer, i.e. normal to the direction of applied pressure, is given by the following expression;

$$\frac{\Delta L}{L} = \frac{\sigma p}{E} \quad (16)$$

where  $p$  is the measured value of applied pressure,  $E$  is Young's Modulus and  $\sigma$  is Poisson's Ratio.

Values of Young's Modulus and Poisson's Ratio were calculated from measurements of the acoustical velocities<sup>21</sup> in the glass for both longitudinal waves,  $V_L$ , and shearwaves,  $V_S$ . The relationship between these wave velocities and the values of Young's Modulus and Poisson's Ratio are given by the following;

$$C_L = V_L^2 \rho = \lambda + 2\mu \quad (17)$$

$$C_S = V_S^2 \rho = \mu \quad (18)$$

and

$$E = \frac{\mu(2\mu + 3\lambda)}{\lambda + \mu} \quad (19)$$

$$\sigma = \frac{\lambda}{2(\lambda + \mu)} \quad , \quad (20)$$

where  $\rho$  is density.

Since apparatus for the measurement of acoustic velocities did not exist in-house, samples were prepared to the required dimensions (1.65 cm x 1.65 cm x 1.27 cm) and sent to the Massachusetts Institute of Technology, where the measurements of  $V_L$  and  $V_S$  were carried out under the guidance of Prof. S. C. Moss using the ultrasonic "pulse-echo" technique. Values of  $E$  and  $\sigma$  were calculated using these values of acoustic velocity and a value of density measured independently. These values are given in Table XIX.

## 2.5.7 Athermalization Results

As previously indicated, the glass compositions chosen for the initial part of this study were designed solely to provide a series of glasses with a wide variety of glass ingredients and a minimum degree of correlation between glass ingredients from one composition to the next. With the realization that the measurement of stress-optical properties would be a time consuming task, it was felt that some preliminary indication of the feasibility of achieving an athermalized glass composition was desired. For this purpose a preliminary figure of merit ( $\alpha n/\alpha$ ) was calculated (cf. Table XII).

One of the more promising compositions in the series, based on this figure of merit, was MG-1204 which contained 1.03 wt%  $Nd_2O_3$ . The  $Nd_2O_3$  concentration of this composition was increased to 2.5 wt% (MG-1750) in order to make the composition a more suitable laser material. The  $Nd_2O_3$  concentration was later increased to 5 wt% (MG-1855) in order to compare results with our standard MG-3835 laser glass. The MG-1204 composition was chosen rather than MG-1270 because the initial calculation of the figures of merit was made using the average value of  $\alpha$ , over the conventional temperature range of 20°C to 300°C which gave values of the figure of merit that were slightly more negative than those given in Table XII. In that initial calculation, the glasses had the same general order of priority, but the MG-1204 glass had a slightly more negative value than the next best glass, MG-1270.

In order to check the degree of athermalization achieved at that stage of the program, 10 pound (4.5 kg) melts of the MG-1750 glass were made. Laser rods of fair optical quality were fabricated from this glass in order to make a direct measurement of the induced optical distortion produced in the rod during the pumping process. These rods were submitted to H. Welling of the U.S. Army Electronics Laboratories at Fort Monmouth, New Jersey, where facilities existed for the measurement of temporal and spatial variations of the optical pathlengths in pumped laser rods.

TABLE XIX. Elastic Constants

Glass Melt No.	Density (g/cm <sup>3</sup> ) $\rho$	Acoustic Velocity <sup>(a)</sup> (cm/sec $\times 10^5$ ) <sup>(c)</sup>		Elastic Constants <sup>(b)</sup> (Dynes/cm <sup>2</sup> $\times 10^{11}$ )		Youngs Modulus (Dynes/cm <sup>2</sup> $\times 10^{11}$ ) E	Poisson's Ratio $\sigma$
		$V_L$	$V_S$	$C_L$	$C_S$		
MG-1191C	2.78	4.828	2.505	6.480	1.744	4.590	0.316
MG-1192E	2.78	4.937	2.810	6.776	2.195	5.529	0.260
MG-1193C	3.51	4.822	2.575	8.161	2.327	6.053	0.301
MG-1194	2.83	6.231	3.773	10.988	4.029	9.754	0.211
MG-1195C	2.75	5.070	3.219	7.069	3.915	6.885	0.121
MG-1196D	3.01	4.923	2.836	7.354	2.421	6.072	0.255
MG-1197F	3.63	4.623	2.627	7.758	2.505	6.320	0.262
MG-1199C	3.75	4.878	2.687	8.923	2.707	6.942	0.282
MG-1200C	2.57	5.159	3.149	6.840	2.549	6.133	0.203
MG-1201B	3.20	4.999	2.853	7.997	2.605	6.556	0.258
MG-1202D	2.78	5.899	3.253	9.674	2.942	7.540	0.281
MG-1203C	2.76	4.902	3.056	6.633	2.577	6.094	0.182
MG-1204D	3.00	4.902	2.816	7.209	2.379	5.965	0.254
MG-1233	3.52	5.643	3.178	11.210	3.555	9.014	0.268
MG-1248	3.07	4.559	2.655	6.381	2.164	5.382	0.243
MG-1263B	2.59	5.173	2.988	6.931	2.312	5.779	0.250
MG-1264B	3.01	4.875	2.838	7.153	2.424	6.030	0.244
MG-1276B	3.35	5.215	2.848	9.111	2.717	6.996	0.288
MG-1467B	2.80	6.233	3.201	10.878	2.869	7.579	0.321
MG-1474	5.70	--	--	--	--	5.404	0.260
MG-1855B	3.05	4.906	2.204	7.341	2.204	5.666	0.285
MG-1894	2.74	5.275	3.052	7.624	2.552	6.342	0.248
MG-1897	2.80	5.588	3.284	8.743	3.020	7.466	0.236
MG-1898B	2.88	5.072	2.977	7.409	2.552	6.315	0.237
MG-1899	3.45	4.523	2.604	7.058	2.339	5.808	0.252
MG-1902B	2.98	5.213	3.055	8.098	2.781	6.886	0.238
MG-1903B	2.69	5.197	3.095	7.265	2.577	6.314	0.225
MG-1906B	3.13	4.735	2.682	7.018	2.251	5.690	0.264
MG-1907	3.33	5.180	2.915	8.935	2.830	7.178	0.268
MG-1911	3.36	4.406	2.542	6.523	2.171	5.430	0.251
MG-1915B	3.30	5.200	2.997	8.923	2.964	7.418	0.251
MG-1917A	2.77	5.057	2.822	7.084	2.206	5.620	0.274
MG-1918	3.32	4.299	2.397	6.136	1.908	4.863	0.274
MG-1919B	2.88	5.705	3.278	9.374	3.905	8.292	0.254
MG-3835	2.63	--	--	--	--	6.84	0.225
MG-1750						6.175	0.268

(a)  $V_L$  = Longitudinal Wave  
 $V_S$  = Shear Wave

(b)  $C_L = V_L^2 \rho$   
 $C_S = V_S^2 \rho$

(c)  $\pm 0.003$

The apparatus for making this measurement is described in the literature.<sup>22</sup> It consists of a single path interferometer with an He-Ne laser light source and a frame camera and a streak camera as recording devices.

A comparison, shown in Table XX, was made of the change in optical pathlength ( $\Delta P$ ) at the center and at the edge of 3 inch (76 mm) long rods of MG-1750 glass and our standard laser glass MG-3835.

---

TABLE XX. Change in Optical Pathlength During Pumping<sup>a</sup>

---

MG-1750	$\Delta P_{\text{center}} = 0.38\lambda$	$\Delta P_{\text{edge}} = 0.38\lambda$
MG-3835	$\Delta P_{\text{center}} = 1.9\lambda$	$\Delta P_{\text{edge}} = 2.7\lambda$

---

<sup>a</sup>Length of laser rod is 3 inches (76 mm),  $\lambda$  is 6328Å, pump energy is 1000 joules.

---

These results are encouraging for two reasons. First, the change in optical pathlength is uniform across the face of MG-1750 laser rod, i.e. there was no optical power induced in the laser rod. In this respect, MG-3835 shows a 40% greater increase in pathlength at the edge of the rod than at the center. This indicates that the degree of athermalization of the MG-1750 composition has been greatly improved with respect to our standard MG-3835 laser glass.

Secondly, the magnitude of the change in pathlength for the MG-3835 glass is 5 to 7 times greater than that of the MG-1750 glass, thus the latter may exhibit less wavelength shift per individual laser spike. In retrospect, the MG-1855 composition would have been more appropriate for comparison with the MG-3835 since it would eliminate any effects due to the difference in Nd<sub>2</sub>O<sub>3</sub> concentration, however, this material was not available at the time.

Based on these encouraging results, the program to develop a suitable method for measuring the stress-optical coefficient of

these glasses was continued and the second generation of athermal glass compositions was added to the study, as previously reported. Funding of the program expired before all of the stress-optical measurements were made, but all results are included in Table XVIII for the sake of completeness. Calculated and experimental evaluation of the degree of athermalization achieved in these glasses was initiated under the contract, but the bulk of the work was carried out in a company-funded program following expiration of contract funds.

As values of the figure of merit and, later, the stress-optical coefficient data became available, the more promising compositions were selected and ten pound (4.5 kg) melts were prepared to provide glass for experimental evaluation of the overall athermal properties of the glass. Initial experimental evaluation of these materials was performed by fabricating laser rods of the material and observing the change in diameter of the output beam of the sample laser as a function of successive firings at known input power. A schematic of the experimental setup is shown in Figure 28.

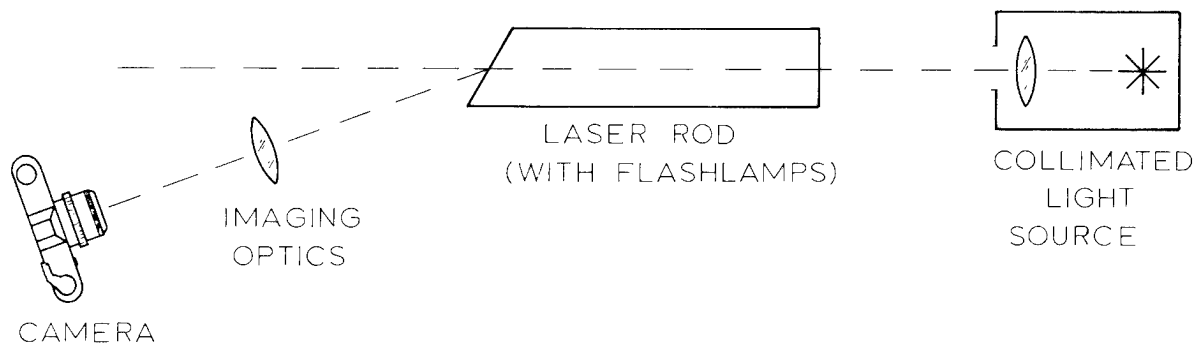


Figure 28. Apparatus for measuring pump-induced thermal distortion.

Test rods were 12 mm diameter x 30.5 cm long with one end flat and normal to the axis and the other end flat but tilted  $5^\circ$  from normal. The rod to be tested was surrounded by four

symmetrically spaced FX-47A-12 xenon flashlamps to provide uniform pumping. The effective pump length was 9-5/8 inches (24.5 cm). A camera with associated imaging optics was provided which recorded a 2x image of the end of the test rod. The percentage change in the diameter of this image is used as an indication of the induced thermal distortion.

Measurements were made on a few glasses and results are given in Table XXI as a function of input power (watts/cm) and number of firings. Measurements were usually made after the first pump pulse and at 5 pulse intervals, however, some difficulties were encountered with rod fracture at the higher power levels.

TABLE XXI. Pump Induced Thermal Distortion

Glass Number	Pump Power (W/cm)	Induced Distortion (%) <sup>a</sup>			
		1st	5th	10th	15th
0835	200	6	12	15	16
1895	285	6	(fractured)	--	--
1899	40	0	0	0	0
	100	0	0	4	
1911	285	0	(fractured)	--	--
1918	50	0	0	0	0
	100	0	0	0	0
	150	0	0	(fractured)-	

<sup>a</sup>Percentage change in image size as a result of 1st, 5th, etc. firing of flashlamps.

This measurement differs from the one summarized in Table XX in several respects. The former measures the distortion produced during a single pulse, while the latter indicates the distortion existing after one and usually several pump pulses. The latter is also a much cruder measurement and was designed primarily as a rapid screening procedure to determine the relative degree of thermally induced distortion.

Subsequent to this program, a more qualitative measurement was made to correlate experimental and calculated evaluation of athermalized materials. In this case, the lens power created in a laser rod of standard configuration was measured by observing the change in focal length of a "lens system" consisting of a 2 diopter lens, plus the laser rod which is illuminated with a collimated beam of  $1.15\text{ }\mu\text{m}$  light. The laser rod was either pumped with a xenon flashlamp at a high repetition rate or was irradiated with a continuous tungsten lamp to simulate various loading conditions.

Results of this study indicated that the correlation between calculated values of difference in  $\Delta P$ 's between the center and edge of the rod, and the experimental measurement of induced power was not always consistent. This led to a reexamination of data used in the calculated values of  $\Delta P$ . The major source of error appears to be the inaccuracy involved in the measurement of the elastic constants, i.e., Young's Modulus and Poisson's Ratio. Samples of the compositions showing the greatest discrepancy in correlation were resubmitted for measurement of the elastic constants. Calculations using these new values of the elastic constants showed quite good correlation between calculated and experimental values.

This suggests that the other values of the elastic constants should be rechecked, and that the values of elastic constants in Table XIX, and values generated therefrom, (B's in Table XVII) should be corrected accordingly. Revised values for selected glasses that were remeasured are given in Table XXII. With accurate values of the elastic constants, it should be possible to make a reliable calculated evaluation of the athermal materials using existing values of the other parameters involved in Equations (4) through (8). The next least reliable parameter in these equations is probably the measurement of the thermal expansion coefficient.

Results of the above company-funded study, using revised data where available, indicated that there were numerous glasses with computed values of average change in pathlength (Eq. 8) which were less than that of our standard laser glass MG-3835, and several which were smaller in magnitude than the improved MG-1750 or MG-1855 glasses. Measured values of induced optical power were obtained with the above modified system on six rods chosen on the basis of low optical distortion and approximately equal  $\text{Nd}_2\text{O}_3$  content. Four of the rods had lower induced power than our standard laser glass. One of these, MG-1918, exhibited no induced power in agreement with the preliminary results of Table XXI.

TABLE XXII. Revised Values of Elastic Constants on  
Selected Glasses

Glass Number	Young's Modulus ( $10^{10}$ dynes/cm <sup>2</sup> )	Poisson's Ratio	Stress Optical Coefficients	
			B <sub>  </sub> (Brewsters)	B <sub>⊥</sub> (Brewsters)
1191	8.4	0.15	1.04	3.47
1894	6.7	0.26	0.76	3.38
1899	6.1	0.24	1.74	4.04
1907	7.75	0.27	0.59	2.77
1911	5.8	0.23	1.99	4.42
1917	6.85	0.22	1.45	4.51

### 3. SUMMARY

One of the first studies performed under this program, initiated in May 1962, was the effect of material impurities (both batch ingredient and crucible) on the transmission of the laser material at its emission wavelength of 1.06  $\mu$ m. The major cause of absorption at this wavelength is the presence of iron in the glass. High purity sources of the major glass ingredient, SiO<sub>2</sub>, were located which contain 3 ppm or less of iron from which glass with an absorption of 0.2%/cm or less is currently made. The search for high purity materials is a continuing one.

Fluorescent lifetime was investigated in an effort to develop materials with desired lifetime characteristics and also as a means of obtaining a better understanding of the mechanisms involved in the laser process. One of the early goals was to develop a material with a long fluorescent lifetime for use as a high energy storage, Q-switch material.

A study of lifetime as a function of composition indicated that lifetime value increases as the ionic radius of the alkali ingredient is increased, i.e., Li to Cs, and to a lesser extent as that of the alkaline earth ingredient is increased, i.e., Ca to Ba. Lifetimes of about 1 ms were obtained by optimizing glass composition. Concentration quenching is slower to develop in these long lifetime materials containing larger alkali ions; for

example, it occurs in the 5-7 wt%  $\text{Nd}_2\text{O}_3$  region for a K,Rb-crown glass compared to 2-3 wt%  $\text{Nd}_2\text{O}_3$  for Na, K-crown glasses.

An analysis of fluorescent intensity as a function of time indicates that the decay process is not a purely exponential one. Results suggest that the decay transition probability for a given  $\text{Nd}^{3+}$ -ion is a function of the degree of coupling between it and neighboring  $\text{Nd}^{3+}$ -ions rather than being associated with a specific site in the glass host, the latter identifiable as a function of glass composition.

Solarization resulting from the ultraviolet emission of the flashlamps used to pump laser systems was investigated as a function of glass composition to determine its effect on the transmission spectra of laser materials and their laser performance.

The addition of  $\text{TiO}_2$ , a UV absorber, to the glass decreases the solarization change in transmission throughout the spectrum rather uniformly but doesn't eliminate it.  $\text{Sb}_2\text{O}_3$ , which changes valence readily, confines the change in transmission to the blue end of the spectrum.  $\text{CeO}_2$ , which changes valence readily and also is an excellent UV absorber, practically eliminates the change in transmission. Combining  $\text{Sb}_2\text{O}_3$  and  $\text{TiO}_2$  reproduces the result obtained with  $\text{CeO}_2$  but with better UV transmission.

The investigation of the effect of the solarization treatment on laser performance indicates, in the case of a glass containing  $\text{Sb}_2\text{O}_3$ , that the initial change in laser performance of a "fresh" laser rod is an aging process independent of the coloration induced by solarization. This aging process took place whether solarization was allowed to occur or not. For the case in which solarization was inhibited during the aging process, the rod was subsequently solarized with no observable degradation of laser performance due to the solarizing process.

Thermal conductivity and specific heat were determined under a subcontract to an independent laboratory for two quite different types of glass, a flint and a crown glass. The results suggest that for silicate glasses, values of these parameters do not change significantly as a function of composition.

A serious problem in the operation of lasers is the optical distortion thermally induced in the cavity due to non-uniform pumping throughout the laser material. An analysis of the factors contributing to the induced changes in optical path-length was carried out which indicated that it might be feasible to develop an athermalized laser material in which the optical

path through a laser system would not be distorted by the existence of thermal gradients. This analysis, carried out independently of the contract, lead to a contract modification to study the effects of composition on the thermal coefficient of refractive index,  $\alpha_n$ , the coefficient of thermal expansion,  $\alpha$ , the stress-optical coefficients,  $B_{\perp}$  and  $B_{\parallel}$ , and the elastic constants which provide values of Young's Modulus,  $E$ , and Poisson's Ratio,  $\sigma$ . An attempt to develop a glass with zero stress birefringence ( $B_{\perp} = B_{\parallel}$ ) and a negative value of  $\alpha_n$  was not successful. Determination of stress-optical coefficient values proved to be the most difficult and most time consuming measurement to perform. The contract expired about the time the latter measurements were being completed and final optimization of the material was not undertaken.

When it became evident that the measurement of the stress-optical coefficient was going to be a rather time consuming process, an experimental material with the most promising ratio of  $\alpha_n/\alpha$  (highest negative value) was evaluated to check the feasibility of the general approach. The optical distortion induced in a 76 mm long rod of this material under typical laser pumping conditions was measured by an independent laboratory in comparison with our commercial laser material. Their results indicated no induced power in the experimental glass at the pump powers used, but a definite induced power in our standard glass. Based on these very encouraging results, a second series of test compositions based on this glass was added to the study.

Results of the study indicated that good correlation can be obtained between measured value of the degree of optical distortion to be expected and values computed from the above parameters. Computations indicated that several of the compositions are better athermal materials than our standard commercially available laser glass. Actual tests on a limited number of materials confirmed this. One of these compositions was judged to be completely athermal, i.e., a rod of the material showed no induced optical power as the input power to the flashlamp was increased to the point at which the laser material fractured thermally.

A study of damage to laser material due to high intensity laser light was initiated under the last contract modification. This phase of the work was deleted before the test equipment was completed because of the magnitude of the problem and the limited funds available.

## APPENDIX I

### THEORETICAL CONSIDERATIONS OF ZERNIKE'S THREE PINHOLE INTERFEROMETER AS APPLIED TO THE MEASUREMENT OF STRESS OPTICAL COEFFICIENTS IN STRIATED GLASSES

#### I.1 INTRODUCTION

The effect of pressure on the optical properties of glass is described by Morey.<sup>15</sup> We adhere to the theory given by Morey. The pressure  $P$  is applied along  $Z$  and the light is propagated along  $Y$  as in Figure I-1. The electric vector is polarized to vibrate along  $Z$  or  $X$ .

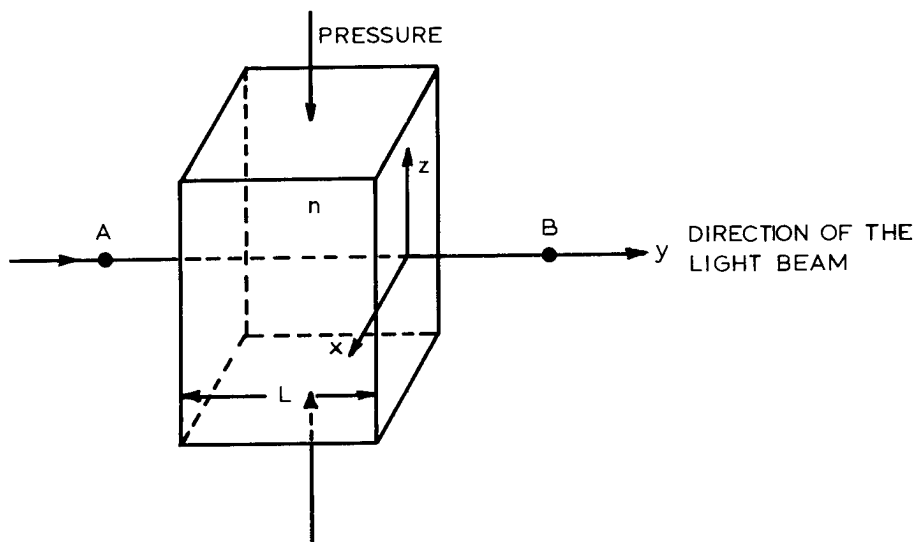


Figure I-1. Convention with respect to the glass sample.  
 $n$  is the refractive index of the isotropic solid  
when no stress is applied.

Let  $X_x$ ,  $Y_y$  and  $Z_z$  be the longitudinal components of strain.  
 Let  $\nu$  be the velocity of light in the glass in the unstrained state. Let  $\nu_x$ ,  $\nu_y$  and  $\nu_z$  denote the velocities with the electric vector vibrating along X, Y and Z respectively. Then, beginning from the relations

$$\begin{aligned}\nu_x - \nu &= q X_x + p Y_y + p Z_z ; \\ \nu_y - \nu &= p X_x + q Y_y + p Z_z ; \\ \nu_z - \nu &= p X_x + p Y_y + q Z_z ;\end{aligned}\tag{1}$$

and introducing

$$X_x = Y_y = \sigma \frac{P}{E} ; \quad Z_z = -\frac{P}{E} ;\tag{2}$$

$P$  = pressure;  $E$  = Young's modulus;  $\sigma$  = Poisson's ratio;  
 then since

$$\frac{\nu_x - \nu}{\nu} = \frac{n - n_x}{n_x} ; \quad \frac{\nu_y - \nu}{\nu} = \frac{n - n_y}{n_y} ; \quad \frac{\nu_z - \nu}{\nu} = \frac{n - n_z}{n_z} ;\tag{3}$$

we obtain with respect to Fig. I-1.

$$\frac{n_z - n}{n_z} \equiv \frac{\Delta n_z}{n_z} \rightarrow \frac{\Delta n_z}{n} = \frac{P}{E} \left[ \frac{q}{\nu} - 2\sigma \frac{p}{\nu} \right] ; \text{ (Z-polarization)}$$

$$\frac{n_x - n}{n_x} \equiv \frac{\Delta n_x}{n_x} \rightarrow \frac{\Delta n_x}{n} = \frac{P}{E} \left[ (1-\sigma) \frac{p}{\nu} - \sigma \frac{q}{\nu} \right] . \text{ (X-polarization)}\tag{4}$$

In summary

$$\frac{\Delta n_z}{n} = \frac{P}{E} \left[ \frac{q}{\nu} - 2\sigma \frac{p}{\nu} \right]; \text{ Z-polarization:}$$

$$\frac{\Delta n_x}{n} = \frac{P}{E} \left[ (1-\sigma) \frac{p}{\nu} - \sigma \frac{q}{\nu} \right]; \text{ X-polarization:} \quad (5)$$

Z along line of pressure X  $\perp$  line of pressure.

The problem is to measure  $\Delta n_z/n$  and  $\Delta n_x/n$  so that the coefficients  $p/\nu$  and  $q/\nu$  can be computed from Eq. 5.

#### I.1.1 General Scheme for Measuring $\Delta n_x/n$ and $\Delta n_z/n$ .

With reference to Fig. I-1, let D be the distance in air from A to B. Let  $\phi$  denote optical path in number of wavelengths.

$$\phi = \phi_0 \text{ for no pressure; } \phi = \phi_a \text{ with pressure applied.} \quad (6)$$

$$\phi_0 = \frac{L(n-1) + D}{\lambda}; \quad \phi_a = \frac{(n+\Delta n-1)(L+\Delta L) + D}{\lambda}. \quad (7)$$

Then

$$\Delta\phi \equiv \phi_a - \phi_0 = \frac{L\Delta n + (n-1)\Delta L}{\lambda}; \quad \Delta n\Delta L \text{ neglected.} \quad (8)$$

$$\therefore \left. \begin{aligned} \frac{\Delta n}{n} &= \frac{\lambda\Delta\phi}{nL} - \frac{\Delta L}{L} \frac{n-1}{n} \quad \text{or, again,} \\ \frac{\Delta n}{n} &= \frac{\lambda\Delta\phi}{nL} - \sigma \frac{P}{E} \frac{n-1}{n}; \quad \frac{\Delta L}{L} = \frac{\sigma P}{E} \end{aligned} \right\}. \quad (9)$$

Either one measures both  $\Delta\phi$  and  $\Delta L$  or measures  $\Delta\phi$  and  $P$  while knowing  $\sigma$  and  $E$ . At the moment we do not plan to measure  $\Delta L$ .

Let

$$\Delta\phi_x = \Delta\phi \text{ for the E-vector along X;}$$

$$\Delta\phi_z = \Delta\phi \text{ for the E-vector along Z, the line of pressure.}$$

Then

$$\frac{\Delta n_x}{n} = \frac{\lambda \Delta\phi_x}{nL} - \frac{\sigma P}{E} \frac{n-1}{n}; \quad \frac{\Delta n_z}{n} = \frac{\lambda \Delta\phi_z}{nL} - \frac{\sigma P}{E} \frac{n-1}{n};$$

$$\Delta n_x \equiv n_x - n; \quad \Delta n_z \equiv n_z - n. \quad (10)$$

We thus have a definite way of obtaining  $\Delta n_x/n$  and  $\Delta n_z/n$  if we arrange to measure the changes of optical path  $\Delta\phi_x$  and  $\Delta\phi_z$ .

## I.2 CHECK ON THE VALUE OF $\Delta\phi_z$ AGAINST POCKELS,<sup>10</sup>

From Eq. (10)

$$\frac{\lambda \Delta\phi_z}{nL} = \frac{\Delta n_z}{n} + \frac{\sigma P}{E} \frac{n-1}{n} \quad (11)$$

Then from Eqs. (11) and (5)

$$\Delta\phi_z = \frac{nL}{\lambda} \frac{P}{E} \left[ \sigma \frac{n-1}{n} + \frac{q}{\nu} - 2\sigma \frac{p}{\nu} \right]; \quad (12)$$

which agrees with Eq. (2) on p. 748 of Pockel's paper.

Let us look also into the value of  $\Delta\phi_x$ . From Eq. (10)

$$\frac{\lambda\Delta\phi_x}{nL} = \frac{\Delta n_x}{n} + \sigma \frac{P}{E} \frac{n-1}{n} \quad (13)$$

Then from Eqs. (13) and (5)

$$\Delta\phi_x = \frac{nL}{\lambda} \frac{P}{E} \left[ \sigma \frac{n-1}{n} + (1-\sigma) \frac{P}{\nu} - \sigma \frac{q}{\nu} \right]. \quad (14)$$

Now, interestingly, we see that from Eqs. (12) and (14) that

$$\Delta\phi_x - \Delta\phi_z = \frac{nL}{\lambda} \frac{P}{E} (1+\sigma) \left[ \frac{P}{\nu} - \frac{q}{\nu} \right]. \quad (15)$$

It can happen that for flint glasses  $q > p$ ; but from Pockel's data  $p$  is usually greater than  $q$ . Thus we must expect that, usually,

$$\Delta\phi_x > \Delta\phi_z. \quad (16)$$

### I.3 COMMENTS ON STRIATED GLASS

Whereas many interferometers can be used to measure the optical path differences  $\Delta\phi_x$  and  $\Delta\phi_z$  for homogeneous glass of high quality, most of the methods must be eliminated when striated glasses are to be measured with a high degree of precision. We would like to measure  $\Delta\phi_x$  and  $\Delta\phi_z$  to about  $\lambda/100$  - even though the glass be quite striated. Thus, the method of the Jamin interferometer, as used by Pockels with great success, fails. Other interferometers, such as the Tyman-Green, fail also because the optical paths of the two arms are too unstable thermally. In so far as possible, the two interfering beams should follow practically parallel paths, and the interferometer, should produce straight fringes even though the glass is quite nonuniform.

Let the beam passing through the glass sample be called the object beam. If the glass is striated, one way out of the difficulty is to arrange to measure the average optical path through a small area of the sample. This suggests the use of the double pinhole interferometer; but further considerations lead one to the choice of the three pinhole method due to Zernike. Certain modifications become desirable.

#### I.4 A ZERNIKE PINHOLE SYSTEM; THE AVERAGING EFFECT OVER A CENTRAL, SMALL PINHOLE

We prefer to begin by considering the configuration of Figure I-2 in which the lenses are omitted.

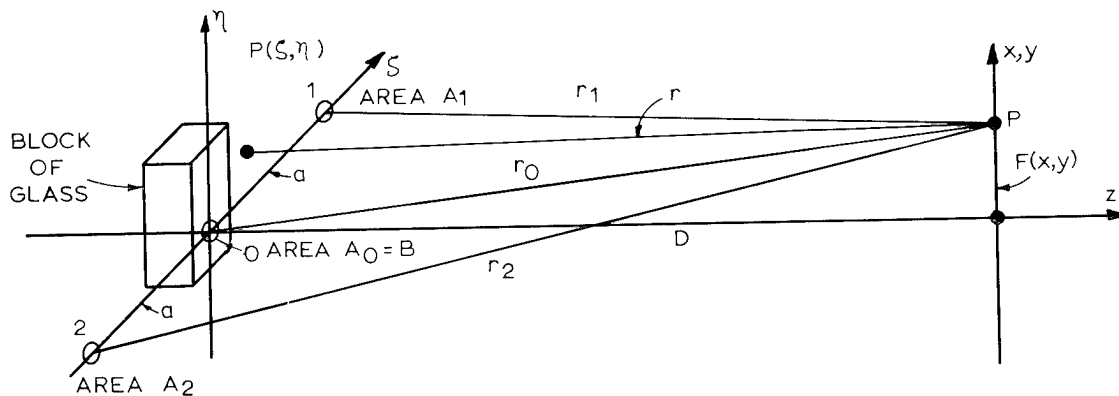


Figure I-2. Pinholes are located at  $\xi = \pm a, \eta = 0$  and at  $\xi = 0, \eta = 0$ . A block of glass is placed behind pinhole #0, the central pinhole. The areas of the pinholes are  $A_1, A_2$  and  $B$ , as indicated. We suppose for convenience that incident upon the plane of the pinholes is a plane wave propagated along  $Z$ . Pinholes #1 and 2 are clear.

If  $P(\xi, \eta)$  is the complex transmittance at the "object plane"  $\xi, \eta$ , then from Huygens' principle the disturbance  $F(x, y) = F(x, y, D)$  is given by

$$F(x,y) = \iint_{\text{over } \xi, \eta \text{ - plane}} P(\xi, \eta) \frac{e^{ikr}}{r} d\xi d\eta ; \quad (17)$$

$$r = \sqrt{(\xi-x)^2 + (\eta-y)^2 + D^2}$$

We are not at liberty to assert that the plane  $Z=D$  falls in the Fraunhofer region so that  $F(x,y)$  need not be a Fourier transform.

We have

$$P(\xi, \eta) = 1 \text{ over pinholes 1 and 2;} \quad (18)$$

$$P(\xi, \eta) = P_0(\xi, \eta) \text{ over the central pinhole.} \quad (19)$$

We assume that all of the pinholes are small - so small that (17) is well approximated by

$$F(x,y) = A_1 \frac{e^{ikr_1}}{r_1} + A_2 \frac{e^{ikr_2}}{r_2} + \iint_{\text{over the central pinhole}} P_0(\xi, \eta) \frac{e^{ikr}}{r} d\xi d\eta \quad (20)$$

We have to consider the remaining integral more carefully when  $P_0(\xi, \eta) \neq \text{constant}$ . Let

$$I_0 = \iint_{\text{over central pinhole}} P_0(\xi, \eta) \frac{e^{ikr}}{r} d\xi d\eta. \quad (21)$$

$P_0(\xi, \eta) \neq \text{constant}$  when the glass sample is striated.

From (17).

$$r = [x^2 + y^2 + D^2 + \xi^2 + \eta^2 - 2(x\xi + y\eta)]^{\frac{1}{2}} = R \sqrt{1 + \frac{\xi^2 + \eta^2}{R^2} - 2\frac{(x\xi + y\eta)}{R^2}} ;$$

$$\text{where } R = r_0 = \sqrt{x^2 + y^2 + D^2} . \quad (22)$$

Now in the experiments  $D$  will be so large relative to  $\sqrt{\xi^2 + \eta^2}$  and  $|x\xi + y\eta|$  that with excellent approximation (22) yields

$$r = R + \frac{\xi^2 + \eta^2}{2R} - \frac{x\xi + y\eta}{R} \quad (23)$$

It suffices to set  $r = R$  in the denominator of (21) to obtain

$$I_0 = \frac{e}{R} \iint_{\text{over the central pinhole}} P_0(\xi, \eta) e^{ik \left[ \frac{\xi^2 + \eta^2}{2R} - \frac{x\xi + y\eta}{R} \right]} d\xi d\eta \quad (24)$$

Further simplifications of Eq. (24) are possible if we restrict  $D$  and therefore  $R$  to be greater than 50 meters, and restrict the diameter of the central pinhole to be equal or less than about 0.34 mm. Then  $\sqrt{\xi^2 + \eta^2} = 0.34/2$ , hence with respect to Eq. (24), with  $\lambda = 0.6328 \times 10^{-3}$  mm,

$$k \frac{\xi^2 + \eta^2}{2R} = \pi \frac{\sqrt{\xi^2 + \eta^2}}{\lambda} \frac{\sqrt{\xi^2 + \eta^2}}{R} < 0.0029 \text{ radians.} \quad (25)$$

Consider next the term  $k \frac{(x\xi + y\eta)}{R}$  along the line  $y = 0$ .

The fringe width produced by the fringes due to the two outer pinholes is given by

$$\frac{x}{R} = \frac{\lambda}{2a} \quad .$$

We now restrict our field of view to points  $x$  so near the axis that, say,  $\frac{x}{R} \leq \frac{\lambda}{2a}$ . Then  $k \frac{x\xi + y\eta}{R} = \frac{kx\xi}{R} \leq k\xi \frac{\lambda}{2a} = \pi\xi/a$ . We have

$a = 7$  mm and  $\xi \leq 0.17$  mm. Hence for points  $x, y$  near the center of the field

$$\frac{k(x\xi + y\eta)}{R} \leq 0.077 \text{ radians.}$$

Under these circumstances, the exponential in Eq. (24) is substantially constant = unity so that

$$I_0 = \frac{e}{R} \iint_{\text{over the central pinhole}} P_0(\xi, \eta) d\xi d\eta \quad (26)$$

Returning to Eq. (20), we may now set  $r_1=r_2=R$  in the denominator and write

$$F(x, y) = \frac{e}{R} \left\{ A_1 e^{ik(r_1 - R)} + A_2 e^{ik(r_2 - R)} + B \frac{\iint P_0(\xi, \eta) d\xi d\eta}{B} \right\} \quad (27)$$

where  $B$  is the area of the central pinhole and  $\iint P_0(\xi, \eta) d\xi d\eta / B$  is the average value of the complex transmittance  $P_0(\xi, \eta)$  over the pinhole.

## 1.5 INTRODUCTION OF THE AVERAGE OPTICAL PATH

The expected glass samples produce the variation  $P_0(\xi, \eta)$  over the central pinhole. We expect that

$$P_0(\xi, \eta) = T e^{i\Delta(\xi, \eta)} \quad (28)$$

where  $T$  is the amplitude transmittance and  $\Delta$  is the optical path through the striated sample of glass.  $T$  will be substantially constant but not  $\Delta(\xi, \eta)$ .

Let  $\Delta_a$  be the average value of the optical path over the area of the pinhole. Then

$$P_0(\xi, \eta) = T e^{i\Delta_a} e^{i[\Delta(\xi, \eta) - \Delta_a]} \quad (29)$$

We assume now that  $\Delta(\xi, \eta) - \Delta_a$  is no larger but that

$$e^{i[\Delta(\xi, \eta) - \Delta_a]} \rightarrow 1 + i [\Delta(\xi, \eta) - \Delta_a] ; \quad (30)$$

i.e. terms  $\frac{[\Delta(\xi, \eta) - \Delta_a]^2}{2}$  and higher ordered terms are negligible.  
Then

$$\begin{aligned}
 I &= \iint_{\text{over central pinhole}} P_o(\xi, \eta) d\xi d\eta = T e^{i\Delta_a} \iint [1 + i(\Delta(\xi, \eta) - \Delta_a)] d\xi d\eta \\
 &= T e^{i\Delta_a} \left\{ B - iB\Delta_a + i \iint \Delta(\xi, \eta) d\xi d\eta \right\} \\
 &= T e^{i\Delta_a} \left\{ B - iB\Delta_a + iB\Delta_a \right\}. \quad (31)
 \end{aligned}$$

In summary from Eq. (31)

$$I = T B e^{i\Delta_a} = \iint_{\text{over central pinhole}} P_o(\xi, \eta) d\xi d\eta \quad (32)$$

For this to be true, the variation  $\Delta(\xi, \eta) - \Delta_a$  must be small enough that in the expansion (30) the term  $\frac{i^2 [\Delta(\xi, \eta) - \Delta_a]^2}{2!}$

and all higher ordered terms are negligible. This offers considerable information about the allowable variation.

Finally in summary from Eqs. (27) and (32) we obtain

$$F(x, y) = \frac{e}{R} \left\{ A_1 e^{ikR} + A_2 e^{ik(r_1 - R)} + T B e^{ik(r_2 - R) + i\Delta_a} \right\}; \quad (33)$$

$A_1$  = area of pinhole 1:

$A_2$  = area of pinhole 2:

$B$  = area of central pinhole.

$T$  = amplitude transmittance of the glass plate.

$\Delta_a$  = average optical path of the glass sample over the area of the central pinhole with  $\Delta$  in radians.

$$R = \sqrt{x^2 + y^2 + D^2}; \quad (33a)$$

$$r_1 = [(x-a)^2 + y^2 + D^2]^{\frac{1}{2}}; \quad r_2 = [(x+a)^2 + y^2 + D^2]^{\frac{1}{2}}. \quad (33b)$$

Comment: When the three pinholes cannot be illuminated uniformly, one can consider  $A_1$ ,  $A_2$  and  $B$  as the product of area of the pinhole and the amplitude of the radiation thereon. It can of course happen that the phase of the radiation incident on the pinholes is not the same. For this case we can generalize Eq. (33) by writing

$$F(x,y) = \frac{e}{R} \left\{ A_1 e^{i\Delta_1} e^{ik(r_1-R)} + A_2 e^{i\Delta_2} e^{ik(r_2-R)} + T B e^{i\Delta_a} \right\} \quad (34)$$

#### I.6 THE FRESNEL THEORY FOR EQUALLY SPACED PINHOLES WITH $A_1 = A_2$ . THE LINE $y = 0$ .

Several considerations show that one should look at the fringes in the vicinity  $x=y=0$ . We shall take  $y=0$  and  $x$  small. Then

$$R = \sqrt{x^2 + D^2} \quad (35)$$

From Eq. 33b and  $y=0$

$$\begin{aligned} r_1 &= \sqrt{x^2 + D^2 + a^2} - 2ax = R \sqrt{1 + \frac{a^2}{R^2} - \frac{2ax}{R^2}}; \\ r_2 &= \sqrt{x^2 + D^2 + a^2 + 2ax} = R \sqrt{1 + \frac{a^2}{R^2} + \frac{2ax}{R^2}}. \end{aligned} \quad (36)$$

We will have  $1 \gg \frac{a^2}{R^2}$  or  $\frac{|2ax|}{R^2}$ . Then approximately

$$\begin{aligned} r_1 &= R \left\{ 1 + \frac{a^2}{2R^2} - \frac{ax}{R^2} - \frac{1}{8} \left( \frac{a^2}{R^2} - \frac{2ax}{R^2} \right)^2 \right\}; \\ r_2 &= R \left\{ 1 + \frac{a^2}{2R^2} + \frac{ax}{R^2} - \frac{1}{8} \left( \frac{a^2}{R^2} + \frac{2ax}{R^2} \right)^2 \right\}. \end{aligned} \quad (37)$$

$$\begin{aligned}
r_1 - R &= \frac{a^2}{2R} - \frac{ax}{R} - \frac{1}{8R^3} (a^4 - 4a^3x + 4a^2x^2) ; \\
r_2 - R &= \frac{a^2}{2R} + \frac{ax}{R} - \frac{1}{8R^3} (a^4 + 4a^3x + 4a^2x^2) .
\end{aligned} \tag{37a}$$

In order to obtain good fringes, the terms in  $x^2$  must be negligible. This will be the case if we observe, as we should, in the vicinity of  $x=y=0$ . Then

$$\begin{aligned}
r_1 - R &= \frac{a^2}{2R} \left( 1 - \frac{a^2}{4R^2} \right) - \frac{ax}{R} \left( 1 - \frac{a^2}{2R^2} \right) ; \\
r_2 - R &= \frac{a^2}{2R} \left( 1 - \frac{a^2}{4R^2} \right) + \frac{ax}{R} \left( 1 - \frac{a^2}{2R^2} \right) .
\end{aligned} \tag{37b}$$

Let the result (37b) be entered into Eq. (34). Then

$$\begin{aligned}
F(x,y) = \frac{e}{R} & e^{ikR} e^{ik\frac{a^2}{2R} \left( 1 - \frac{a^2}{4R^2} \right)} e^{i\frac{\Delta_1 + \Delta_2}{2}} e^{i\frac{\Delta_2 - \Delta_1}{2}} e^{i\frac{kax}{R} \left( 1 - \frac{a^2}{2R^2} \right)} \\
& \left\{ A_2 e^{-i\frac{\Delta_2 - \Delta_1}{2}} e^{-i\frac{kax}{R} \left( 1 - \frac{a^2}{2R^2} \right)} + A_1 e^{-i\frac{\Delta_1 + \Delta_2}{2}} e^{-i\Delta_a} \right. \\
& \left. + T B e^{-ik\frac{a^2}{2R} \left( 1 - \frac{a^2}{4R^2} \right)} \right\} .
\end{aligned} \tag{38}$$

The irradiance  $H(x,y)$  is given by

$$H(x,y) = |F(x,y)|^2 . \quad \text{Hence} \tag{39}$$

$$\begin{aligned}
H(x,y) = \frac{1}{R^2} & \left| A_2 e^{i\frac{\Delta_2 - \Delta_1}{2}} e^{i\frac{kax}{R} \left( 1 - \frac{a^2}{2R^2} \right)} + A_1 e^{-i\frac{\Delta_2 - \Delta_1}{2}} e^{-i\frac{kax}{R} \left( 1 - \frac{a^2}{2R^2} \right)} \right. \\
& \left. + T B e^{-i\frac{\Delta_1 + \Delta_2}{2}} e^{-i\Delta_a} e^{-ik\frac{a^2}{2R} \left( 1 - \frac{a^2}{4R^2} \right)} \right|^2
\end{aligned} \tag{40}$$

Case  $A_1 = A_2 = A$

$$H(x,y) = \frac{1}{R^2} \left| 2A \cos \left[ \frac{kax}{R} \left( 1 - \frac{a^2}{2R^2} \right) + \frac{\Delta_2 - \Delta_1}{2} \right] \right. \\ \left. + T B e^{i\Delta_a} e^{-i\frac{\Delta_1 + \Delta_2}{2}} e^{-ik\frac{a^2}{2R} \left( 1 - \frac{a^2}{4R^2} \right)} \right|_2 \quad (41)$$

(Like pinholes 1 and 2).

In handling and interpreting Eq. (41), it is helpful to set

$$\Phi \equiv \Delta_a - \frac{\Delta_1 + \Delta_2}{2} - k \frac{a^2}{2R} \left( 1 - \frac{a^2}{4R^2} \right). \quad (42)$$

Then

$$H(x,o) = H(x) = \frac{1}{R^2} \left| 2A \cos \left[ \frac{kax}{R} \left( 1 - \frac{a^2}{2R^2} \right) + \frac{\Delta_2 - \Delta_1}{2} \right] + T B e^{i\Phi} \right|_2 \\ R \equiv \sqrt{x^2 + D^2} \quad (43)$$

We remark first that sinusoidal fringes do not appear except where  $x$  is so small that with excellent approximation

$$R = D. \quad (44)$$

Of considerable practical importance, the main effect of having  $\Delta_2 \neq \Delta_1$  is to shift the sinusoidal fringes that occur near  $x=y=0$ . This shift is of no importance to our present application of the Zernike method.

It is always possible to find a  $D$ , Fig. I-2, such that

$$\Phi = \pm \mu \frac{\pi}{2}; \quad \mu \text{ an odd integer.} \quad (45)$$

Then with  $x$  small

$$H(x) = \frac{1}{D^2} \left| 2A \cos \left[ \frac{kax}{D} \left( 1 - \frac{a^2}{2D^2} \right) \right] + T B e^{\pm i\mu \frac{\pi}{2}} \right|^2 \quad (46)$$

whence

$$H(x) = \frac{1}{D^2} \left\{ 4A^2 \cos^2 \left[ \frac{kax}{D} \left( 1 - \frac{a^2}{2D^2} \right) \right] + T^2 B^2 \right\}; \quad (47)$$

$$\pm \mu \frac{\pi}{2} = \Delta_a - \frac{\Delta_1 + \Delta_2}{2} - k \frac{a^2}{2D} \left( 1 - \frac{a^2}{4D^2} \right); \quad \mu \text{ odd}. \quad (48)$$

### I.7 ON THE USE OF A COLLIMATOR AND TELESCOPE

The arrangement of Fig. I-2 is hardly practical; so we utilize the configuration of Fig. I-3.

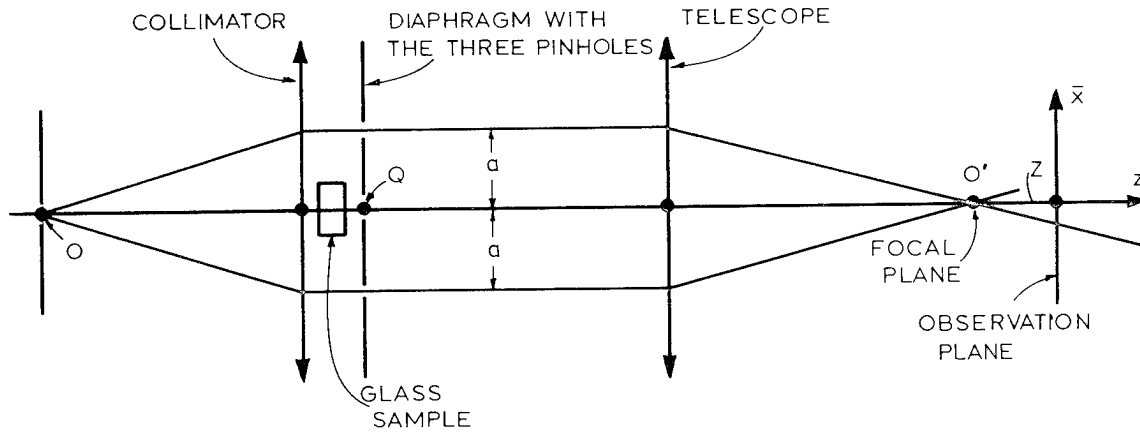


Figure I-3. The preferred optical system. Light from a laser is focused upon a small pinhole at  $o$ . The observation plane is at the distance  $z$  from the focal plane  $o'$  of the telescope. We observe this observation plane by a 100 $\times$  microscope.



Newton's formula  $(D+b)$  and  $z$  are the object and image distance, respectively, from the focal points  $G_1$  and  $G_2$ . From Eq. (49)

$$D = -\left(\frac{f^2}{z} + b\right) \text{ or } \frac{1}{D} = -\frac{z}{f^2 + bz} . \quad (50)$$

We may think of distance  $z$  as the out-of-focus distance.

Let us apply (50) to the result (47). Then

$$H(x) = \frac{1}{D^2} \left\{ 4A^2 \cos^2 \left[ \frac{kax}{D} \left( 1 - \frac{a^2}{2D^2} \right) \right] + T^2 B^2 \right\} , \text{ with} \quad (51)$$

$D$  given by Eq. (50). Now in (48), the glass plate is so thick that  $\mu$  is going to be some large, positive, odd number. Thus we choose the + sign and write

$$\Delta_a = \mu \frac{\pi}{2} + \frac{\Delta_1 + \Delta_2}{2} - \frac{ka^2}{2} \frac{z}{f^2 + bz} \left( 1 - \frac{a^2}{4} \frac{z^2}{(f^2 + bz)^2} \right) . \quad (52)$$

At this point, we neglect  $a^2/2D^2$  as compared to unity and  $\frac{a^2}{4} \frac{z^2}{(f^2 + bz)^2}$  as compared to unity. This does mean that we should be looking in the region where  $z$  is small, that is, near focus. Eqs. (51) and (52) now assume their practical form

$$H(x) = \frac{1}{D^2} \left[ 4A^2 \cos^2 \left( \frac{kax}{D} \right) + T^2 B^2 \right] ; \quad (53)$$

$$\Delta_a = \mu \frac{\pi}{2} + \frac{\Delta_1 + \Delta_2}{2} - \frac{ka^2 z}{2(f^2 + bz)} . \quad (54)$$

As pointed out by Van Heel, we now see that  $\Delta_a$  is linear in the out-of-focus distance  $z$ , Fig. I-4, when  $b=0$ , i.e. when the plane of the pinholes is located at the 1st focal plane of the telescope. Our experiments have confirmed this conclusion.

To summarize matters up to this point, we choose  $\Phi = \mu \frac{\pi}{2}$  where  $\Phi$  is given by Eq. (42). Then the irradiance  $H(x)$  is given by Eq. (53) provided the two outer pinholes have equal area and are equally illuminated. The fringe settings for Eq. (53) are sharp, i.e. the values of  $z$  at which the fringes assume this doubled appearance are sharp. The values of  $z$  at which  $\Phi = 0, \pm \pi, \pm 2\pi$ , etc. are not sharp and are not a good measure of  $\Delta_a$ . We utilize Eq. (54) as follows. With an initial pressure<sup>a</sup> on the glass sample, Fig. I-3, and for the assigned direction of vibration of the electric vector

$$\left(\Delta_a\right)_0 = \mu \frac{\pi}{2} + \frac{\Delta_1 + \Delta_2}{2} - \frac{k a^2 z_0}{2(f^2 + bz_0)} \quad (55a)$$

For the pressure  $P_1$

$$\left(\Delta_a\right)_1 = \mu \frac{\pi}{2} + \frac{\Delta_1 + \Delta_2}{2} - \frac{k a^2 z_1}{2(f^2 + bz_1)} \quad ; \quad (55b)$$

since we alter  $z$  so as to keep the order number  $\mu$  the same and since neither  $\Delta_1$  nor  $\Delta_2$  are altered. Thus

$$\left(\Delta_a\right)_1 - \left(\Delta_a\right)_0 = - \frac{ka^2}{2} \left[ \frac{z_1}{f^2 + bz_1} - \frac{z_0}{f^2 + bz_0} \right] \quad (55c)$$

Then with  $b=0$  or negligible

$$\left(\Delta_a\right)_1 - \left(\Delta_a\right)_0 = - \frac{ka^2}{2f^2} (z_1 - z_0) = \frac{\pi}{\lambda} \frac{a^2}{f^2} (z_0 - z_1) \quad (55d)$$

$$\text{In case } \left(\Delta_a\right)_1 > \left(\Delta_a\right)_0, \quad z_0 > z_1, \quad (55e)$$

a fact which we confirm experimentally.

We seek next to introduce the actual coordinate  $\bar{x}$  of the plane of observation  $D'$  of Fig. I-4. To do this, we use the simplified Fig. I-5. This indicates the first order optics that become involved.

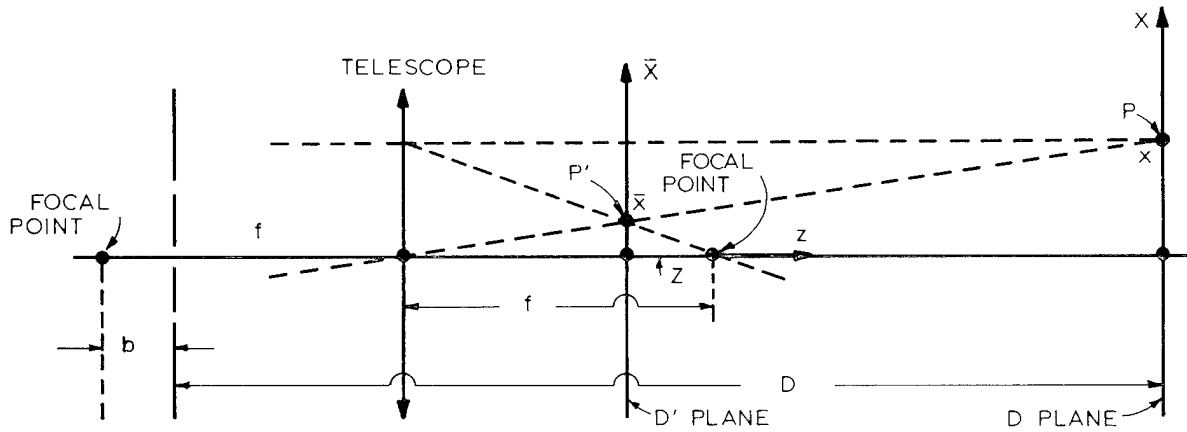


Figure I-5. Illustrating the first order connection between  $\bar{x}$  and  $x$ .

From Fig. I-5, if  $|M|$  = magnification

$$|M| = \frac{f+z}{D-(f-b)} = \frac{f+z}{D-f+b} = \frac{\bar{x}}{x} \quad (56)$$

where  $z < 0$  in the figure. We should have

$$M = \frac{(\text{image distance})}{f} = \frac{-z}{f} . \quad (57a)$$

Let us check this matter. From Eqs. (50) and (56)

$$M = \frac{f+z}{-\frac{f^2+zb}{z} - f+b} = \frac{(f+z)z}{-f^2 - zb + zb - zf} = \frac{z(f+z)}{-f(f+z)} = -\frac{z}{f} . \quad (57b)$$

$$\therefore x = \frac{\bar{x}}{M} = -\frac{\bar{x}f}{z} . \quad (58)$$

With reference to Eq. (53)

$$\frac{ax}{D} = -\frac{a}{D} \frac{\bar{x}f}{z} = -\frac{a\bar{x}f}{z} \frac{(-z)}{f^2+zb} = \frac{af\bar{x}}{f^2+zb} . \quad (59)$$

$$H(\bar{x}) = \frac{1}{D^2} \left\{ 4A^2 \cos^2 \left( \frac{kax}{f + \frac{b}{f}} z \right) + T^2 B^2 \right\} . \quad (60)$$

At  $b=0$ , not only is  $\Phi$  or  $\Delta_a$  linear in the out-of-focus distance  $z$  but also the fringe width for fields near  $x=y=0$  is constant. We have from (60)

$$H(\bar{x}) = \frac{1}{D^2} \left\{ 4A^2 \cos^2 \left( \frac{kax}{f} \right) + T^2 B^2 \right\} \text{ or,} \quad (61)$$

more conveniently, since the external factor is unimportant

$$H(\bar{x}) = 4A^2 \cos^2 \left( \frac{kax}{f} \right) + T^2 B^2 , \quad (61a)$$

holding for outer pinholes having the same area.

Also from Eq. (42) for  $\Phi$  with  $R \rightarrow D$  and  $\frac{1}{D} = \frac{-z}{f^2}$  with  $a^2/4R^2$  negligible

$$\Phi = \Delta_a + \frac{\Delta_1 + \Delta_2}{2} + \frac{ka^2}{2f^2} z = \Delta_a + \frac{\Delta_1 + \Delta_2}{2} + \frac{\pi}{\lambda} \frac{a^2}{f^2} z . \quad (62)$$

where  $\Delta_a$ ,  $\Delta_1$  and  $\Delta_2$  are to appear in radians. For highly corrected telescopes and well centered systems we may take

$$\Delta_1 = \Delta_2 = 0 . \quad (62a)$$

At our settings that produce the distribution (61), we set  $z$  so that  $\Phi = \mu \frac{\pi}{2}$ ,  $\mu$  odd.

## APPENDIX II

### TOLERANCE STUDIES ON THE INTERFEROMETER

#### II.1 EFFECT OF DEFOCUSING THE COLLIMATOR

In setting up the system of Figure 23, it is assumed that with collimators and telescopes of 15 inch focal length one is likely to set point O only within  $\pm 1/4$  inch of the first focal point of the collimator. Similarly, one is likely to set Q only within  $\pm 1/4$  inch of the first focal point of the telescope.

We will now show that, fortunately, a defocusing of the collimator does not introduce error into our measurement of pathlength change.

Suppose first that in Figure 23 the pinhole O falls to the left of the first focal point of the collimator. Then, in the absence of the telescope lens, O would be focused at a point O' at a great distance,  $\ell_o$ , from the plane of the three pinholes as shown in Figure II-1. Let us suppose for simplicity that the system is centered and is highly corrected. Then, the phase at the two outer pinholes will be given by

$$e^{ikC_e - ikR} = e^{ikC_e - ik\sqrt{a^2 + \ell_o^2}} \quad (1)$$

and the phase at the central pinhole will be given by

$$e^{ikC_e - ik\ell_o} e^{i\Delta_a} \quad , \quad (2)$$

where C measures the total pathlength from O to O' and  $\Delta_a$  is the average additional pathlength introduced by the glass sample.

We may now find the solution to the Fresnel problem as done previously (cf. previous Appendix Sections I.4, I.5, and I.6 wherein D corresponds to the present  $\ell_o$ ). For simplicity let the two outer pinholes have the same area A. Our solution for  $F(x,0) = F(x)$  will be that of Eq. (38) of the previous semi-annual report in the above mentioned Appendix wherein

$$\Delta_1 = \Delta_2 = k(C - \sqrt{a^2 + \ell_o^2}) \quad ; \quad \Delta_2 - \Delta_1 = 0; \quad (3)$$

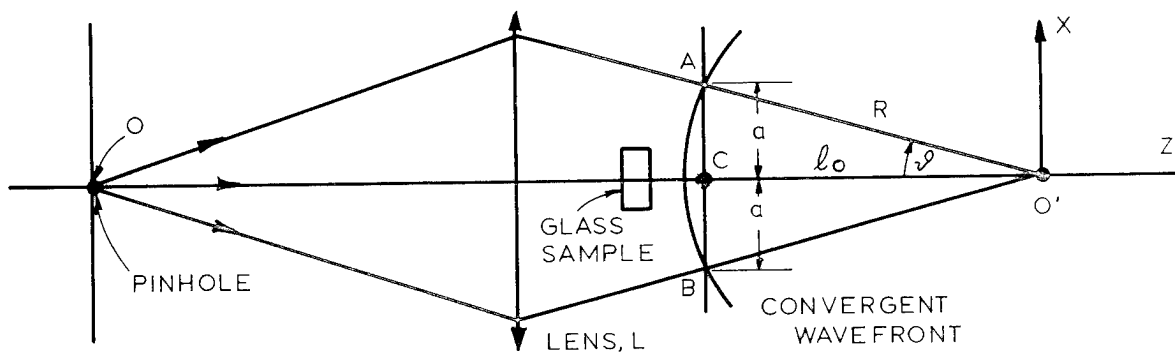


Figure II-1. Illumination of the pinholes A, B and C in convergent light.

and  $\Delta_a$  is replaced by

$$\Delta_a + k(C - l_0) . \quad (4)$$

Maintaining the approximation expressed in Eq. 44 of that Appendix and ignoring the unimportant external factors one obtains, for the case  $A_1 = A_2 = A$ ,

$$F(x) = 2A \cos \left[ \frac{kax}{l_0} \left( 1 - \frac{a^2}{2l_0^2} \right) \right] + T B e^{i\Phi}, \text{ where} \quad (5)$$

$$\Phi \equiv \Delta_a + k \left[ \sqrt{l_0^2 + a^2} - l_0 \right] - \frac{ka^2}{2l_0} \left[ 1 - \frac{a^2}{4l_0^2} \right]. \quad (5a)$$

With the system of Fig. 1 the defocusing of the collimator will be kept small enough so that  $l_0$  will remain great and will be so large relative to  $a$  of Fig. II-1 that we may accept as before the approximation

$$F(x) = 2A \cos \left( \frac{kax}{l_0} \right) + T B e^{i\Phi} ; \quad (6a)$$

$$\Phi = \Delta_a + k \left[ \sqrt{l_0^2 + a^2} - l_0 \right] - \frac{ka^2}{2l_0} . \quad (6b)$$

Solution in the Fresnel plane when the collimator is defocused to produce slightly convergent light.

Let the telescope be inserted so that the three pinholes are at the front focal plane of the telescope and  $O'$  is now brought to focus at  $O''$ , as in Figure II-2, and in accordance with Newton's formula

$$f^2 = -l_o z \text{ or } \frac{1}{l_o} = -\frac{z}{f^2} \quad (7)$$

where  $z$  is the distance measured from the back focal plane of the telescope to  $O''$ . Then from Eqs. 6 and 7

$$\Phi = \Delta_a + k \left[ \sqrt{l_o^2 + a^2} - l_o \right] + \frac{ka^2 z}{2f^2} \quad (8)$$

But

$$\sqrt{l_o^2 + a^2} - l_o \rightarrow \frac{a^2}{2l_o} \quad (9)$$

$\therefore$

$$\Phi = \Delta_a + \frac{ka^2}{2} \left( \frac{z}{f^2} + \frac{1}{l_o} \right) \quad (10)$$

Now, if  $\Delta_a = 0$ , then  $\Phi$  should equal to zero when  $z$  is the location of the star image formed by the collimator and telescope. From Eq. 10, with  $\Delta_a = 0$  and  $\Phi = 0$ ,

$$-z l_o = f^2 ; \text{ Newton's formula.} \quad (11)$$

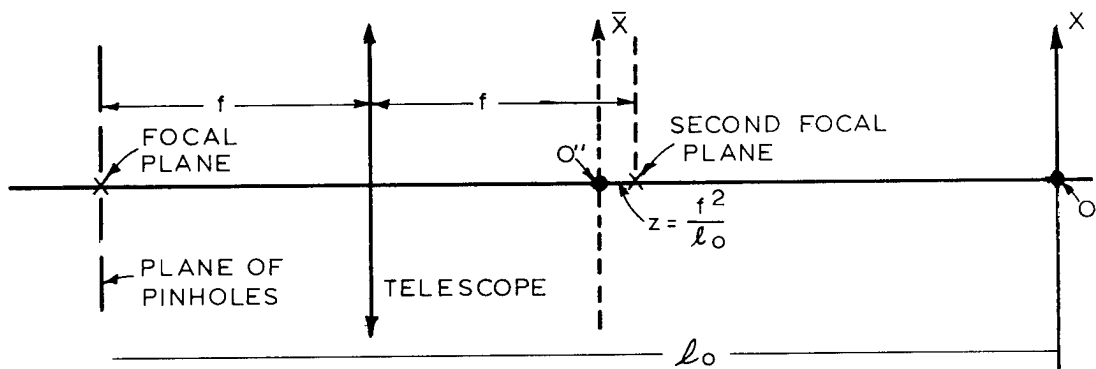


Figure II-2. Location of the star image  $O'$  as formed by collimator alone and of the new image  $O''$  when a telescope is added with its front focal plane coincident with the plane of pinholes.

Therefore when  $\Delta_a = 0$  the plane  $z$  in which  $\Phi = 0$  is the plane of the image of the illuminating pinhole  $O$ .

It follows from Eq. (8) that since  $\sqrt{\ell_o^2 + a^2} - \ell_o$  is constant and that if  $z$  is altered so that  $\Phi$  is fixed at  $\mu \frac{\pi}{2}$  where  $\mu$  is a particular odd integer, then

$$(\Delta_a)_2 - (\Delta_a)_1 = \frac{ka^2}{2f^2} (z_1 - z_2) \quad (12)$$

This means that defocusing the collimator so as to obtain slightly convergent light will introduce no error in the measurement of

$(\Delta_a)_2 - (\Delta_a)_1$ . Also, we have seen that  $\Phi$  continues to remain linear in  $z$  provided that the plane of the three pinholes is the front focal plane of the telescope.

Consideration of the case of the slightly diverging beam in which the collimator is defocused so as to image  $O'$ , Figure II.2 at a great distance  $\ell_o$  to the left of the three pinholes yields instead of Eq. 10

$$\Phi = \Delta_a + \frac{ka^2}{2} \left( \frac{z}{f^2} - \frac{1}{\ell_o} \right). \quad (13)$$

The position given by  $z\ell_o = f^2$  is now that of the final "star image"  $O''$ . The conclusions drawn above hold again.

In conclusion: Defocusing of the collimator in the arrangement of Figure 23 by relatively slight amounts will not alter the accuracy of the measurement of the phase differences

$$(\Delta_a)_2 - (\Delta_a)_1.$$

## II.2 TOLERANCE ON THE ANGULAR ORIENTATION OF THE INCIDENT ELECTRIC VECTOR IN THE X-Z METHOD

In this method, described in Section 2.5.5.3, the incident E-vector is intended to vibrate either along  $Z$  or along  $X$ . We examine here how closely one must set  $E$  along  $Z$  or along  $X$ . In doing so, it suffices to consider the setting with respect to  $Z$  since the same tolerance must apply with respect to the  $X$ -setting.

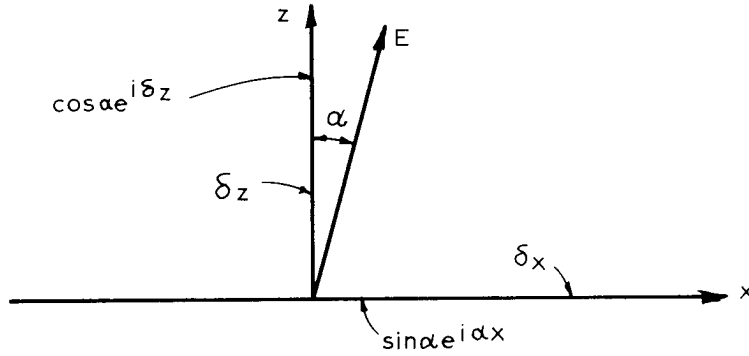


Figure II-3. Convention with respect to establishing a tolerance for the angle  $\alpha$  in the X-Z method.

First, we note that for the two outer, clear pinholes the E-vector remains unchanged in phase, amplitude and direction upon passing through these pinholes. But such is not the case for the light traversing the glass and the central pinhole. Let the strength of the incident E-vector be unity. Then for the E-vector emerging from the central pinhole,

$$\text{Z-component} = \cos \alpha e^{i\delta_z} ;$$

$$\text{X-component} = \sin \alpha e^{i\delta_x} ; \quad (14)$$

where  $\delta_z$  and  $\delta_x$  are the retardations of the strained glass for the Z and X-components, respectively. Since no analyzer is used, the fringes are due to interference of the combined electric vectors that oscillate along the line of vibration of the incident electric vector inclined at angle  $\alpha$  with respect to Z.

Let  $P_r$  denote the projection of the vector described by Eq. 14 upon the direction E. Then

$$P_r = \cos^2 \alpha e^{i\delta_z} + \sin^2 \alpha e^{i\delta_x} = \cos^2 \alpha e^{i\delta_z} [1 + \tan^2 \alpha e^{i(\delta_x - \delta_z)}] \quad (15)$$

As regards the E-vector emerging from the central pinhole, the only part of it that is of any use in forming the interference fringes is that having amplitude and phase given by the complex number  $P_r$ . In case  $\alpha=0$ , the correct value, then simply

$$P_r = e^{i\delta_z}$$

where  $\delta_z$  is the phase that we want to measure. Let

$$\psi \equiv 1 + \tan^2 \alpha e^{i(\delta_x - \delta_z)} \equiv 1 + \tan^2 \alpha e^{i\Delta} ; \quad (16)$$

$$\Delta \equiv \delta_x - \delta_z$$

Then

$$\theta = \arg(\psi) \quad (17)$$

is the error in the phase of the disturbance leaving the central pinhole produced by setting  $\alpha \neq 0$ .

Now

$$\psi = 1 + \tan^2 \alpha \cos \Delta + i \tan^2 \alpha \sin \Delta . \quad (18)$$

$\therefore$

$$\tan \theta = \frac{\tan^2 \alpha \sin \Delta}{1 + \tan^2 \alpha \cos \Delta} , \text{ whence}$$

$$\tan^2 \alpha = \frac{\tan \theta}{\sin \Delta - \cos \Delta \tan \theta} \quad (19)$$

Since both  $\alpha$  and  $\theta$  will be small, we have approximately

$$\alpha = \frac{\sqrt{\theta}}{\sqrt{|\sin \Delta - \theta \cos \Delta|}} \quad (20)$$

The smallest value of  $\alpha$  occurs when  $\Delta$  is near  $\pi/2$ . Hence we take as the tolerance on  $\alpha$

$$|\alpha| \leq \sqrt{\theta} . \quad (21)$$

If the error  $\theta = 1^\circ$  (corresponding to a phase error of  $\lambda/360$ ) is permitted as upper maximum, then

$$|\alpha| \leq \sqrt{\frac{1}{57.3}} \text{ radians} = 7.56^\circ . \quad (22)$$

Correspondingly, the error in the angular setting of the  $\lambda/2$ -plate is  $7.56/2 = 3.78^\circ$ . These are very liberal tolerances. Actually, it is easy to set the  $\lambda/2$  plate within  $\pm 0.2^\circ$  of the correct position.

Experiment showed that the  $\lambda/2$ -plate ought not to be rotated as much as  $1^\circ$  from its correct position but that  $\pm 0.2^\circ$  or even  $\pm 0.3^\circ$  is acceptable. Therefore, no problem arises in setting the  $\lambda/2$ -plate accurately enough in the X-Z method.

### II.3 TOLERANCE ON THE ANGULAR ORIENTATION OF THE ANALYZER IN THE $45^\circ$ METHOD

In this method, the incident E-vector vibrates at  $45^\circ$  with X and Z and the analyzer is set along either X or Z. Consider, Figure II-4, a setting error  $\alpha$  of the analyzer. With the incident polarization P at  $45^\circ$ , emerging from the central pinhole will be

$$\begin{aligned} e^{i\delta_z}/\sqrt{2} & \text{ as z-component ;} \\ e^{i\delta_x}/\sqrt{2} & \text{ as x-component .} \end{aligned} \quad (23)$$

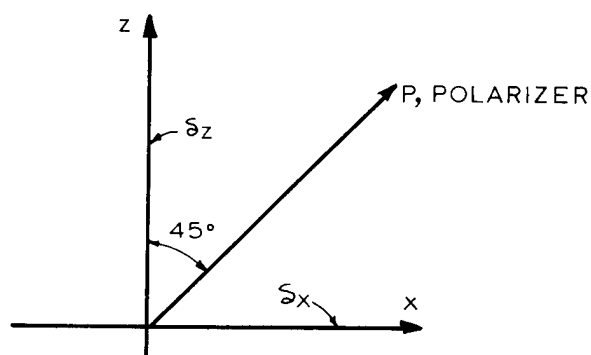


Figure II-4a

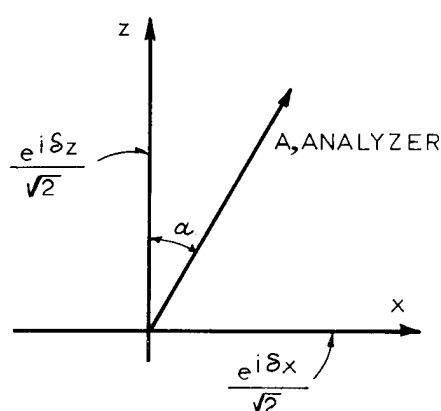


Figure II-4b

Polarized light emerges from the two outer pinholes vibrating along P and undisturbed in amplitude and phase. We have to project all of the disturbances upon the direction of the analyzer in determining the distribution of irradiance in the interference fringes.

The projection of the disturbance (23) upon the analyzer is given by the complex number

$$A = \frac{\cos\alpha}{\sqrt{2}} e^{i\delta_z} + \frac{\sin\alpha}{\sqrt{2}} e^{i\delta_x} = \frac{\cos\alpha}{\sqrt{2}} e^{i\delta_z} [1 + \tan\alpha e^{i\Delta}] , \quad (24)$$

$\Delta \equiv \delta_x - \delta_z$ , the relative retardation.

With the setting of Figure 4b, one is seeking information about  $\delta_z$ . The information will be correct at  $\alpha=0$  where

$$A = e^{i\delta_z} / \sqrt{2} . \quad (25)$$

But with  $\alpha \neq 0$  the disturbance A from the central pinhole will depart in phase from the amount  $\delta_z$  by the error  $\theta$  where

$$\theta = \arg (1 + \tan\alpha e^{i\Delta}) = \arg [1 + \cos\Delta \tan\alpha + i \sin\Delta \tan\alpha] . \quad (26)$$

In the complex Z-plane we have, as in Figure II-5,

$$\tan\theta = \frac{\sin\Delta \tan\alpha}{1 + \cos\Delta \tan\alpha} . \quad (27)$$

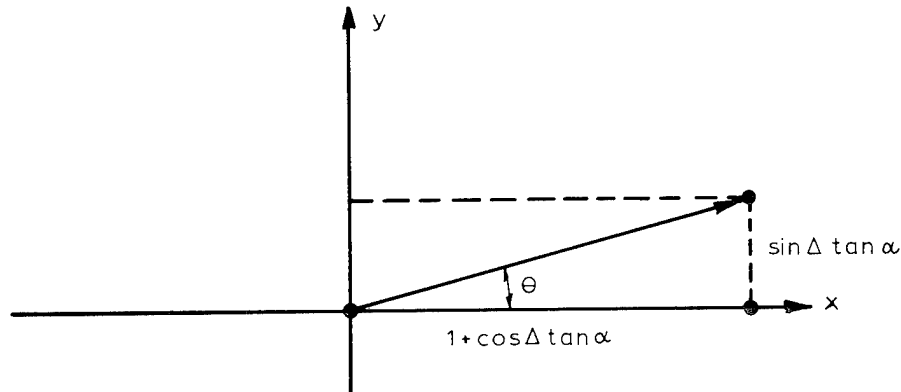


Figure II-5. Representation of the phase error  $\theta$  in the complex Z-plane.

(27)

Then since  $\theta$  and  $\alpha$  will be small

$$\theta = \frac{\alpha \sin \Delta}{1 + \alpha \cos \Delta} \rightarrow \alpha \sin \Delta \quad (28)$$

Whence, approximately,

$$|\alpha| = \left| \frac{\theta}{\sin \Delta} \right|. \quad (29)$$

Since  $|\alpha|$  is smallest when  $|\sin \Delta| = 1$ , we take as our tolerance on  $\alpha$

$$|\alpha| \leq |\theta| \quad (30)$$

Again, we ask that  $\theta$  shall not exceed  $1^\circ$  so that the phase error shall not exceed  $\lambda/360$ . Thus, our tolerance on the setting of the analyzer from its correct position is

$$|\alpha| \leq 1^\circ \quad (31)$$

in the  $45^\circ$ -method.

This tolerance is not difficult to meet.

We conclude that whether one uses the X-Z method or the  $45^\circ$  method the tolerances on the "polarizer" or analyzer settings are large enough so that no difficulty need be expected.

#### II.4 TOLERANCES WITH RESPECT TO IMPERFECT SAMPLES IN THE THREE-PINHOLE, ZERNIKE METHOD

Experiment has indicated that in the presence of striae one must mount the three pinholes so that they ride with the sample. In the following we assume that at least the central pinhole is attached to the sample. In determining the precision with which the samples are to be fabricated the following factors should be considered;

- (A) Effects of non-uniformity of optical path between the polished faces due to the presence of wedge or lack of flatness.
- (B) Non-uniformity of strain in a wedged sample.

- (C) Wedge between the polished faces can cause the diffraction pattern from the central pinhole not to overlap those from the two side holes.
- (D) The relation of wedge-angle to autocollimation.

## II.5 TOLERANCE ON WEDGE-ANGLES AS RELATED TO THE NEED FOR AUTOCOLLIMATION

We refer here to wedge between the two polished faces. The tolerance on wedge-angle becomes so liberal that one can ignore it provided that upon autocollimation one takes the trouble to distinguish carefully between the two images produced by reflection from the two polished faces. Owing to the presence of striae, the image reflected from the second surface is usually blurred.

The penalty for paying no attention to this matter will be to keep the wedge-angle down to about 1 minute of arc in order to control the tilt of the sample as the pressure is altered. We assume that proper care will be taken during autocollimation so that no tolerance beyond the normal care taken in the optical shop need be assigned relative to the matter of controlling the tilt of the sample.

## II.6 TOLERANCE ON WEDGE ANGLES AS REGARDS OBTAINING RELIABLE MEASUREMENT OF THE AVERAGE OPTICAL PATH

Fortunately, this aspect of the measurement does not require the assignment of tolerance of wedge-angles beyond routine practice in the optical shop.

From Eqs. (31) and (32) in Section I.5 of Appendix I we have to consider the integral

$$I = \iint_{\substack{\text{over central} \\ \text{pinhole}}} P_o(\zeta, \eta) d\zeta d\eta = T e^{i\Delta_a} \iint_{\substack{\text{over central pinhole}}} e^{i[\Delta(\zeta, \eta) - \Delta_a]} d\zeta d\eta \quad (32)$$

where  $\Delta_a$  is the averaged optical path over the pinhole. Let

$$\psi \equiv \iint_{\substack{\text{over central pinhole}}} e^{i[\Delta(\zeta, \eta) - \Delta_a]} d\zeta d\eta \quad (33)$$

We have to keep firmly in mind that in measuring the stress-optical coefficients we measure  $\arg(I)$  at two different pressures and then subtract these arguments (phases) from each other with the aim of measuring in this way

$$\Delta = (\Delta_a)_{\text{at } P=P_2} - (\Delta_a)_{\text{at } P=P_1} \quad (34)$$

For this to be true our experimental conditions must be such that

$$\text{Arg}(\psi) = \text{constant, independent of pressure.} \quad (35)$$

It is not necessary that  $\arg(\psi) = 0$ .

Assume for simplicity that the incident wavefront is normal to the optic axis. The effect of a wedged sample is to incline this wavefront into oblique incidence upon the central pinhole. Without loss of generality we may regard  $\xi, \eta$  to be oriented so that correspondingly  $\Delta(\xi, \eta) = \Delta(\xi) = \Delta_a + K\xi$  (36)

$$\text{where } K = \frac{2\pi}{\lambda} (n-1) A ; A = \text{angle of the wedge.} \quad (37)$$

Then from Eqs. (33) and (36)

$$\psi = \iint_{\text{over central pinhole}} e^{iK\xi} d\xi d\eta \quad (38)$$

Let the central pinhole be circular with area B. Then, introducing polar coordinates

$$\psi = \int_0^{\sqrt{\frac{B}{\pi}}} \int_0^{2\pi} e^{iK\rho\cos\theta} \rho d\rho d\theta = 2\pi \int_0^{\sqrt{\frac{B}{\pi}}} J_0(K\rho) \rho d\rho . \quad (39)$$

$$\psi = \pi \frac{B}{\pi} 2 \frac{J_1\left(K \sqrt{\frac{B}{\pi}}\right)}{K \sqrt{\frac{B}{\pi}}} \quad (40)$$

Then since  $\frac{B}{\pi} = R_c^2 = \text{radius of the central pinhole,}$

$$\psi = 2B \frac{J_1(KR_c)}{K R_c} ; \quad \underline{\text{real}} ; \quad (41)$$

$R_c = \text{radius of central pinhole; } B = \pi R_c^2 ;$

$K = \frac{2\pi}{\lambda} (n-1) A ; A = \text{angle of the wedge.}$

Hence if the polished faces form a simple wedge,

$$\arg(\psi) = 0 \text{ for all pressures} \quad (42)$$

irrespective of the wedge angle. Hence we do not have to assign a tolerance on the wedge angle from the considerations of this section. This conclusion was unexpected.

## II.7 TOLERANCE ON SURFACE FLATNESS AS REGARDS OBTAINING RELIABLE MEASUREMENT OF THE AVERAGE OPTICAL PATH

It will not be possible to examine here all possible variations from surface flatness; but the special case studied here suggests strongly that as regards measuring  $[(\Delta_a)_{P_2} - (\Delta_a)_{P_1}]$  properly from the restricted viewpoint of this section, no tolerances need be assigned to surface flatness beyond the quality which is routine in our optical shop.

We can expect that for radially symmetric surface deviations from flatness

$$\Delta(\zeta, \eta) = \Delta_a + \sigma(\zeta^2 + \eta^2) \quad (43)$$

when the central pinhole is placed over the center of the irregularity. Then from Eqs. (32) and (33)

$$\psi = \iint_{\text{over central pinhole}} e^{i\sigma(\zeta^2 + \eta^2)} d\zeta d\eta. \quad (44)$$

Let the central pinhole be circular with radius  $R_c$  and area  $B$ . Upon converting to polar coordinates, we obtain

$$\psi = 2\pi \int_0^{\sqrt{\frac{B}{\pi}}} e^{i\sigma\rho^2} \rho d\rho = 2\pi \int_0^{R_c} e^{i\sigma\rho^2} \rho d\rho ;$$

$$\psi = -\frac{i\pi}{\sigma} e^{iz} \Big|_0^{\sigma R_c^2} = \frac{i\pi}{\sigma} [1 - e^{i\sigma R_c^2}] . \quad (45)$$

As  $\sigma R_c^2 \rightarrow 0$ ,

$$\psi \rightarrow \frac{i\pi}{\sigma} (-i) \sigma R_c^2 = B ; I \rightarrow T B e^{i\Delta_a} . \quad (45a)$$

We observe from (45) that whereas  $\arg(\psi)$  is not in general equal to zero (the exception occurs when  $\sigma R_C^2 \rightarrow 0$ ) it is in a given set-up a constant independent of pressure. Hence this type of surface error (and we can suspect all others) need not be assigned tolerances beyond the quality which is routine in our optical shop. This is, of course, fortunate.

## II.8 TOLERANCE IMPOSED ON THE ANGLE OF THE WEDGE IN ORDER THAT THE DIFFRACTION PATTERNS SHALL OVERLAP PROPERLY

It turns out that a tolerance on the angle of wedge between the two polished surfaces needs to be imposed in order that the light diffracted from the three pinholes shall overlap properly in the plane of observation. In calculating this tolerance, we need consider only the far Fresnel region as in Section I.4 of Appendix I where it is estimated that said Fresnel plane is in excess of 50 meters, in our proposed optics, from the plane of the pinholes in the absence of the telescope.

First, for pinholes of about 0.34 mm diameter the radius  $r_a$  of the "Airy disk" in the observation plane is given approximately by

$$r_a = \frac{0.61 \lambda}{N.A.} = \frac{0.61 \times 0.6328 \times 10^{-3}}{\frac{0.34}{2 \times 5 \times 10^4}} = 114 \text{ mm} \quad (46)$$

Secondly, the spacing of the fringes produced by light from the two outer pinholes of separation  $2a = 14 \text{ mm}$  is given by

$$\frac{x}{R} = \frac{\lambda}{2a} \quad \text{whence}$$

$$x = \text{spacing} = \frac{0.6328 \times 50}{14} = 2.3 \text{ mm} \quad (47)$$

This is in the far Fresnel plane for which  $R = 50 \text{ m}$ . About 100 fringes would then be seen across Airy disks that overlap completely. If the three pinholes are separated by 7 mm and have the same diameter, as is our case, we obtain in the observation plane corresponding to  $R = 50 \text{ m}$ , under idealized conditions three overlapping and interfering diffraction disks each about 114 mm in diameter with their centers displaced each by 7 mm. The effect of placing a glass wedge over the central pinhole is to displace the Airy disk produced by the central pinhole. It is recommended

that this Airy disk be displaced no more but that the irradiance produced by it at the midpoint between the centers of the two outer Airy disks drops to only 90% of its value at the diffraction head.

Approximately,  $\left[2 \frac{J_1(Z)}{Z}\right]^2 = 0.90$  for  $Z = 0.64$ . This means that the central diffraction disk should not be displaced in excess of

$$\frac{0.64}{3.83} \times 114 = 20 \text{ mm.} \quad (48)$$

The angle  $\alpha$  through which light from the central pinhole can be deviated should, then, not exceed

$$\alpha = \frac{20}{5 \times 10^4} = 0.0004 \text{ radians.} \quad (49)$$

The angle of the glass wedge is about twice this value of  $\alpha$  since  $n$  is roughly 1.5. Thus the angle  $A$  of the glass wedge should obey the tolerance

$$A \leq 0.0008 \text{ radians} = 2.7 \text{ minutes.} \quad (50)$$

We regard this as a conservative estimate - meaning that slightly larger angles may prove to be tolerable.

We note that experimentally all of our glass samples that were tested gave good, straight fringes.

## II.9 TOLERANCE ON THE TILT OF THE SAMPLE

The most damaging effect of the tilt of the sample from perpendicularity to the incident beam is the change in tilt that may be produced upon changing the applied pressure. The following considerations are based upon Fig. II-6 and apply to a single passage of light through the sample.

Let the normal to the sample be tilted by the amount  $\theta$  from the axis A B of the instrument. Then with respect to Fig. II-6

$$l = \frac{L}{\cos\phi} ; \quad z = l \cos(\theta - \phi) = L \frac{\cos(\theta - \phi)}{\cos\phi} \quad (51)$$

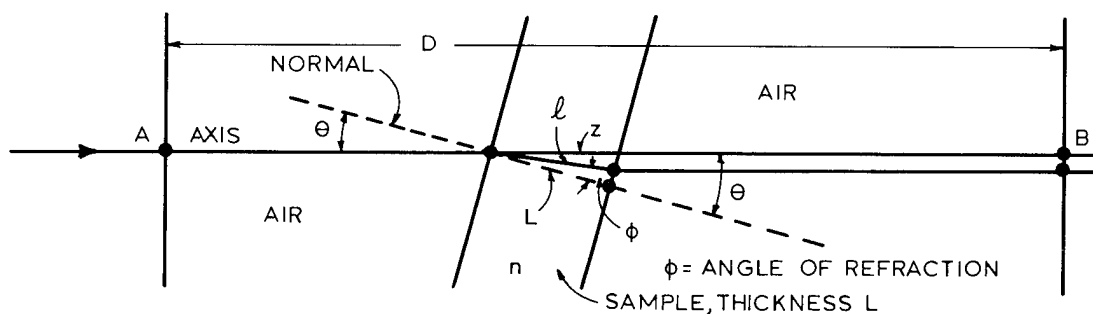


Figure II-6. Convention with respect to tilt of the sample.

Let

$$\Delta = \text{optical path from A to B} = D - z + n l.$$

$$\therefore \Delta = D - L \frac{\cos(\theta - \phi)}{\cos\phi} - \frac{nL}{\cos\phi} . \quad (52)$$

$$\text{Let } \Delta_0 = \Delta_{\theta=0} = D - L + nL. \quad (53)$$

Define

$$\delta = \Delta - \Delta_0 = \text{change in optical path due to tilt.} \quad (54)$$

One finds quite directly from (52) - (54) that

$$\delta = L \left[ \frac{n(1-\cos\phi)}{\cos\phi} + \frac{\cos\phi - \cos(\theta-\phi)}{\cos\phi} \right] \text{ or}$$

$$\frac{\delta}{L} = 1 + \frac{n(1-\cos\phi)}{\cos\phi} - \frac{\cos(\theta-\phi)}{\cos\phi} ; \sin\theta = n \sin\phi ; \text{ any } \theta. \quad (55)$$

For small  $\theta$ , write  $\cos\phi = 1 - \frac{\phi^2}{2}$  ;  $\theta = n\phi$ . Then

$$\frac{\delta}{L} = \frac{\theta^2}{2} \frac{n-1}{n} \quad \text{and} \quad \theta = \sqrt{\frac{2n}{n-1} \frac{\delta}{L}} . \quad (56)$$

Hence for small tilts about the normal position the optical path error  $\delta$  varies as  $\theta^2$ .

TABLE II.1 TOLERANCES  $\theta$  AS COMPUTED FROM EQ. (56)

Error $\delta$	n	L (mm)	$\theta$ (min)	$\lambda$ ( $\mu\text{m}$ )
$\lambda/1000$	1.5	10	1.88	0.5
$\lambda/1000$	1.5	10	2.12	0.6328
$\lambda/100$	1.5	10	6.70	0.6328
$\lambda/100$	1.6	10	3.55	0.6328

It appears from this table that the tolerances on tilt are quite liberal; but such is not the case when the sample is not normal to the incident beam before the added tilt occurs. For example, if the sample has originally the tilt  $\theta_0 = 0.1^\circ$ , then if this tilt is altered to  $0.15^\circ$  by changing the pressure,  $\delta/\lambda$  changes from 0.00802 to 0.01803 due to change of tilt alone.

This means that a change of tilt of 3 minutes causes an error in  $\delta$  of 0.01 wavelength - an amount large enough to interfere with the accuracy of our measurements. If  $\theta_0 = 0.1^\circ$ , the added tilt should be constrained to about one minute.

Eq. (56) is accurate enough for  $0 \leq \theta \leq 2^\circ$ , a range which, surely, should not be exceeded for experimental reasons. From Eq. (56)

$$\frac{\delta_1 - \delta_0}{\lambda} = \frac{L}{\lambda} \frac{n-1}{2n} (\theta_1^2 - \theta_0^2) . \quad (57)$$

A definite tolerance on  $\theta_1$  cannot be assigned without knowing  $\theta_0$ . Since it is desirable to measure the optical path differences to  $0.01\lambda$ , it is suggested that  $\theta_1$  be restricted with respect to  $\theta_0$  such that

$$\frac{L}{\lambda} \frac{n-1}{2n} (\theta_1^2 - \theta_0^2) \leq 2 \times 10^{-3} \quad (58)$$

In conclusion, it is suggested that the head of a collimating device be placed just beyond the pinhole O, Fig.II-3 for measuring how nearly normal the surfaces of the glass sample are to the incident beam. Means for adjustment should be provided so that Eq. (58) remains satisfied. Motion of the cross-hairs in two, perpendicular directions is indicated.

## II.10 ADDITIONAL COMMENTS ON THE TOLERANCE

### ON TILT OF THE SAMPLE

A tolerance on tilt of the sample as discussed in I.8 of the previous Appendix can be estimated from Eq. (56) of that report as follows:

$$\frac{\delta}{\lambda} = \frac{n-1}{n} \frac{L}{\lambda} \frac{\theta^2}{2} ; \quad \frac{d(\delta/\lambda)}{d\theta} = \frac{n-1}{n} \frac{L}{\lambda} \theta ; \quad (59)$$

where  $\theta$  is the angle between the axis of the instrument (more particularly, the rays of the incident light beam) and the normal to the plate being tilted.

The autocollimator device we have designed for the final apparatus is estimated to permit us to monitor  $\theta$  to at least 10 sec. of arc. Adjusting screws will permit the readjustment of the sample to at least 0.0001 radians or about 21 sec. If we call for a change in  $(\delta/\lambda)$  after readjustment of not more than 0.001, then the angle of tilt  $\theta$  must not exceed

$$\theta = \frac{n}{n-1} \frac{\lambda}{L} \frac{d\left(\frac{\delta}{\lambda}\right)}{d\theta} = \frac{1.5}{0.5} \frac{0.6328 \times 10^{-3}}{10} \frac{0.001}{0.0001} \text{ so that}$$

as a tolerance on  $\theta$

$$\theta \leq 0.00190 \text{ radians} \approx 7 \text{ minutes.}$$

This tolerance should be easy to maintain mechanically. With the proposed collimating system, one will not be able to measure the 7 minutes; but setting within these 7 minutes should be easy.

# REFERENCES

1. E. Snitzer, Phys. Rev. Lett., 7, (12), p 444, 15 Dec. 1961.
2. G. E. Peterson and P. M. Bridenbaugh, J. Opt. Soc. Am., 54, p 644, May 1964.
3. R. F. Woodcock, J. Opt. Soc. Am., 53, p 523, April 1963.
4. C. C. Robinson, J. Chem. Phys., 54, (8), p 3572, 15 April 1971.
5. W. A. Weyl, "Coloured Glasses," Pub. by Soc. of Glass Technology, Sheffield, 1951.
6. V. J. Johnson, Ed. "A Compendium of Properties of Materials at Low Temperature, Phase I," NBS Cry. Eng. Lab., Boulder, Colorado, pp 3.5001, Dec. 1959.
7. G. W. Morey, "The Properties of Glass," The Reinhold Publishing Corp., New York, p 428, 1938.
8. Unpublished proposal to ONR, April 1964, see also Snitzer, E., Appl. Opt. 5, p 1487, Oct. 1966.
9. F. W. Quelle, Appl. Opt., 5, p 633, April 1966.
10. F. Pockels, Ann. Physik, 7, (4), p 745, 1902.
11. Jena Glass, Hovestadt Trans. by J. D. & A. Everett, Macmillan & Co., London, p 186, 1902.
12. T. Kishii, Proc. 4th International Glass Congress, p 244.
13. F. P. Hall, Am. Ceram. Soc., 13, p 182, 1930.
14. S. Kumar, Glastechn. Ber., Special Issue, V. International Glass Congress, 32K, Part V, p 26, 1959.
15. G. W. Morey, "Properties of Glass," Reinhold Publishing Corp., New York, 2nd Ed., p 442, 1954.
16. L. H. Adams, and E. D. Williamson, J. Wash. Acad. 9, p 609, 1919.
17. F. Pockels, Ann. Physik, 7 (4), p 745, 1902, 9 (4), p 220, 1902 and 11 (4), p 651, 1903.

#### REFERENCES

18. F. Zernike, J. Opt. Soc. Am., 40, p 326, 1950.
19. B. Vittoz, Helv. Phys. Acta 26, p 400, 1953.
20. A.C.S., van Heel, Physica XXIV, p 529, 1958.
21. H. B. Huntington, "Elastic Constants of Crystals," Solid State Physics, Vol. 7, Academic Press Inc., New York, p 213, 1958.
22. H. Welling and C. J. Beckart, J. Opt. Soc. Am. 56, p 611, May 1966.

UNCLASSIFIED

Security Classification

## DOCUMENT CONTROL DATA - R &amp; D

(Security classification of title, body of abstract and indexing annotation must be entered when the overall report is classified)

1. ORIGINATING ACTIVITY (Corporate author) American Optical Corporation Research Division Southbridge, MA 01550		2a. REPORT SECURITY CLASSIFICATION UNCLASSIFIED	
		2b. GROUP N/A	
3. REPORT TITLE  NEODYMIUM LASER GLASS IMPROVEMENT PROGRAM			
4. DESCRIPTIVE NOTES (Type of report and inclusive dates) Final Report 1 May 1962-1 March 1971			
5. AUTHOR(S) (First name, middle initial, last name)  Richard F. Woodcock			
6. REPORT DATE July 1973		7a. TOTAL NO. OF PAGES 124	7b. NO. OF REFS 22
8a. CONTRACT OR GRANT NO. Nonr 3835(00)		9a. ORIGINATOR'S REPORT NUMBER(S)  598 F	
b. PROJECT NO.  7300		9b. OTHER REPORT NO(S) (Any other numbers that may be assigned this report)	
c.  ARPA Order No. 306			
10. DISTRIBUTION STATEMENT  Distribution of this report is unlimited			
11. SUPPLEMENTARY NOTES  Project DEFENDER ABSTRACT		12. SPONSORING MILITARY ACTIVITY Office of Naval Research Department of the Navy Arlington, Virginia 22217	

This final report describes work carried out over a nine-year period to improve the properties and performance of Nd-laser glass. One of the first tasks was the reduction of absorption at 1.06  $\mu\text{m}$  to a 0.1-0.2%/cm level by the identification and elimination of such impurities as iron.

Fluorescent lifetime was investigated; (1) as a function of host glass composition to provide data on the range of values attainable for this important parameter, and (2) as a function of time, temperature and  $\text{Nd}_2\text{O}_3$  concentration to provide insight into the nature of the  $\text{Nd}^{3+}$ -ion site and its effect on emission.

The degree of discoloration due to solarization by the pump source and its effect on laser performance was investigated as a function of glass composition.

Theory was evolved for the design of an "athermal" laser material based on the hypothesis that thermally induced optical distortion resulting from thermal expansion and associated stress-optical effects can be counterbalanced by direct thermally induced index changes if proper glass composition and cavity design are chosen. Descriptions are given of the measuring techniques, which are unique in many cases, for determining coefficients of the above temperature and pressure effects as a function of glass composition. Several compositions showed theoretically predicted and experimentally verified marked improvement over our commercial laser material.

DD FORM 1 NOV 65 1473

UNCLASSIFIED

Security Classification

UNCLASSIFIED

Security Classification

14. KEY WORDS	LINK A		LINK B		LINK C	
	ROLE	WT	ROLE	WT	ROLE	WT
Lasers Laser Glass Neodymium Laser Glass Glass Melting Glass Measurements Athermalization Interferometry Solarization Stress Optical Coefficients Stress Birefringence Optical Transmission Fluorescent Lifetime						

UNCLASSIFIED

Security Classification